

NASA Contractor Report 179448

---

# **Analysis of Structural Response Data Using Discrete Modal Filters**

---

Lawrence C. Freudinger

---

G 0635, PR A78043C  
May 1991



National Aeronautics and  
Space Administration

---

# Analysis of Structural Response Data Using Discrete Modal Filters

---

Lawrence C. Freudinger  
Dryden Flight Research Facility  
Edwards, California

Prepared for  
NASA Dryden Flight Research Facility  
Edwards, California  
Under Contract G 0635, PR A78043C

1991



National Aeronautics and  
Space Administration

Dryden Flight Research Facility  
Edwards, California 93523-0273

**CONTENTS**

<b>ABSTRACT</b>	<b>1</b>
<b>ACKNOWLEDGEMENTS</b>	<b>1</b>
<b>NOMENCLATURE</b>	<b>1</b>
<b>INTRODUCTION</b>	<b>2</b>
<b>MATHEMATICAL BACKGROUND</b>	<b>3</b>
Reciprocal Modal Vectors . . . . .	3
Decoupled Frequency Response . . . . .	4
Decoupled Operating Data . . . . .	5
<b>APPLICATIONS</b>	<b>5</b>
<b>ANALYTICAL SYSTEM APPLICATION</b>	<b>6</b>
Objectives and Procedure . . . . .	6
Analytical System Results and Discussion . . . . .	6
<b>EXPERIMENTAL APPLICATION</b>	<b>19</b>
Experiment Objectives and Procedure . . . . .	19
Modal Test Results . . . . .	20
Perturbed System Analysis Results and Discussion . . . . .	20
<b>CONCLUDING REMARKS</b>	<b>69</b>
<b>RECOMMENDATIONS</b>	<b>69</b>
<b>REFERENCES</b>	<b>71</b>

## LIST OF TABLES

Table 1. Modal assurance criterion matrix: analytical system . . . . .	11
Table 2. Frequency and damping values for analytical systems . . . . .	13
Table 3. Relationship between baseline and 50% mass perturbation . . . . .	18
Table 4. Estimated modes from truss: baseline configuration . . . . .	23

## LIST OF FIGURES

Figure 1. Mass, stiffness, and damping matrices of baseline analytical system . . . . .	9
Figure 2. Typical synthesized frequency response function . . . . .	9
Figure 3. RMV-decoupled frequency responses of baseline analytical system . . . . .	10
Figure 4. Effect of spatial undersampling for first analytical mode . . . . .	12
Figure 5. Effect of spatial undersampling for third analytical mode . . . . .	12
Figure 6. Effects of perturbing mass (1,1): analytical mode 1 . . . . .	14
Figure 7. Effects of perturbing mass (1,1): analytical mode 2 . . . . .	14
Figure 8. Effects of perturbing mass (1,1): analytical mode 3 . . . . .	15
Figure 9. Effects of perturbing mass (1,1): analytical mode 4 . . . . .	15
Figure 10. Effects of perturbing mass (1,1): analytical mode 5 . . . . .	16
Figure 11. Effects of perturbing mass (1,1): analytical mode 6 . . . . .	16
Figure 12. Decoupling performance for unaltered mode shape: analytical mode 1 . . . . .	17
Figure 13. Decoupling performance for unaltered mode shape: analytical mode 4 . . . . .	17
Figure 14. Truss test structure overview . . . . .	24
Figure 15. Driving point measurements (17y) for all test configurations . . . . .	25
Figure 16. Driving point measurements (28x) for all test configurations . . . . .	26
Figure 17. Driving point measurements (56y) for all test configurations . . . . .	27
Figure 18. Typical multiple coherence measurements . . . . .	28
Figure 19. Nonlinearity check: highest and lowest force level (17y top, 28x bottom) . . . . .	29
Figure 20. Reciprocity check for baseline configuration (17y – 56y) . . . . .	30
Figure 21. Reciprocity check for baseline configuration (17y – 28x) . . . . .	30
Figure 22. Time invariance check: driving point (17y/17y) . . . . .	31
Figure 23. Time invariance check: driving point (28x/28x) . . . . .	31
Figure 24. Overview of decoupled responses for first seven flexible modes . . . . .	32
Figure 25. Decoupled FRFs for different active references: mode 1 (rigid body yaw) . . . . .	33
Figure 26. Decoupled FRFs for different active references: mode 2 (rigid body roll) . . . . .	34
Figure 27. Decoupled FRFs for different active references: mode 3 (rigid pitch/roll) . . . . .	35
Figure 28. Decoupled FRFs for different active references: mode 4 (rigid body pitch) . . . . .	36
Figure 29. Decoupled FRFs for different active references: mode 5 (lateral first bending) . . . . .	37
Figure 30. Decoupled FRFs for different active references: mode 6 (vertical first bending) . . . . .	38
Figure 31. Decoupled FRFs for different active references: mode 7 (lower mast torsion) . . . . .	39
Figure 32. Decoupled FRFs for different active references: mode 8 (mast vertical bending) . . . . .	40
Figure 33. Decoupled FRFs for different active references: mode 9 (upper mast/crossarm lateral bending) . . . . .	41

Figure 34. Decoupled FRFs for different active references: mode 10 (lateral second bending) . . . . .	42
Figure 35. Decoupled FRFs for different active references: mode 11 (upper mast torsion) . . . . .	43
Figure 36. Decoupled FRFs for different active references: mode 12 (crossarm YZ-plane bending) . . . . .	44
Figure 37. Comparison of decoupled FRF for 80, 40, and 20 degrees of freedom (mode #1) . . . . .	45
Figure 38. Comparison of decoupled FRF for 80, 40, and 20 degrees of freedom (mode #2) . . . . .	46
Figure 39. Comparison of decoupled FRF for 80, 40, and 20 degrees of freedom (mode #3) . . . . .	47
Figure 40. Comparison of decoupled FRF for 80, 40, and 20 degrees of freedom (mode #4) . . . . .	48
Figure 41. Comparison of decoupled FRF for 80, 40, and 20 degrees of freedom (mode #5) . . . . .	49
Figure 42. Decoupled FRFs for 80, 40, and 20 degrees of freedom (mode #6; 1 mass added) . . . . .	50
Figure 43. Decoupled FRFs for all configurations: mode #5 (lateral first bending) . . . . .	51
Figure 44. Decoupled FRFs for all configurations: mode #6 (vertical first bending) . . . . .	52
Figure 45. Decoupled FRFs for all configurations: mode #7 (lower mast torsion) . . . . .	53
Figure 46. Decoupled FRFs for all configurations: mode #8 (mast vertical bending) . . . . .	54
Figure 47. Decoupled FRFs for all configurations: mode #9 (upper mast/crossarm lateral bending) . . . . .	55
Figure 48. Decoupled FRFs for all configurations: mode #10 (lateral second bending) . . . . .	56
Figure 49. Decoupled FRFs for all configurations: mode #11 (upper mast torsion) . . . . .	57
Figure 50. Decoupled FRFs for all configurations: mode #12 (crossarm YZ-plane bending) . . . . .	58
Figure 51. Baseline mode shape: first lateral bending (mode #5) . . . . .	59
Figure 52. Configuration #2 mode shape containing baseline first lateral bending . . . . .	60
Figure 53. Configuration #2 mode shape containing baseline first lateral bending . . . . .	61
Figure 54. Configuration #3 mode shape containing baseline first lateral bending . . . . .	62
Figure 55. Configuration #3 mode shape containing baseline first lateral bending . . . . .	63
Figure 56. Configuration #4 mode shape containing baseline first lateral bending . . . . .	64
Figure 57. Baseline mode shape: upper mast/crossarm lateral bending (mode #9) . . . . .	65
Figure 58. Configuration #2 mode shape containing baseline mode #9 . . . . .	66
Figure 59. Configuration #3 mode shape containing baseline mode #9 . . . . .	67
Figure 60. Configuration #4 mode shape containing baseline mode #9 . . . . .	68

## ABSTRACT

This thesis describes the application of reciprocal modal vectors to the analysis of structural response data. Reciprocal modal vectors are constructed using an existing experimental modal model and an existing frequency response matrix of a structure and can be assembled into a matrix that effectively transforms the data from the physical space to the modal space within a particular frequency range. In other words, the weighting matrix necessary for modal vector orthogonality (typically the mass matrix) is contained within the reciprocal modal matrix.

The ability to extract the response of a particular mode from a system due to whatever forces may be acting on it has broad applicability, from operating data analysis and force identification to vibration control. The underlying goal of this work is mostly directed toward observing the modal state responses in the presence of unknown, possibly closed loop forcing functions, thus having an impact on both operating data analysis techniques and independent modal space control techniques. This study investigates the behavior of reciprocal modal vectors as modal filters with respect to certain calculation parameters and their performance with perturbed system frequency response data.

## ACKNOWLEDGEMENTS

This thesis topic was made possible by past research activity of the Structural Dynamics Research Laboratory in the area of discrete modal filter theory, which was supported under NASA Grant NAG-1-942. I would like to express my gratitude to the current members of the laboratory who provided guidance and/or assistance to me in this work. Many thanks to Stuart Shelley and Dr. Randy Allemang for their efforts in planning, guidance, and supervisory roles. In addition, I would like to thank Jerry Pan and Alex Wang for enlightening discussions on orthogonal bases, and Filip Deblauwe and Allyn Phillips for sharing their programming skills with me.

Also, I would like to thank Mike Kehoe and NASA Dryden Flight Research Facility for providing the opportunity to pursue my lofty ideas. I certainly could not have accomplished this if it weren't for their understanding, sacrifice, and support.

Lastly, I am indebted to my lovely wife Catherine whose sense of humor and continuing sacrifices are very much appreciated and critical ingredients of the successful completion of this work.

## NOMENCLATURE

$\{\dots\}$	column vector
$[\dots]$	matrix
$[\dots]^H, [\dots]^{T*},$ $[\dots]^{*T}$	Hermetian operation: complex conjugate transpose
$[\dots]^T$	transpose of a matrix (same for vector)
$[\dots]^*$	complex conjugate of a matrix (same for vector)
$[\dots]^\dagger$	pseudoinverse of a matrix
$[\dots]_{pq}$	dimensions of a matrix: $p$ rows and $q$ columns
$f$	input excitation force (function of frequency or time implied)
$G_{xx}$	response power spectral matrix
$[H(\omega)]$	frequency response matrix (frequency dependency usually inferred)
$j$	$\sqrt{-1}$
$\{l\}_r$	participation vector for mode $r$

$N$	number of significant modes within given frequency range
$N_i$	number of excitation sources ( <i>a.k.a.</i> system inputs; references)
$N_o$	number of transducers (measurement degrees of freedom)
$x$	system response (function of frequency or time implied)
$\zeta_r$	viscous damping ratio for mode $r$
$\lambda_r = \sigma_r + j\omega_r$	complex eigenvalue for mode $r$ (system pole)
$\{\phi\}_r$	mode shape for mode $r$
$\{\Psi\}_r$	reciprocal modal vector for mode $r$
$\omega$	frequency variable, radians per second
$\omega_r$	damped natural frequency of $r^{th}$ mode

## INTRODUCTION

The well-known result that mode shapes of linear reciprocal systems possess a *weighted* orthogonality property has often limited the applicability of experimental modal analysis. Since the required weighting matrix in the physical space—often the mass matrix—is typically not known, most current techniques for validating the orthogonality of estimated modal vectors require simplifying assumptions or have been an approximation at best. Subsequent mathematical studies using experimental modal models are very dependent on the accuracy of the supplied modal model, thus establishing a need for quantifying the accuracy of the modal parameters.<sup>[1,2]</sup>

A new type of modal parameter called the reciprocal modal vector (RMV) was recently introduced to complete the modal model and check the orthogonality of modal vectors.<sup>[2]</sup> A matrix whose columns are a set of reciprocal modal vectors is called a reciprocal modal matrix or a discrete modal filter (although there are other ways of calculating modal filters). The continuous domain counterpart of the modal filter had been previously introduced about a decade ago in the controls community in order to deal with the problem of control spillover.<sup>[3,4]</sup> By definition, reciprocal modal vectors are orthogonal to the modal vectors in a given frequency range. In theory, the inner product of the reciprocal modal matrix and the modal matrix should be the identity matrix. In practice, this inner product only approximates the identity matrix, consequently providing insight to the actual orthogonality of the estimated modes. A reciprocal modal vector is calculated by using the traditional modal parameters estimated for a given mode and the frequency response function (FRF) matrix that was used in deriving the parameters.

This orthogonality condition implies that, for symmetric systems, the reciprocal modal vectors are actually the transpose of the modal matrix postmultiplied by the weighting matrix necessary for orthogonality, which is extracted from the FRF measurements. This weighting matrix would be the mass matrix in the typical analytical case of proportional viscous damping. However, since no assumptions have been made on the nature of the underlying analytical model, the reciprocal modal vector is independent of discretization uncertainties and other invalid assumptions associated with an analytical model. Instead, the reliability of the reciprocal modal vectors should be affected by inaccuracies in the estimated model and the FRF measurements.<sup>[1]</sup>

In addition to this inner product matrix, referred to as the orthogonality indicator matrix, the reciprocal modal vectors provide a means for “decoupling” the original FRF matrix and/or other measurement matrices. In the case of the original FRF matrix, one should expect this decoupling to produce functions resembling single-degree-of-freedom (SDOF) FRF plots. This decoupled FRF is analogous to the enhanced FRF technique.<sup>[5]</sup> In the case of operating data from the same (time-invariant) system, one should expect to see the forced response of each particular mode due to whatever forcing function is acting on the system.

The primary goal of this work is mostly directed toward observing the modal state responses in the presence of unknown, possibly closed loop forcing functions, thus having an impact on both operating data analysis techniques

and independent modal space control techniques. Specifically, this study looks at the decoupling of certain baseline (or open loop) FRF matrices and also the decoupling of FRF matrices corresponding to systems that are perturbed from the baseline (or, equivalently, subject to unmeasured closed loop forcing functions). It is hoped that this work will contribute to the eventual implementation of a practical tool for monitoring the dynamics of a structure in the presence of unknown or unmeasurable closed loop forces.

This thesis briefly outlines the theoretical development of the reciprocal modal vectors and some of its aforementioned uses, presents the results of a verification study with an analytical model, and presents the results of a study to observe the decoupling behavior with experimental data. The theoretical development is an extension of that found in the references<sup>[1,2]</sup> to accommodate multiple input frequency response data. Additional discussions on the applications of reciprocal modal vectors and modal filters can also be found in the references.<sup>[1,2,6]</sup>

## MATHEMATICAL BACKGROUND

### Reciprocal Modal Vectors

The frequency response of a linear, time-invariant reciprocal system can be represented as the triple matrix product

$$[H]_{N_o \times N_i} = [\Phi]_{N_o \times 2N} \left[ \frac{Q_r}{j\omega - \lambda_r} \right]_{2N \times 2N} [L]_{2N \times N_i}^T \quad (1)$$

where the  $r^{th}$  row of  $[L]^T$  represents a subset of the mode shape coefficients for mode  $r$  corresponding to the input points and where the center matrix is diagonal. Only the center matrix is a function of frequency. It is assumed in this discussion that the frequency response function matrix  $[H]$  and corresponding estimates of the modal parameters ( $\{\phi\}$ ,  $Q_r$ , and  $\lambda_r$ ) are available. By observing that the roots of the system appear in complex conjugate pairs, the above equation can be rewritten as

$$[H]_{N_o \times N_i} = [\Phi]_{N_o \times N} \left[ \frac{Q_r}{j\omega - \lambda_r} \right]_{N \times N} [L]_{N \times N_i}^T + [\Phi^*]_{N_o \times N} \left[ \frac{Q_r^*}{j\omega - \lambda_r^*} \right]_{N \times N} [L^*]_{N \times N_i}^T \quad (2)$$

This equation is a matrix version of the more familiar partial fraction expansion of the frequency response matrix. The  $N$  scaled outer products  $\{\phi\}Q_r\{l\}^T$  and their complex conjugates comprise the residue matrices for each of the  $r$  modes in the system. The columns  $\{\phi\}$  of the matrix  $[\Phi]$  are the mode shapes of the system. The matrix dimensions will henceforth be excluded from the mathematical notation for brevity. The  $r^{th}$  reciprocal modal vector  $\{\Psi\}$  is defined as<sup>[1,2]</sup>

$$\{\Psi\}_r^T \{\phi\}_s = \delta_{rs} \quad (3)$$

where  $\delta_{rs}$  is unity if  $r$  is equal to  $s$  and zero otherwise. Inspection of equation (3) infers that our solution for the set of  $N$  reciprocal modal vectors is found quickly via the pseudoinverse on the modal matrix. However, while the pseudoinverse may indeed be a useful solution procedure, errors in the estimated mode shapes will be propagated and no mechanism exists to account for modes that may be active within a particular frequency range but for some reason has not been included in the modal matrix (such as rigid body modes and modes that resonate just outside the frequency range considered). Thus, it is desirable to find a solution approach that considers these facts.

If the inner product of the  $r^{th}$  modal vector is formed with equation (2) and utilizing the orthogonality property of equation (3), the emergence of a decoupling action can be observed:

$$\{\Psi\}_r^T [H] = \frac{Q_r}{j\omega - \lambda_r} \{l\}_r^T + \{\Psi\}_r^T \{\phi\}_r^* \frac{Q_r^*}{j\omega - \lambda_r^*} \{l\}_r^{T*} \quad (4)$$

Note that there remains in the equation a contribution from the complex conjugate root. Equation (4) is easily rearranged and transposed so that it can be expressed equivalently as

$$\left[ [H]^T - \frac{Q_r^*}{j\omega - \lambda_r^*} \{l\}_r^* \{\phi\}_r^{*T} \right] \{\Psi\}_r = \frac{Q_r}{j\omega - \lambda_r} \{l\}_r \quad (5)$$

which is of the form shown in equation (6).

$$[A(\omega_i)] \{\Psi\}_r = \{b(\omega_i)\}_r \quad (6)$$

Equation (5) is a fundamental equation that relates the reciprocal modal vector to the modal vectors through the FRF matrix. Assuming that both a modal model and a corresponding frequency response function database exist, equation (6) can be written for several spectral lines (for each mode) such that an overdetermined solution for the  $r^{th}$  reciprocal modal vector is formed:

$$\begin{bmatrix} [A(\omega_1)] \\ [A(\omega_2)] \\ \vdots \\ [A(\omega_k)] \end{bmatrix}_r \{\Psi\}_r = \begin{Bmatrix} \{b(\omega_1)\} \\ \{b(\omega_2)\} \\ \vdots \\ \{b(\omega_k)\} \end{Bmatrix}_r \quad (7)$$

From which the solution is clearly

$$\{\Psi\}_r = \begin{bmatrix} [A(\omega_1)] \\ [A(\omega_2)] \\ \vdots \\ [A(\omega_k)] \end{bmatrix}_r^\dagger \begin{Bmatrix} \{b(\omega_1)\} \\ \{b(\omega_2)\} \\ \vdots \\ \{b(\omega_k)\} \end{Bmatrix}_r \quad (8)$$

Several observations can be made from equation (7). First, one would expect different results depending on which spectral lines were included in the solution. In fact, one should intuitively expect the reciprocal modal vector to be orthogonal only to modes that have significant response within the spectral lines included in the computation. Second, in real applications, the dimensions of the solution can become relatively large, possibly pushing computational requirements beyond what is considered practical. Reference 2 discusses a recursive least squares version of equation (7) which can be used in order to speed solution time if necessary.

The orthogonality of the modes can now be checked by calculating the orthogonality indicator matrix, which is the inner product of the reciprocal modal matrix and the modal matrix

$$[E] = [\{\Psi_1\}\{\Psi_2\}\dots\{\Psi_N\}]^T [\{\phi_1\}\{\phi_2\}\dots\{\phi_N\}] \quad (9)$$

For a high fidelity modal model, one would expect the orthogonality indicator matrix to closely approximate the identity matrix. When this is not the case, this matrix offers some insight into which modes (or which reciprocal modal vectors) are poor estimates.<sup>[2]</sup>

## Decoupled Frequency Response

In addition to measuring modal model validity via the orthogonality indicator matrix, reciprocal modal vectors are useful for other things as well. One application is the decoupled FRF. The decoupled FRF is analogous to the enhanced FRF used in the complex mode indicator function<sup>[5,7]</sup> and is essentially a spatial filter that uncouples the FRF matrix into its constitutive single-mode response functions. The fundamental distinction is that the reciprocal modal vectors contain the effects of the weighting matrix which may be merely the mass matrix or more generally linear combinations of the [M], [C], and [K] matrices.

The expression for the decoupled FRF can be found by postmultiplying equation (4) by an appropriate weighting vector for the columns of [H]. By first considering [H] to be square it becomes apparent that the reciprocal vector would be an appropriate choice. It may not, however, be the optimum choice when dealing with a non-square measurement matrix [H]. Nevertheless, for the typical case of  $N_i$  inputs, a subset of the reciprocal vector corresponding to the input points will be denoted with a "tilde" overscore. Thus equation 10

$$\{\Psi\}_r^T [H] \{\tilde{\Psi}\}_r = \frac{Q_r \left( \{l\}_r^T \{\tilde{\Psi}\}_r \right)}{j\omega - \lambda_r} + \frac{Q_r^* \left( \{\Psi\}_r^T \{\phi\}_r^* \right) \left( \{l\}_r^{T*} \{\tilde{\Psi}\}_r \right)}{j\omega - \lambda_r^*} \quad (10)$$

is an appropriate expression for the decoupled FRF. Note that this is clearly proportional to the  $r^{th}$  modal coordinate. The second term on the right hand side represents the contribution of the complex conjugate pole. Also note that several other versions of a decoupled FRF can be derived by rearranging the equation or postmultiplying by a different choice of vector. In addition, the  $r^{th}$  modal coordinate that is extracted is unique only to within some complex scalar depending on both the chosen scaling and the number of columns in the FRF matrix.

### Decoupled Operating Data

The decoupling effect of the reciprocal modal vectors is not limited to the FRF matrix used in its calculation. The decoupling of outputs irrespective of the inputs can be investigated by considering the input-output relationship for a linear time-invariant system, commonly written as

$$\{x\} = [H]\{f\} \quad (11)$$

By premultiplying by a particular reciprocal modal vector and substituting equation (4), equation (12) can be formulated.

$$\{\Psi\}_r^T \{x(\omega)\} = \frac{Q_r \left( \{l\}_r^T \{f(\omega)\} \right)}{j\omega - \lambda_r} + \frac{Q_r^* \left( \{\Psi\}_r^T \{\phi\}_r^* \right) \left( \{l\}_r^{T*} \{f(\omega)\} \right)}{j\omega - \lambda_r^*} \quad (12)$$

Equation (12) indicates that the reciprocal modal vector also provides the necessary linear combination of the outputs that yield the response of the  $r^{th}$  mode to the inputs, whatever they happen to be. Thus, the reciprocal modal vector clearly provides a transformation from the physical space to the modal space for operating data. Moreover, even though the mathematics have been worked out in the frequency domain, this decoupling action should also be observed if  $\{x\}$  is observed in the time domain.

In practice,  $\{x(\omega)\}$  may not be available. Instead,  $\{x(\omega)\}$  is replaced by a column of the output spectral density matrix  $G_{xx}$ . In this case the output vector must be amplitude-corrected at each frequency with the element corresponding to the chosen column of  $G_{xx}$ . In other words, a column of  $G_{xx}$  is  $\{x(\omega)\}x_q(\omega)^*$  where  $x_q(\omega)$  is the response of the  $q^{th}$  reference variable. In this case  $x_q(\omega)$  (which is complex in general) cannot be found but the magnitude from the  $q^{th}$  entry of the  $q^{th}$  column of  $G_{xx}$  can be determined.

The application of the reciprocal modal vector to decoupling operating data is interesting because it implies that one should be able to observe a particular mode from a set of sensors independently from other modes without knowledge of, or restrictions on, the excitation forces driving the system. This makes sense even if the excitation is closed loop, causing a shift in the apparent frequency and/or damping of the mode. However, it is not guaranteed that the response of the  $r^{th}$  mode to open or closed loop excitation will always resemble a single mode response.

## APPLICATIONS

This section outlines both the results of an analytical study performed to verify that the reciprocal modal vectors decouple the FRF matrix and an experimental study to investigate the performance of the reciprocal vectors with

realistic data. Both cases utilized software written by the author that operates from within the Structural Dynamics Research Laboratory's MODAL software package.

Except where noted, little attention was paid to the orthogonality indicator matrix. This is because the main interest in these studies involved frequency domain behavior of the decoupled frequency responses. Insufficient experience exists to interpret detailed meaning from the indicator matrix with respect to frequency domain performance.

## **ANALYTICAL SYSTEM APPLICATION**

### **Objectives and Procedure**

A six-degree-of-freedom proportionally damped system was used to verify that the reciprocal modal vectors actually decouple the frequency response matrix. A full FRF database (all six columns) was generated so that a variety of reference sets, including single reference FRF matrices could be considered. No noise was added to the synthesized frequency responses. The [M], [C], and [K] matrices for the (baseline) model are shown in figure 1 and a plot of a typical synthesized FRF is shown in figure 2.

In addition, similar frequency response function matrices were generated for four "perturbed" systems. The FRF matrices were processed with reciprocal vectors from the baseline system in an attempt to provide insight to their performance under varying degrees of changes to the system. The perturbed systems that were considered are summarized as follows:

- Mass matrix modification: 10 percent increase in 1 mass (1,1 position)
- Mass matrix modification: 50 percent increase in 1 mass (1,1 position)
- Mass matrix modification: 90 percent decrease in all masses
- Stiffness matrix modification: 900 percent increase in all matrix elements

The first two perturbed systems were similar to the baseline system in every respect except for the magnitude of the mass in the (1,1) position, which was increased by 10 percent and 50 percent respectively. The intent of this exercise was to observe the behavior of the baseline reciprocal modal vectors with a perturbed system that has modified mode shapes. Modifications (3) and (4) result in significant changes in modal frequency and damping values but leave the mode shapes unchanged relative to the baseline system.

Another way of viewing the first two perturbed systems is to view them as the baseline system with closed loop forcing functions applied at the first degree of freedom. The closed loop forcing function is a pure inertial force and can be considered unmeasured. The idea is to view the FRF matrices of the perturbed systems as closed loop frequency responses due to some unknown closed loop control.

There were several objectives of the analytical study, which can be summarized as follows:

Investigate sensitivity of RMV decoupling performance (baseline measurements only) to choice of reference (column of FRF matrix).

Investigate degradation in performance when system is spatially undersampled.

Investigate decoupling performance when system is perturbed from the baseline.

### **Analytical System Results and Discussion**

The results of calculating the reciprocal modal vectors with various spectral lines (see equation (8)) and various references indicated that the calculation was insensitive to which spectral lines were chosen or which references

(columns of the full FRF matrix) were used - the reciprocal vectors consistently yielded satisfactory results (this would not be expected with realistic or otherwise noisy data). However, orthogonality was violated as soon as less than six-degrees-of-freedom were included in the calculation.

Figure 3 shows the decoupled FRFs for the six modes when the mode shapes were scaled to unity modal scaling factor, clearly indicating perfect decoupling of the FRF matrix. This result was verified in the orthogonality indicator matrix for these reciprocal vectors, which closely approximates the identity matrix—the sum of the magnitudes of all off-diagonal entries was less than  $1.0E-6$ .

To emphasize the significance of the orthogonality indicator matrix in another way, the modal assurance criterion (MAC) provides a measure of the linear relationship between vectors of equal length.<sup>[8]</sup> Table 1 shows a standard MAC calculation between the calculated mode shapes and the corresponding reciprocal modal vectors used to decouple the FRF matrix as mentioned above. It shows that the MAC values between two different modal vectors or two different reciprocal modal vectors are small yet non-zero. More importantly, it also shows that the MAC “submatrix” between modal vectors and reciprocal modal vectors is diagonal. This submatrix is essentially the same as the orthogonality indicator matrix. This is significant because it shows how the MAC calculation can be used as an orthogonality check between modes by comparing each mode with the set of reciprocal modes.

While considering all six output degrees of freedom (DOF) resulted in perfect decoupling, removing a DOF from the calculation resulted in decoupled responses that did not resemble single modes. This is essentially a violation of orthogonality because of spatial undersampling. This result is discussed in more detail below.

Figure 4 shows the resulting single-mode response functions for the first mode for six separate calculations, each calculation neglecting a different DOF. Figure 5 shows similar calculations for the third mode. Comparison of these two plots indicate that the effects of spatial undersampling will vary from mode to mode, depending on which DOF is neglected. Intuitively, the effects are most likely related to a particular DOFs participation in each mode.

These two figures serve to point out the fact that while undersampling can destroy the orthogonality property of the reciprocal vectors, the effects of the undersampling can vary dramatically with the choice of measurement location and the particular mode being extracted from the measurements. This may be an important consideration when one does not have the luxury of a large number of sensors and/or when dealing with a distributed parameter system. In other words, one requires the number of independent degrees of freedom to be greater than or equal to the number of modes active in the frequency range in order to identify the modes. In this analytical case, at least six independent measurements are required for orthogonality, even if one was interested in extracting the response of only a single mode.

On the other hand, these two figures show a certain amount of robustness in the decoupling effect even when the outputs were undersampled. Specifically, except for one of the curves in figure 5, all of the decoupled responses in the vicinity of the particular modes natural frequency overlay each other. In addition, all of the curves are dominated by the mode that was supposed to be extracted. Again, with the exception of one of the curves in figure 5, suppression of undesired modes is at least 20 dB.

A comment is in order here about how the reciprocal modal vectors were calculated. Equation (7) shows a submatrix for each spectral line with  $N_i$  rows in it. The total number of rows in the overdetermined matrix is therefore a multiple of  $N_i$ . In the implemented algorithm, the analyst specifies a number of spectral lines  $k$  which defines a bandwidth which is subsequently centered on each modal frequency. The total number of rows in the coefficient matrix, then, is  $kN$  times  $N_i$ , where  $N$  is the number of modes being considered in the calculation. Programming restrictions limited the total number of rows to about 200, which was more than adequate for the analytical system considered here. The perturbed system results discussed below utilized reciprocal vectors that were calculated from an FRF matrix with the first five of a possible six columns.

The perturbed system results for the analytical model are shown in figures 6 through 11 and in figures 12 and 13. The frequency and damping values for the baseline and perturbed systems are tabulated in table 2. Each figure cor-

responds to one of the six baseline modes. Each of these figures show 3 decoupled FRFs, each of them representing a different FRF matrix that was processed with the *same* reciprocal vector. That reciprocal vector was calculated with the baseline system mode shape and the baseline FRF matrix.

For figures 6 through 11, the three decoupled FRFs correspond to the baseline FRF matrix, the FRF matrix for the system with a 10 percent increase in the first mass element, and the FRF matrix for the system with a 50 percent increase in the first mass element. In several of these plots the curve corresponding to the 10 percent modification is almost identical to the baseline curve (the curve that looks like a single degree of freedom system). For figures 12 and 13, the baseline result is compared with the results from decreasing the mass matrix uniformly by a factor of 10 and from increasing the stiffness matrix by a factor of 10 (for only two representative modes).

The results show that the reciprocal vectors did an excellent job of decoupling the FRF matrix corresponding to the 10 percent increase in the first mass and even managed to do a reasonable job of decoupling the FRF matrix corresponding to a 50 percent increase in the first mass, with the possible exception of the apparently strong coupling that occurs between modes 4 and 5 (figs. 9 and 10). More is said about this later.

Perfect decoupling behavior was observed for the two perturbed systems which had mode shapes consistent with the baseline system. Comparisons of the baseline decoupled mode and these perturbed systems for two modes are shown in figures 12 and 13. This result indicates that the reciprocal vector performance is independent of frequency and damping of the baseline mode. In other words, these results show that the reciprocal modal vector is strictly a spatial filter that provides the correct coordinate transformation from the physical space to the modal space of the baseline system.

There are several useful interpretations for the perturbed system results that did not display ideal decoupling. Clearly the decoupling performance is directly related to accuracy of the mode shape. In the first pair of perturbed systems, the modified system has different mode shapes than the baseline system, thus altering the weighting necessary for ideal decoupling. The second pair of perturbed systems reinforce this viewpoint because they display perfect decoupling even for grossly modified frequency and damping values for each mode.

From a system modification viewpoint, where one makes the assumption that the modified modes are a linear combination of the original modes, the “side peaks” may represent the contribution of each particular baseline mode in the modes of each of the two modified systems. From this viewpoint, the 10 percent mass modification clearly has had only a minor effect on the modes of the modified system, whereas the 50 percent modification has fairly dramatically altered the mode shapes. This idea is supported by calculating the linear combination of the baseline modes that will yield each of the modes in the 50 percent perturbed system (table 3). While no definitive conclusion can be drawn from cursory inspection, there appears to be a correlation between the peak values in the plots for each mode and the rows in table 3. These results imply that reciprocal modal vectors may be of value in correlating predicted and actual effects of structural modifications. In addition, it might be possible to update the reciprocal vectors based on results similar to this such that the modified system can be decoupled.

Lastly, a closed-loop system view offers another perspective. Adding a mass to a specific degree of freedom is analogous to providing a closed loop forcing function that provides a force directly proportional to the acceleration of that degree of freedom. This forcing function naturally has its most significant components at resonant frequencies where acceleration levels are relatively high. The end result is that the response of the open loop system to closed loop forces is being observed, which does not result (in this case) in a classic single-mode response. The results of decoupling the perturbed system FRFs thus offer insight into the relationship between the modal parameters of the open and closed loop systems.

As an aside, an interesting observation was made concerning the relationship of the reciprocal modal vectors to the modal vectors. Specifically, it was noticed that the reciprocal vector is the modal vector times the mass matrix—which in this case is diagonal—times some other constant which is different for each mode. Thus, in this case at least, the weighting matrix necessary for modal orthogonality can indeed be extracted from the FRF matrix and is contained within the reciprocal vectors as previously suggested. This observation was not pursued any further.

$$M = \begin{bmatrix} 100 & 0 & 0 & 0 & 0 \\ 0 & 7 & 0 & 0 & 0 \\ 0 & 0 & 9 & 0 & 0 \\ 0 & 0 & 0 & 9 & 0 \\ 0 & 0 & 0 & 0 & 5 \\ 0 & 0 & 0 & 0 & 5 \end{bmatrix} \quad C = 0.01 * M$$

$$K = \begin{bmatrix} 260 & -100 & 0 & 0 & -50 & -10 \\ -100 & 350 & -100 & -100 & 0 & -50 \\ 0 & -100 & 180 & 0 & 0 & 0 \\ 0 & -100 & 0 & 220 & 0 & 0 \\ -50 & 0 & 0 & 0 & 60 & -10 \\ -10 & -50 & 0 & 0 & -10 & 70 \end{bmatrix}$$

Figure 1. Mass, Stiffness, and Damping matrices of Baseline Analytical System

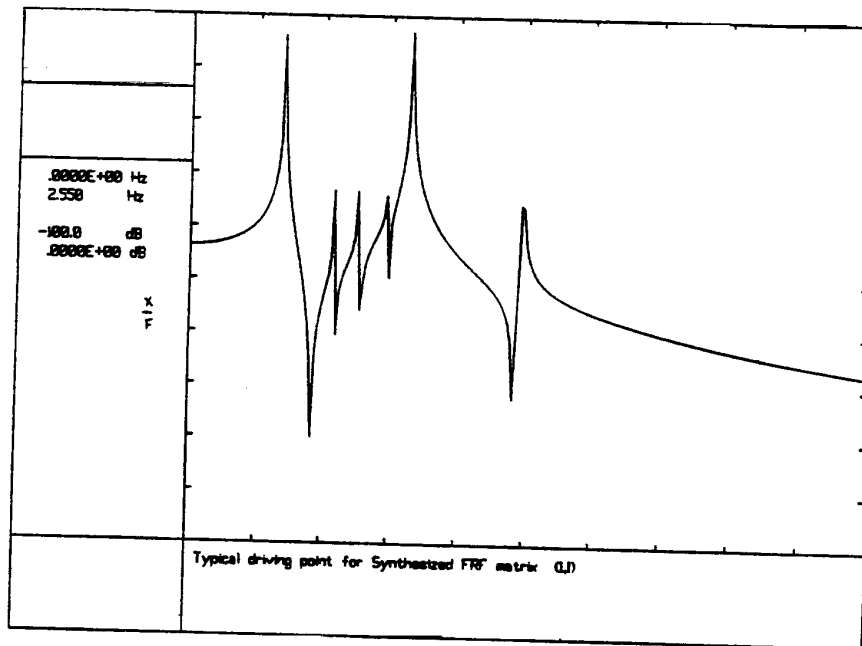


Figure 2. Typical Synthesized Frequency Response Function

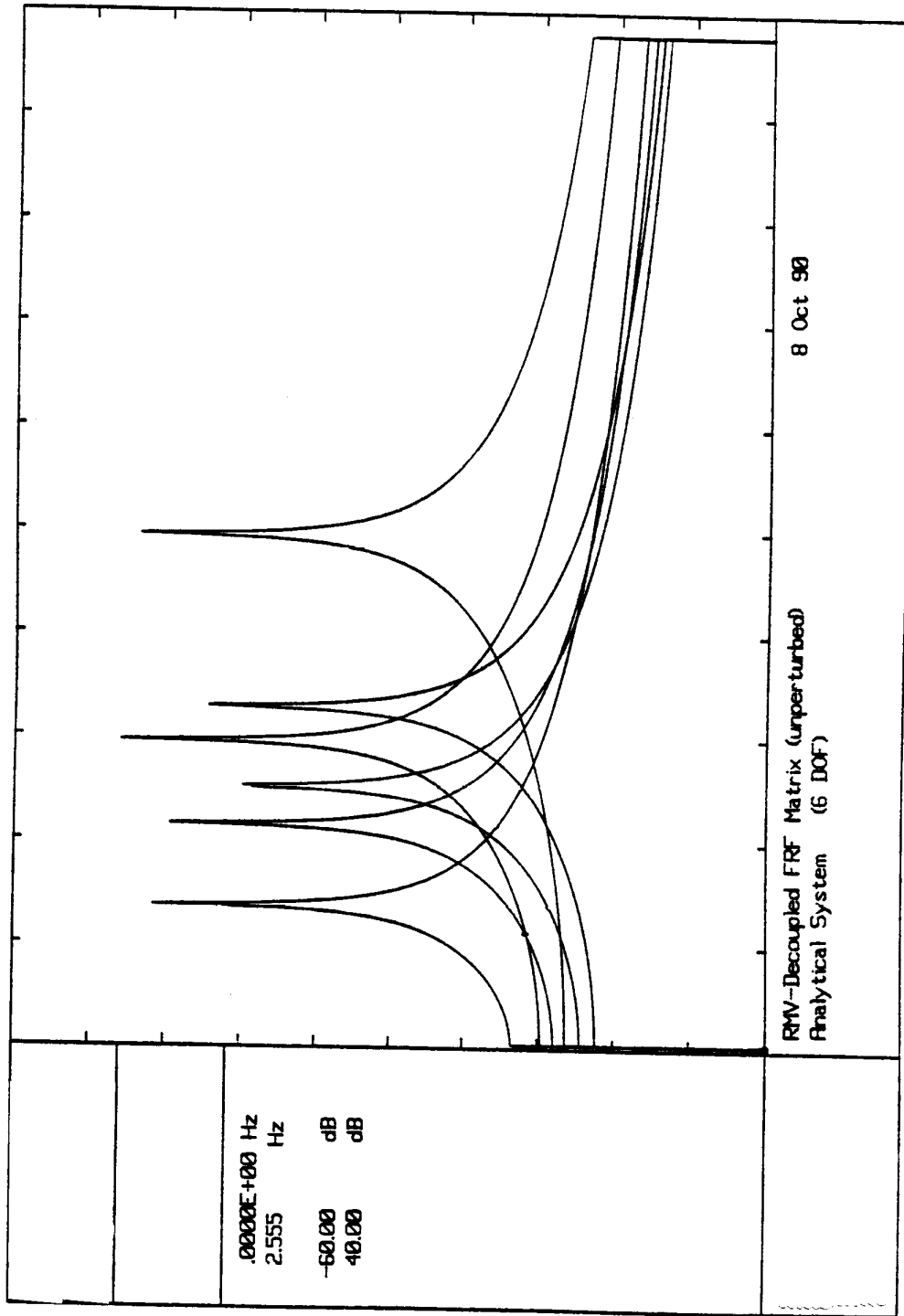


Figure 3. RMV-Decoupled Frequency Responses of Baseline Analytical System

Table 1. Modal assurance criterion matrix: analytical system.

Mode number	Modal assurance criterion											
	Modal Vectors			Reciprocal modal vectors								
	1	2	3	4	5	6	1	2	3	4	5	6
1	1.00000											
2	0.01120	1.00000										
3	0.03066	0.02696	1.00000									
4	0.00490	0.00062	0.00335	1.00000								
5	0.03209	0.02538	0.00029	0.00057	1.00000							
6	0.00201	0.00000	0.01004	0.00161	0.00167	1.00000						
1	0.91847	0.00000	0.00000	0.00000	0.00000	0.00000	1.00000					
2	0.00000	0.93386	0.00000	0.00000	0.00000	0.00000	0.01258	1.00000				
3	0.00000	0.00000	0.92172	0.00000	0.00000	0.00000	0.03785	0.03536	1.00000			
4	0.00000	0.00000	0.00000	0.99077	0.00000	0.00000	0.00328	0.00061	0.00211	1.00000		
5	0.00000	0.00000	0.00000	0.00000	0.94557	0.00000	0.02632	0.02020	0.00004	0.00004	1.00000	
6	0.00000	0.00000	0.00000	0.00000	0.00000	0.98158	0.00573	0.00033	0.01218	0.00141	0.00232	1.00000

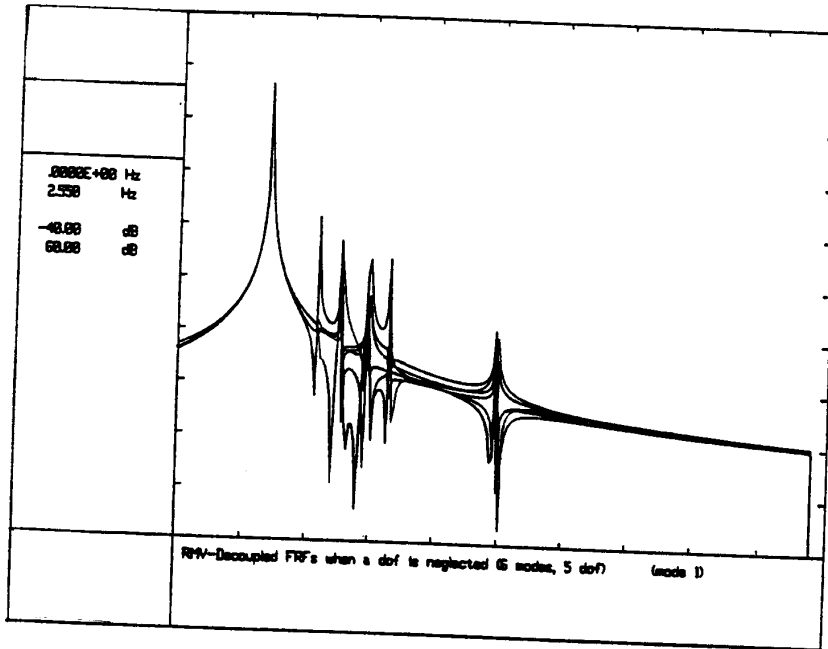


Figure 4. Effect of Spatial Undersampling for First Analytical Mode

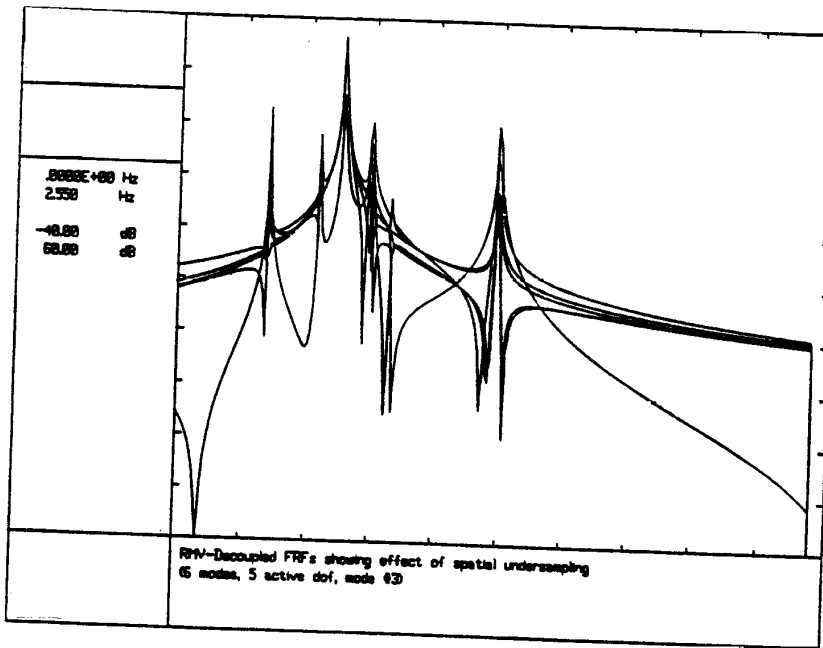


Figure 5. Effect of Spatial Undersampling for Third Analytical Mode

Table 2. Frequency and damping values for analytical systems.

Mode number	Baseline		10% perturbation		50% perturbation		[M] decreased 90%		[K] increased 900%	
	Frequency (Hz)	Damping (% critical)	Frequency (Hz)	Damping (% critical)	Frequency (Hz)	Damping (% critical)	Frequency (Hz)	Damping (% critical)	Frequency (Hz)	Damping (% critical)
1	0.351	0.227	0.348	0.225	0.335	0.215	1.109	0.718	1.109	0.072
2	0.549	0.145	0.549	0.145	0.548	0.144	1.737	0.458	1.737	0.046
3	0.643	0.124	0.642	0.124	0.637	0.121	2.032	0.392	2.032	0.039
4	0.755	0.105	0.754	0.105	0.724	0.092	2.388	0.333	2.388	0.033
5	0.839	0.095	0.813	0.092	0.765	0.101	2.652	0.300	2.652	0.030
6	1.264	0.063	1.260	0.063	1.250	0.063	3.997	0.199	3.997	0.020

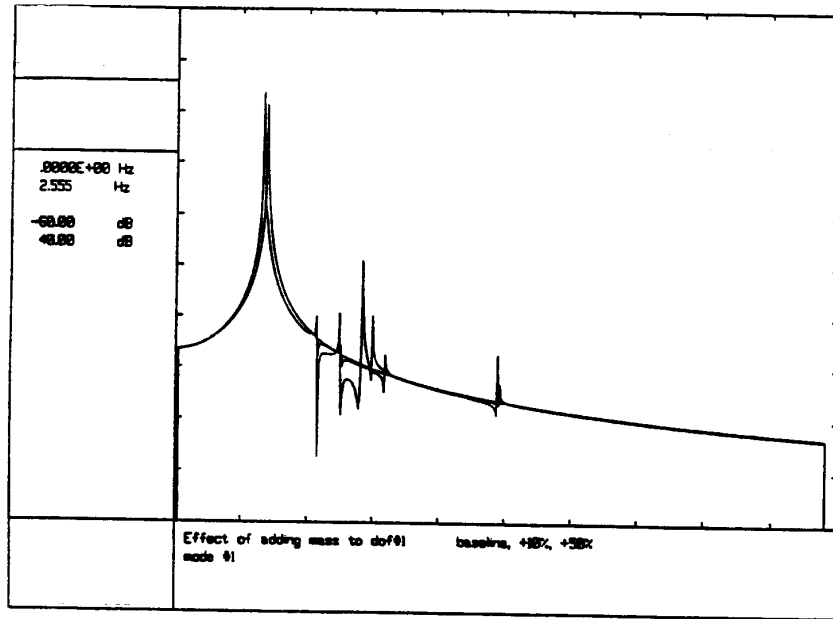


Figure 6. Effects of Perturbing Mass (1,1): Analytical Mode 1

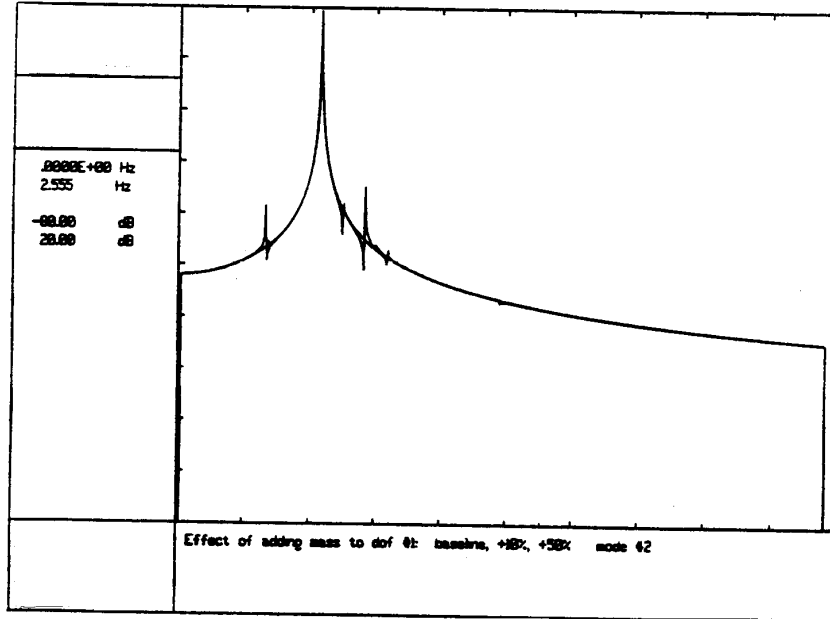


Figure 7. Effects of Perturbing Mass (1,1): Analytical Mode 2

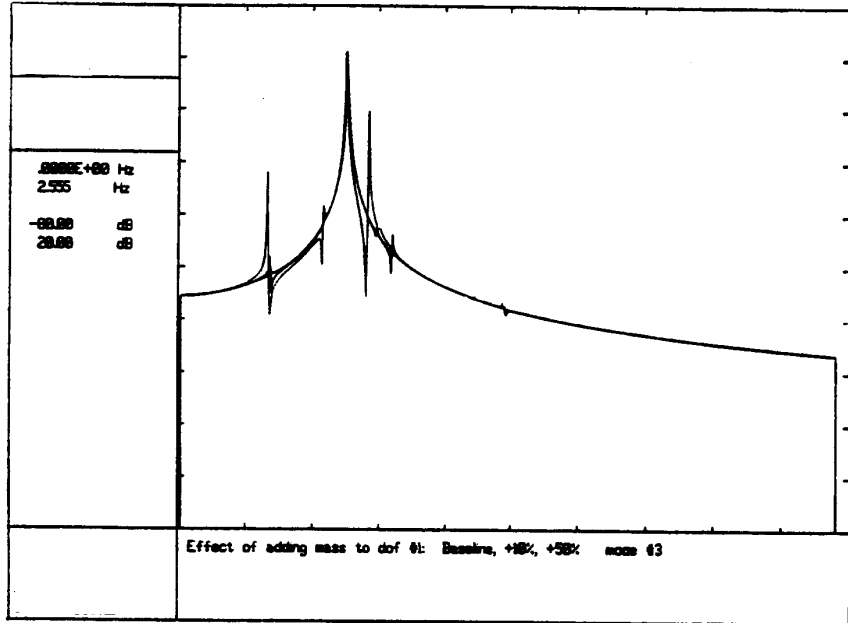


Figure 8. Effects of Perturbing Mass (1,1): Analytical Mode 3

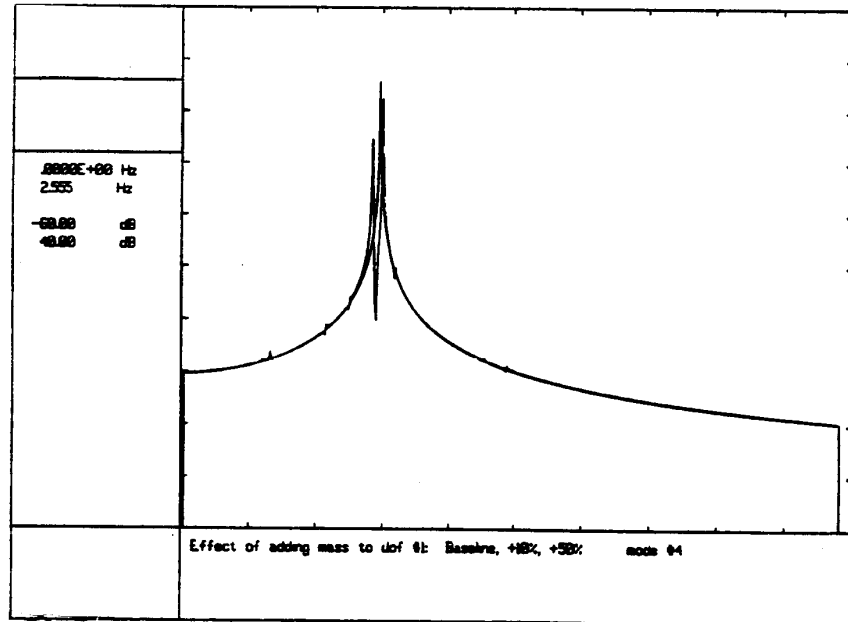


Figure 9. Effects of Perturbing Mass (1,1): Analytical Mode 4

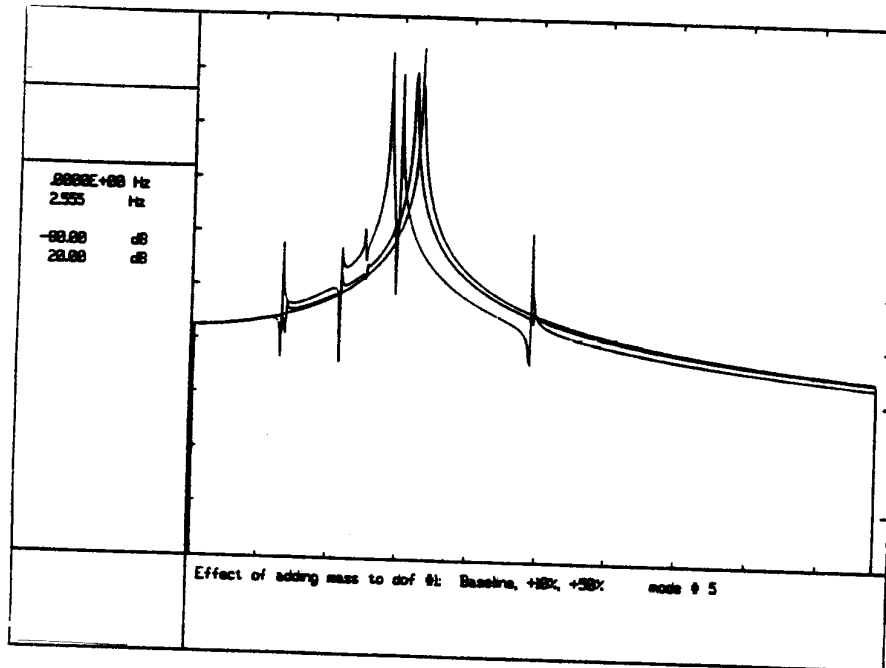


Figure 10. Effects of Perturbing Mass (1,1): Analytical Mode 5

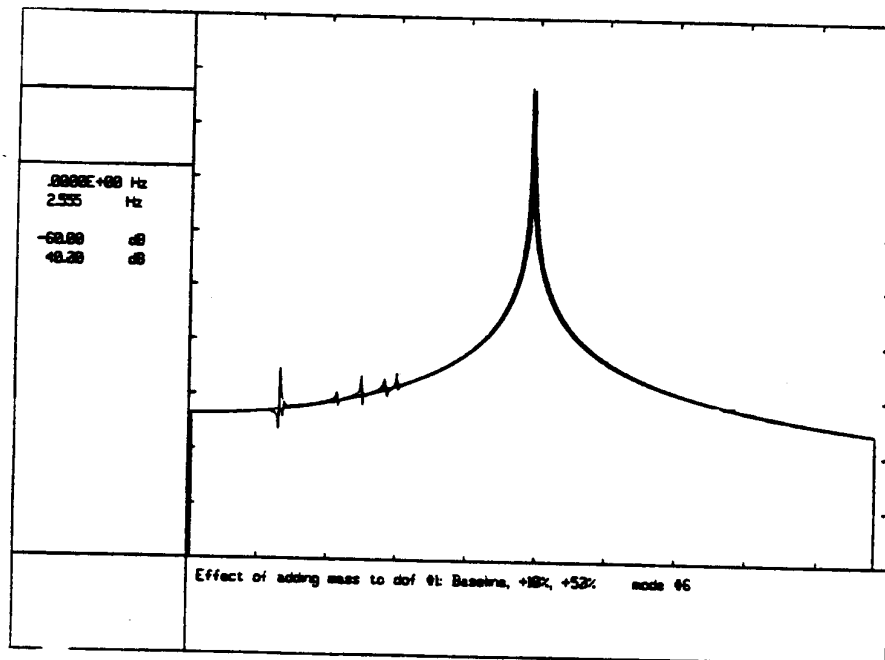


Figure 11. Effects of Perturbing Mass (1,1): Analytical Mode 6

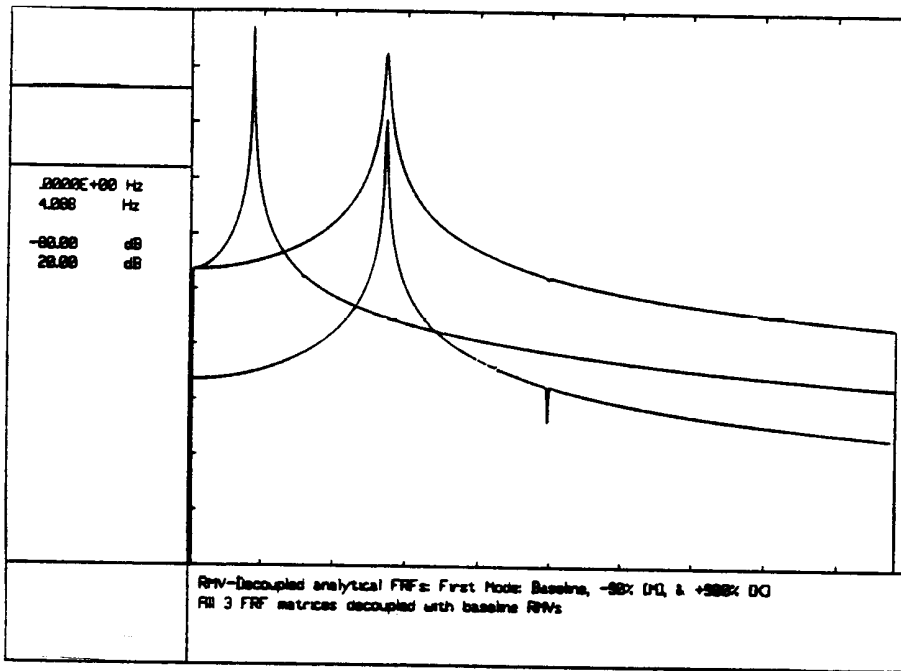


Figure 12. Decoupling Performance for Unaltered Mode Shape: Analytical Mode 1

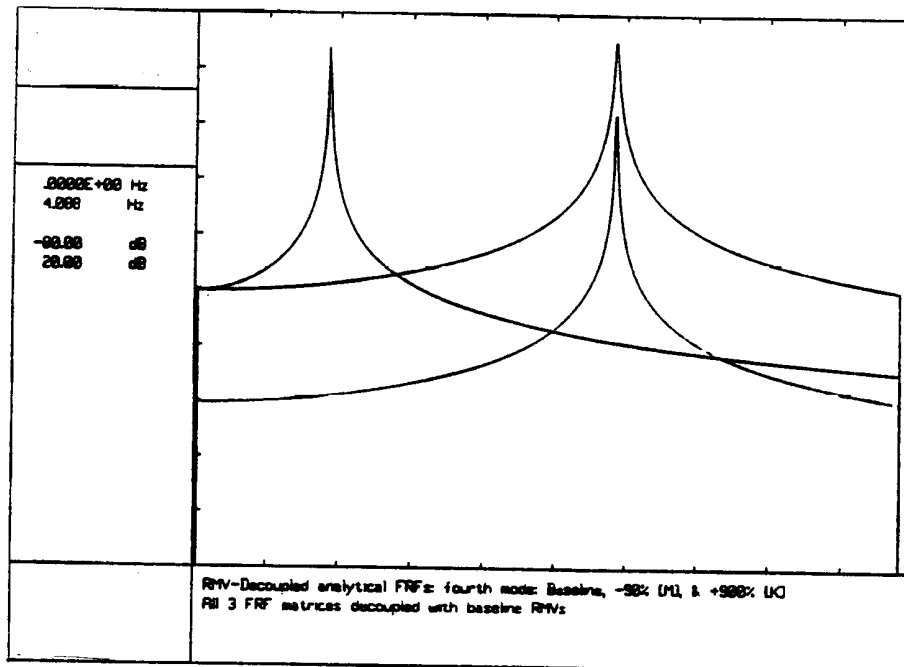


Figure 13. Decoupling Performance for Unaltered Mode Shape: Analytical Mode 4

**Table 3. Relationship between baseline and 50% mass perturbation.**

Frequency (Hz)	abs(inv([PHI_0])*[PHI_50%])					
	0.34	0.55	0.64	0.72	0.77	1.25
0.35	1.006	0.043	0.072	0.189	0.082	0.039
0.55	0.014	1.003	0.050	0.087	0.034	0.011
0.64	0.013	0.025	0.978	0.256	0.082	0.019
0.76	0.008	0.010	0.042	0.562	0.839	0.019
0.84	0.030	0.031	0.114	0.708	0.534	0.110
1.26	0.004	0.004	0.011	0.044	0.023	0.985

## EXPERIMENTAL APPLICATION

In order to investigate the performance of the reciprocal modal vectors with realistic data, a modal test of a 3-dimensional truss structure was performed and a modal model subsequently estimated from the data. In addition, time histories of the transducer outputs were collected from the baseline configuration and several discrete mass-additive modifications were made in order to observe the decoupling effects with data from perturbed systems.

The truss test structure is a plastic node and rod assembly designed to mimic some of the dynamic behavior that might be encountered with large flexible structures, such as the proposed space station, Freedom. The structure was chosen primarily because there is ongoing research with this testbed in the area of modal identification and control.<sup>[9]</sup> Figure 14 provides an overview of the test structure.

The structure contains 6 1/2-in. thick aluminum plates with provisions for mounting inertial mass actuators; four of these actuators were selectively mounted to provide different configurations representing perturbed systems. Each actuator, as used, weighed approximately 32.5 lb and provided sufficient perturbations to the mass matrix to grossly alter the baseline modal parameters. The baseline structure weight (with six aluminum plates) was approximately 186 lb. The actuators served as dead weight only—no control signals were provided to them.

### Experiment Objectives and Procedure

The main objective of the modal test and subsequent analysis was to identify the vibratory modes of the truss below 25 Hz and assess the ability of the reciprocal modal vectors to decouple frequency response data for the baseline configuration and three additional configurations (described below). In addition to overall performance, the subsequent analysis was to investigate the following:

- Sensitivity of RMV decoupling performance to choice of reference (column of FRF matrix).

- Changes in decoupling performance as the number of measurement degrees-of-freedom are reduced by reasonable amounts.

- Decoupling performance when the system is perturbed from the baseline. The perturbations consisted of bolting 32.5 lb masses to aluminum plate bulkheads. Part of this goal was to reveal the feasibility of using reciprocal vectors for tracking a particular mode when the system is subject to significant and unmeasured closed loop forcing functions, which were simulated by the attached masses.

A total of four configurations were selected for testing. The baseline configuration consisted of no attached actuator masses, while the other three configurations consisted of 1, 2, and 4 additional masses, respectively. The locations for these masses are indicated in figure 14. Frequency response data were acquired and stored for each configuration.

The modal test was a standard multiple input burst random test using three simultaneous inputs and 80 output degrees-of-freedom. A 0-25 Hz frequency range of interest was identified from previous experience as being adequate to encompass approximately the first seven flexible modes of the system. Data acquisition was accomplished using the VISTA software package from Hewlett Packard (Palo Alto, California) running on an engineering workstation from the same manufacturer. Response transducers consisted of STRUCTCEL accelerometers, each having a nominal sensitivity of one volt per g after signal conditioning. Frequency domain data involved typically 100 averages of baseband information up to 25 Hz with a frequency resolution of approximately 0.0625 Hz. The excitation burst duration was 75 percent of each time block acquired, and because sufficient response damping was observed within the time block, no data windowing was necessary.

## Modal Test Results

In general, the modal data is of relatively high quality. Driving point frequency response measurements are shown in figures 15 through 17. These figures also serve to compare the changes in the measurements to the baseline configuration. Multiple coherence plots indicated the absence of any gross signal processing errors (see fig. 18), but consistently displayed relatively poor coherence below approximately 1.0 to 2.5 Hz. This phenomena is attributable to nonlinear behavior in the elastic cords supporting the structure and the fact that the transducer performance degrades and exciter performance drops off below that frequency range. In addition, limitations in the feasible excitation level assured poor signal-to-noise ratios at low frequencies.

For the baseline configuration, a nonlinearity check was performed by exciting the structure at a representatively low level, twice that level, and three times that level. Figure 19 shows a comparison of representative low level and high level driving point measurements, which indicate that only minor nonlinearities exist. These nonlinearities are relatively insignificant, leading to the conclusion that subsequent linear parameter estimation techniques should be valid. Since the high level excitation caused sufficient structural response to raise concerns about structural integrity, the medium level excitation was used for the remainder of the testing.

In addition, reciprocity checks were used to verify both the absence of any gross calibration errors and/or the absence of any gross non-reciprocal behavior. Reciprocity is synonymous with a self-adjoint system and is one of the basic assumptions in most structural models. Two typical reciprocity checks are shown in figures 20 and 21 for the baseline system, which do not indicate any major problems although the reciprocity is clearly not perfect.

Lastly, a time invariance check was performed at the conclusion of the testing to check whether any structural changes occurred to the baseline system during the testing. Figures 22 and 23 show two before-and-after overplots of FRFs indicating only minor time dependent changes in the baseline system. The most dramatic changes occurred in the rigid body modes (explainable by intentional alterations of the elastic support system) and a mode around 22 Hz.

Modal parameters were estimated from the baseline data using the complex mode indicator function technique.<sup>[7]</sup> This technique is extremely easy to use and provides excellent results in the presence of low modal coupling. An attempt was made to estimate the rigid body modes as well as the flexible modes to see if the rigid body modes could also be decoupled from the measurements. A total of 12 modes were identified from the baseline data and are described in table 4.

## Perturbed System Analysis Results and Discussion

The reciprocal modal vectors did a very good job of decoupling the baseline FRF matrix, as can be seen in figure 24, which shows the resulting single mode response functions for seven of the eight flexible modes (all modes are shown in subsequent plots). The overall decoupling performance for the rigid body modes was only fair, and improved performance would be expected with better estimates of those modes.

The default set of calculation parameters for the reciprocal vectors consisted of all 80-degrees-of-freedom active using FRF data from all three references. All modal frequencies were considered in the calculation. As previously mentioned, programming limitations prevented an arbitrarily large number of rows in the solution matrix. Consequently, the default number of spectral lines per mode was 5 (15 if each reference is considered separately), resulting in a solution matrix with 180 rows.

In general, sensitivity of decoupling performance to the choice of reference FRF information varied from mode to mode. Decreasing the number of degrees-of-freedom tended to reduce the variance in the decoupled FRF plots for both the baseline and perturbed system data. Lastly, comparison of decoupled FRFs of the perturbed systems with the corresponding perturbed system mode shapes verified that the reciprocal modal vectors can do a good job

of tracking the  $r^{th}$  modal coordinate provided the perturbed system mode shape is not severely altered from the baseline system. The details of these results are discussed below.

Figures 25 through 36 show the decoupling of the baseline FRF matrix for each mode for 4 different choices of reference input information (i.e., four combinations of columns of the FRF matrix were considered). The first of these choices was all available columns used simultaneously and the other three choices were each of the three available columns considered separately. This means that the reciprocal vectors were calculated in this case using either multiple reference (all three) data or single reference data. In addition, a reciprocal vector that was calculated using only one reference only operated on the frequency responses for that reference. This is important because it explains why these plots display significantly different amplitudes for different references (and why the decoupled response for all three references together is always greater than the other three).

At least two observations deserve mention for the baseline FRF plots. First, some references clearly outperform others for individual modes, especially for the rigid body modes. For example, figure 26 shows the second rigid body mode (rigid body roll). In this case one of the exciters (17y) has unacceptable results while the same reference is the best performer for the sixth mode, shown in figure 30. Also, some modes appeared to be sensitive to the choice of reference while others did not (e.g., fig. 32 versus fig. 33). Secondly, the decoupling effect for the baseline FRFs is, in general, excellent, as evidenced by inspection of figure 24. Note that this figure contains only the flexible modes dominated by motion in the x-y plane. The last mode is spatially orthogonal to the excitation and therefore is not generally considered one of the modes targeted for detailed study although figure 36 indicates that reasonably acceptable decoupling was achieved for the baseline data.

These results agree with the intuitive notion that a reference which excites a mode fairly well will also decouple it fairly well. The comparison of these plots, however, provide a slightly more quantitative measure of how well the mode can be decoupled.

The plots just discussed all utilized the full 80-DOF experimental model. Figures 37 through 41 show the baseline decoupling performance as the number of degrees of freedom are reduced for the rigid body modes and the first flexible mode. All other flexible modes showed results similar to figure 41, and have thus been omitted for brevity.

In these figures, both 40-DOF and 20-DOF results are compared with the 80-DOF baseline. In all cases, all three references were active. Selection of which subset of the 80-DOF to use was somewhat arbitrary. The 40-DOF case corresponded roughly to dividing the structure down the YZ-plane centerline and considering only the +X side (except all driving points were retained). The 20-DOF case was a subset of the 40-DOF set and arbitrarily took every other point (and turned off all z-direction DOFs).

The most striking observation for these plots is the improved performance one can get by *reducing* the number of DOF. While one might typically think that more DOF would produce better results, this observation indicates that less DOF may have certain advantages. Specifically, the curves corresponding to less DOF have a tendency to be smoother than the curves using more DOF. However, the reduced variance is more likely attributable to the fact that the least squares solutions for each of the three sets of reciprocal vectors maintained roughly the same number of rows in the solution matrix (see eq. (7)). This means that the solution for the 20-DOF case was four times more overdetermined than the 80-DOF case. Similar results were obtained when the reciprocal vectors were used to decouple the FRF databases for the perturbed systems. An example of this is given in figure 42, showing the effect of the number of DOF for the configuration with only one mass added for the second flexible mode. The baseline curve for this mode is included in this plot for comparison.

The ability of the baseline reciprocal modal vectors to decouple each of the three perturbed system FRF matrices is shown for the flexible modes only in figures 43 through 50. Each figure contains the results of decoupling four FRF matrices with the same reciprocal modal vector (from the baseline system). Each plot shows the modal coordinate response for a particular baseline mode as extracted from each of the four available FRF matrices (baseline, 1 mass,

2 masses, and 4 masses attached respectively). The default calculation parameters were used for these reciprocal vectors (80-DOF, all three references, 5 spectral lines surrounding each mode).

In general, the addition of the masses resulted in significant alterations in all of the modal parameters, including the mode shapes. The resulting responses of the open loop modal coordinates do not, therefore, resemble single DOF systems in general. However, there are important observations relative to objective #3 that merit discussion. Specifically, the decoupled FRFs provide valuable information on a particular baseline mode in the presence of unmeasured closed loop forces. This information includes closed loop eigenvalues and some indication of relative changes in the closed loop eigenvector (mode shape).

In order to verify these observations, two baseline modes were chosen and compared with mode shapes estimated from the perturbed FRF matrices. The hypothesis to be tested suggested that if the decoupled FRF of a perturbed system reasonably approximated a single DOF system, then the mode shape of the perturbed system closely resembled the baseline mode and the modal frequency shifted to the frequency indicated by the decoupled FRF. Conversely, if the decoupled FRF of the perturbed system did not resemble a single DOF system, then the mode shapes of the perturbed system whose frequencies correspond to peaks in the decoupled FRF will contain a certain amount of motion resembling the baseline mode being considered.

The two modes chosen were first lateral bending mode (mode #5) and the mode dominated by lateral bending of the upper mast and crossarm of the truss (mode #9). Figures 43 and 47, respectively, are the corresponding decoupled FRFs that will be part of the discussion below. These two modes were chosen because the extracted modal coordinates displayed relatively simple behavior in the perturbed systems.

In addition, the upper mast/crossarm bending mode displayed the interesting behavior of both an almost negligible effect from one added mass and a significant effect with two added masses before again resembling a single DOF system with four added masses.

Relevant mode shapes from the baseline and perturbed FRF databases for the first lateral bending mode are shown in figures 50 through 55. These modes correspond to the modal frequencies indicated to be the primary locations for the first lateral bending mode in each configuration as indicated in figure 43.

Comparison of the perturbed system mode shapes (figs. 52 through 56) with the baseline mode shape (fig. 51) for the first lateral bending mode indicates that the reciprocal modal vector is indeed capable of tracking a mode shape as the system is subject to unmeasured closed loop forces.

When one mass was added, the corresponding decoupled FRF (fig. 43) indicates two separate frequencies for the first mode, one at 6.5 Hz and the other at 7.2 Hz. Figures 52 and 53 show the extracted mode shapes at 6.5 and 7.2 Hz. Inspection of these figures indicates the presence of the expected shape. In fact, the almost pure lateral bending mode shown in figure 52 hinted that the original mode may not have been an accurate estimate of the true lateral bending mode shape to begin with; but other explanations of this anomaly may exist (this matter was not investigated in detail).

Figures 54 and 55 show two modes extracted from the two-mass database that contain significant lateral bending motion at 6.1 and 6.6 Hz respectively. These modes each contain both lateral and vertical bending motion. The corresponding curve in figure 43 predicts both of these frequencies, although the higher frequency mode appears as only a minor glitch in the plot. This coupling is more obvious in figure 44. Comparison of the two-mass curve in figure 42 with the corresponding curve in figure 43 leads to several possible conjectures to explain why the 6.6 Hz mode is barely discernible in figure 42, one of them being simply the relative scaling between the modes. This particular phenomenon is not well-understood.

The four-mass configuration has a mode at 5.4 Hz that is very much like the original lateral bending mode and is shown in figure 56. The fact that this mode more closely resembles the baseline mode than the two-mass configuration is reflected in the corresponding decoupled FRFs. Specifically, the four-mass configuration mode has significantly attenuated high-frequency components relative to the two-mass configuration (fig. 42).

Relevant mode shapes from the baseline and perturbed FRF databases for the upper mast/crossarm bending mode are shown in figures 57 through 60. These modes correspond to the modal frequencies indicated to be primary locations for the first lateral bending mode in each configuration as indicated in figure 47. Note that the third configuration (2 masses added) does not even closely resemble a single DOF system.

The decoupled FRF for the one-mass configuration indicates negligible changes in this mode, with a minor increase in frequency—from 17.4 Hz to 17.5 Hz. Comparison of figures 57 and 58 verify this to be true.

For the two-mass configuration, however, the decoupled FRF indicates that this mode shape essentially does not exist in the two mass configuration. Instead, the decoupled FRF indicates that this mode has been distributed among the other modes, with the baseline shape being most prominent around 14.9 Hz. The estimated mode shape from this database at 14.9 Hz can be seen to contain this mode (fig. 59), but obviously contains contributions from other baseline modes.

When all four masses are added, however, the decoupled FRF indicates that this mode is once again a mode of the system, this time at a drastically reduced frequency. Figure 60 verifies that the mode reappears at 11.1 Hz when all four masses are attached.

Table 4. Estimated modes from truss: baseline configuration.

Mode	Frequency (Hz)	Zeta (%)	Dominant motion
1	1.17	1.96	Rigid body yaw
2	1.41	1.79	Rigid body roll
3	1.74	4.09	Rigid body pitch/roll
4	2.94	3.55	Rigid body pitch
5	7.67	0.76	First lateral bending
6	8.25	1.15	First vertical bending
7	14.63	0.94	Lower mast torsion
8	15.36	1.00	Mast vertical bending
9	17.39	0.89	Upper mast/crossarm lateral bending
10	18.02	0.82	Second lateral bending
11	21.84	1.01	Upper mast torsion
12	24.67	0.86	Crossarm YZ-plane bending

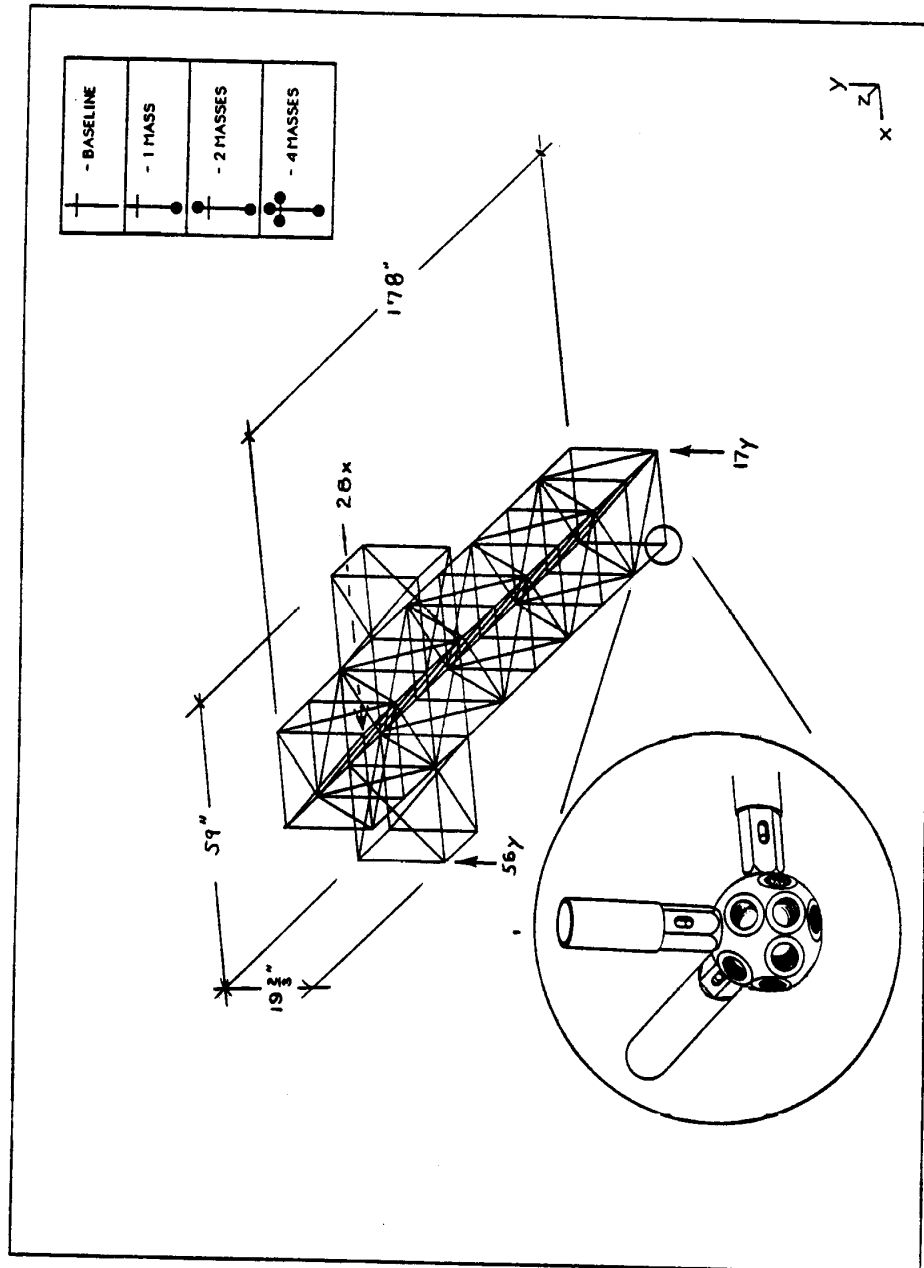


Figure 14. Truss Test Structure Overview

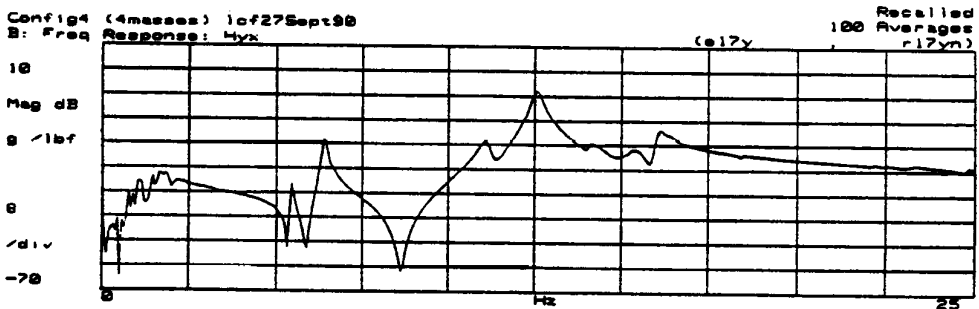
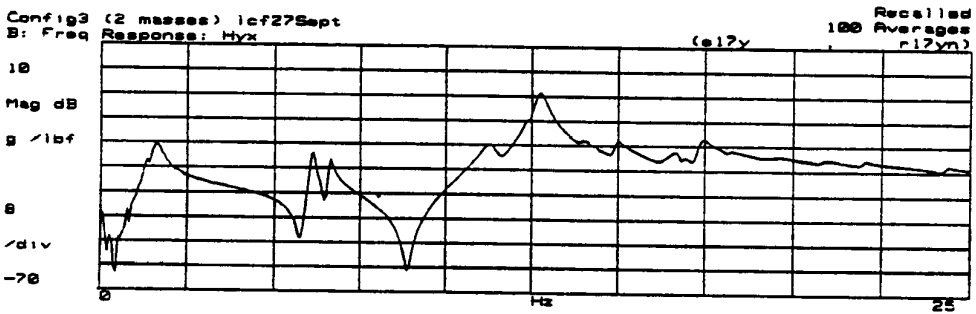
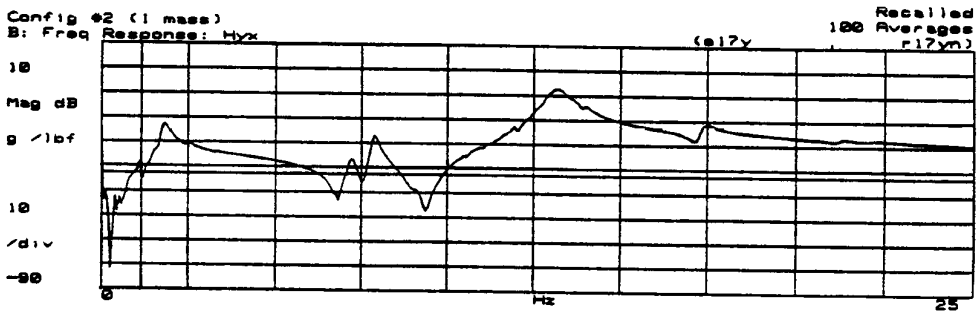
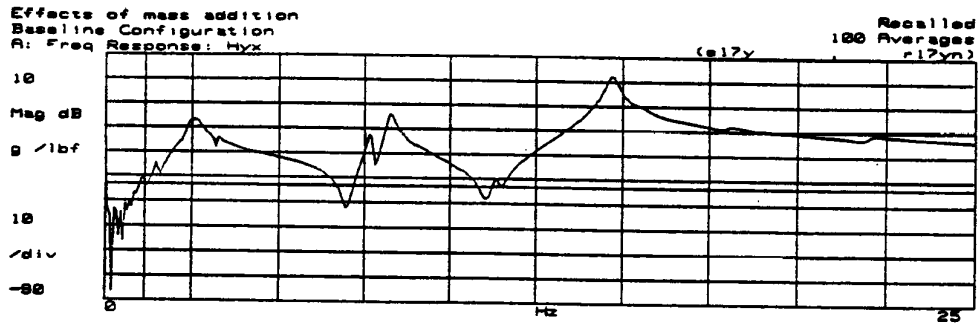


Figure 15. Driving Point Measurements (17y) for All Test Configurations

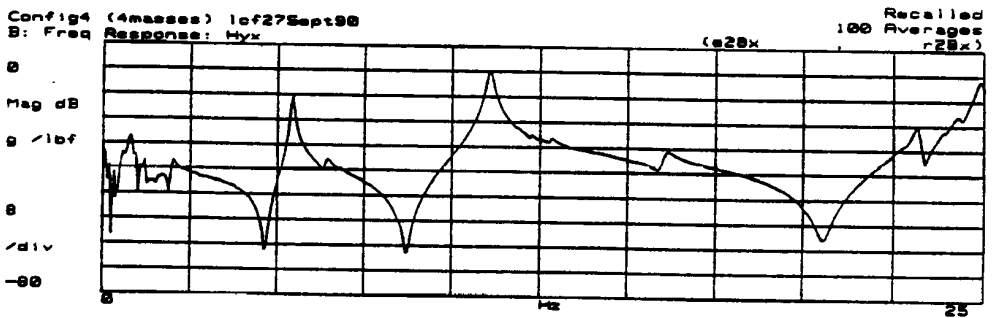
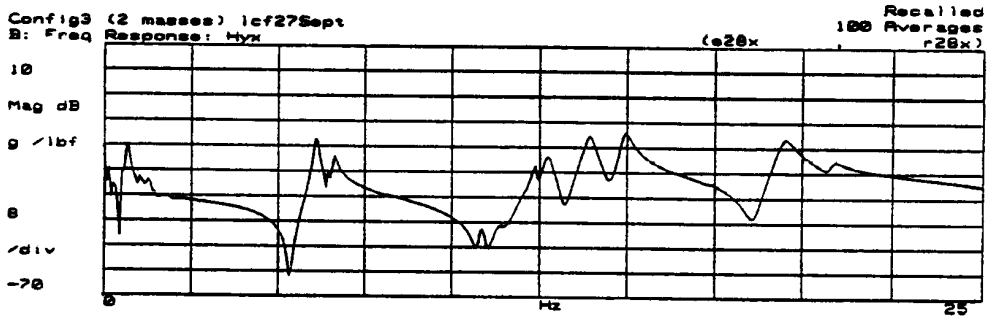
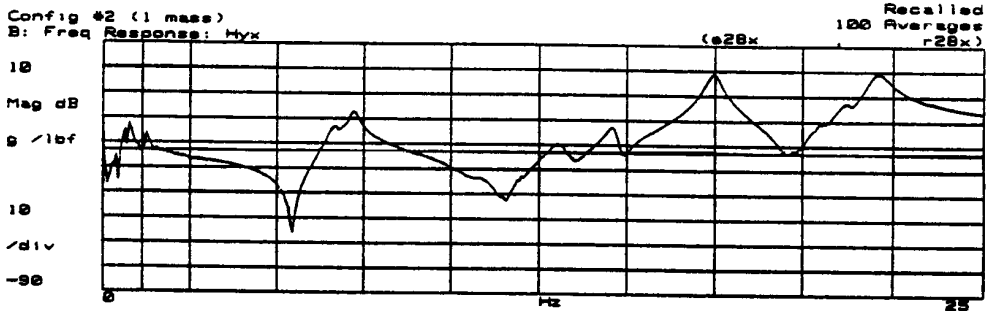
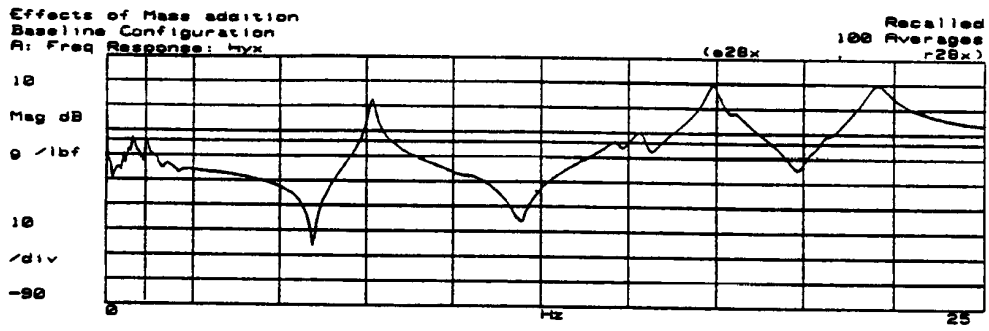


Figure 16. Driving Point Measurements (28x) for All Test Configurations

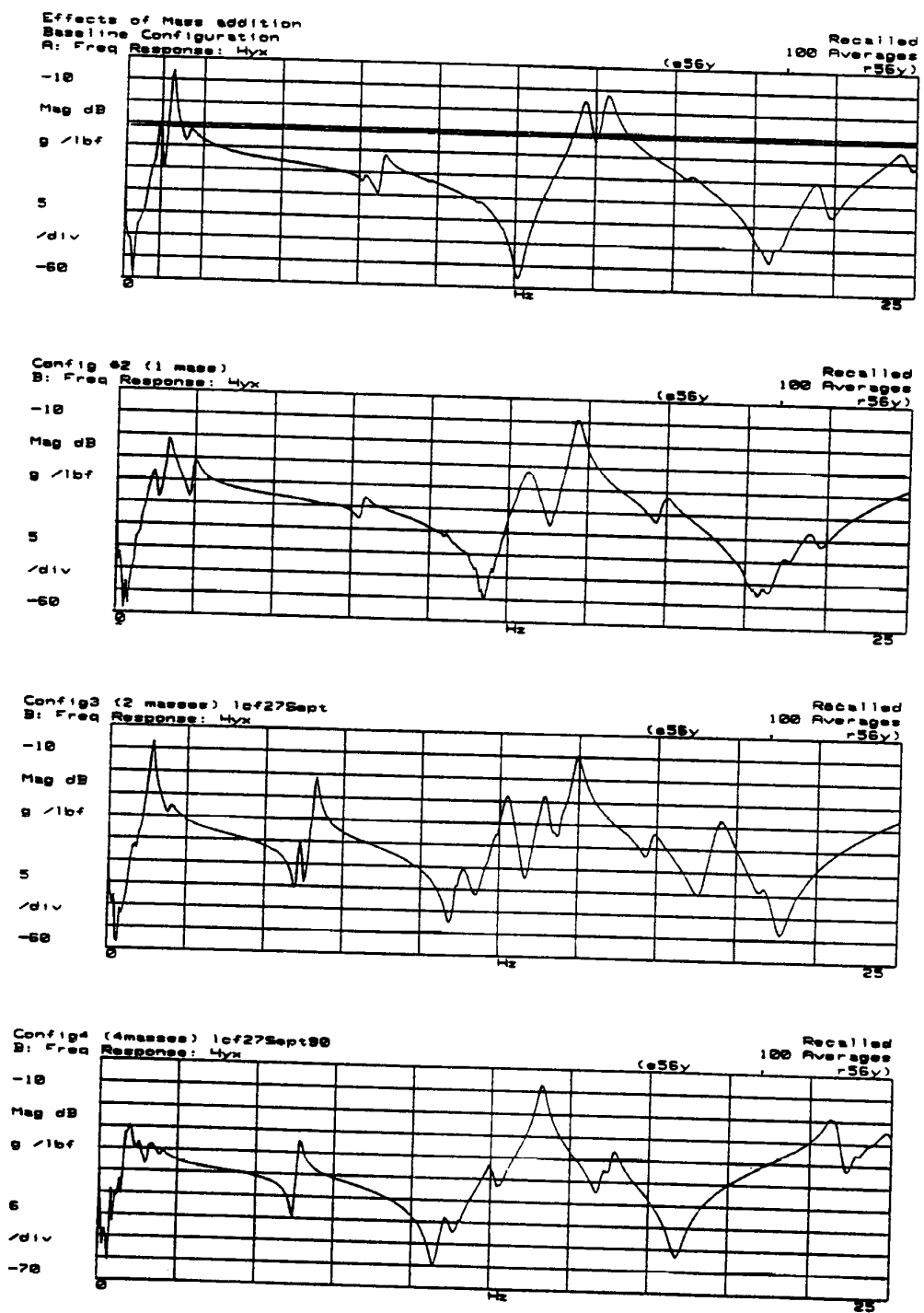


Figure 17. Driving Point Measurements (56y) for All Test Configurations

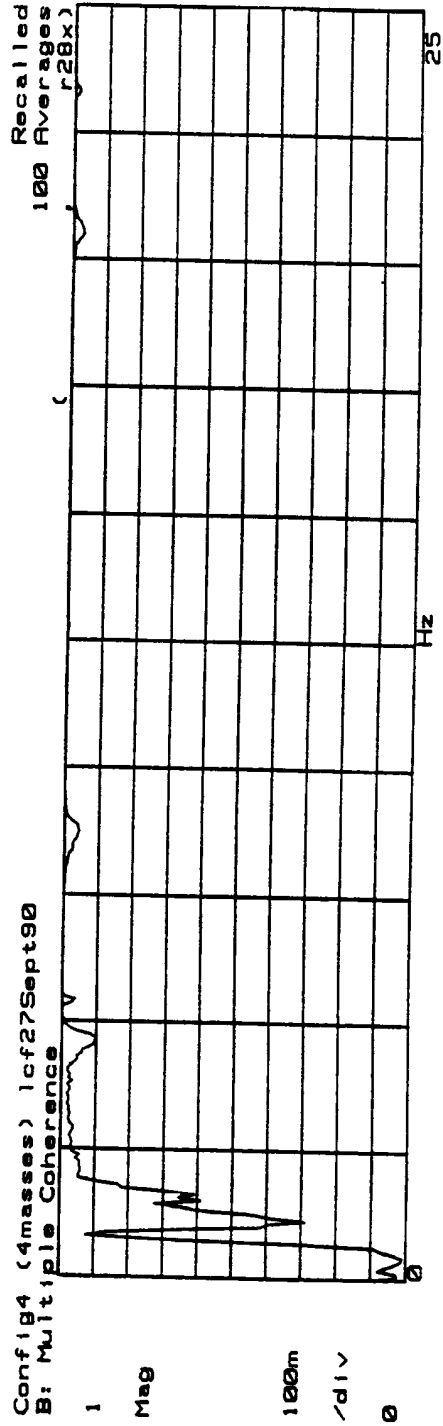
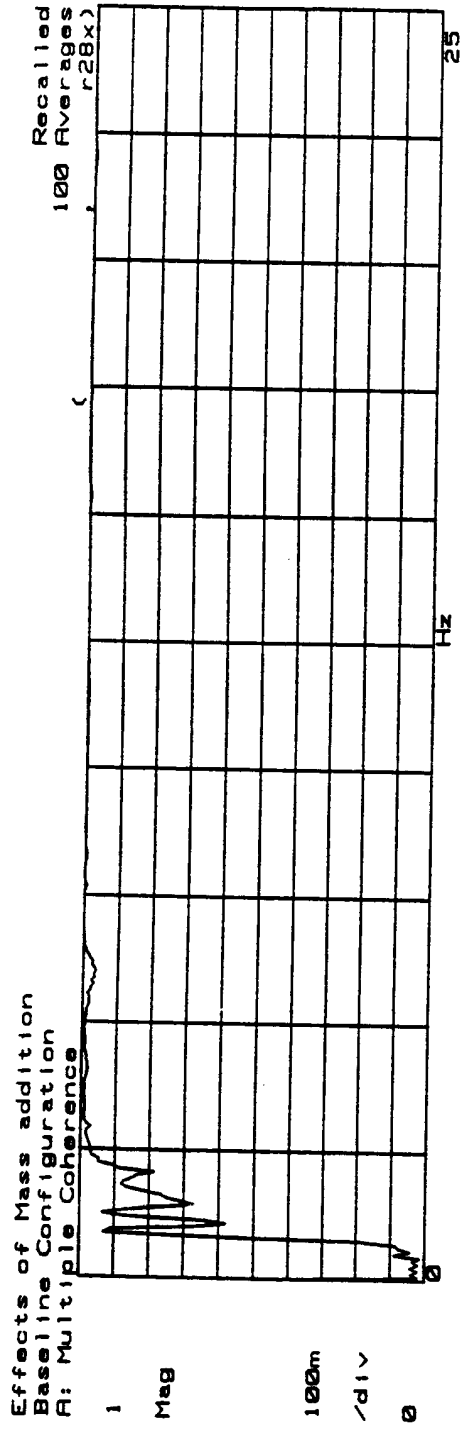


Figure 18. Typical Multiple Coherence Measurements

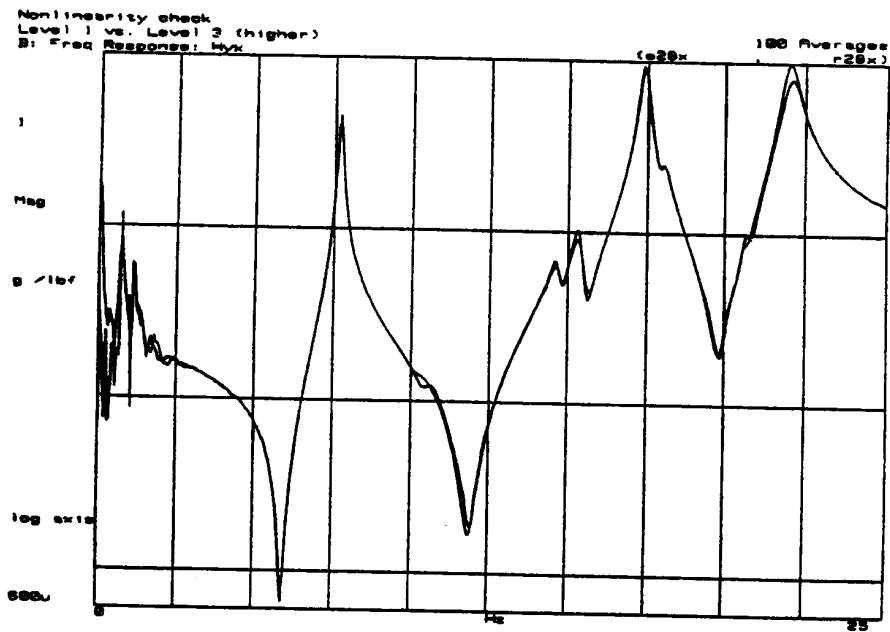
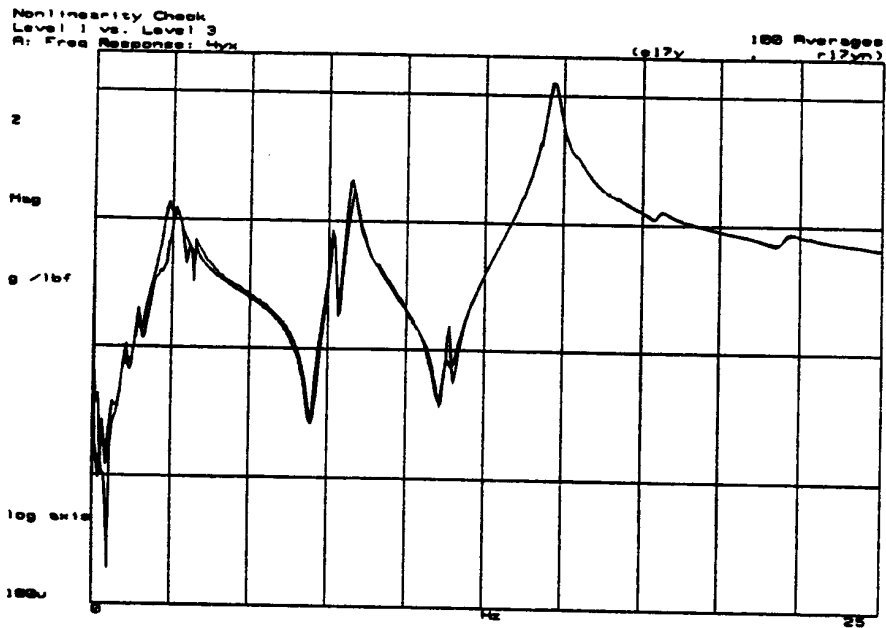


Figure 19. Nonlinearity Check: Highest and Lowest Force Level (17y top, 28x bottom)

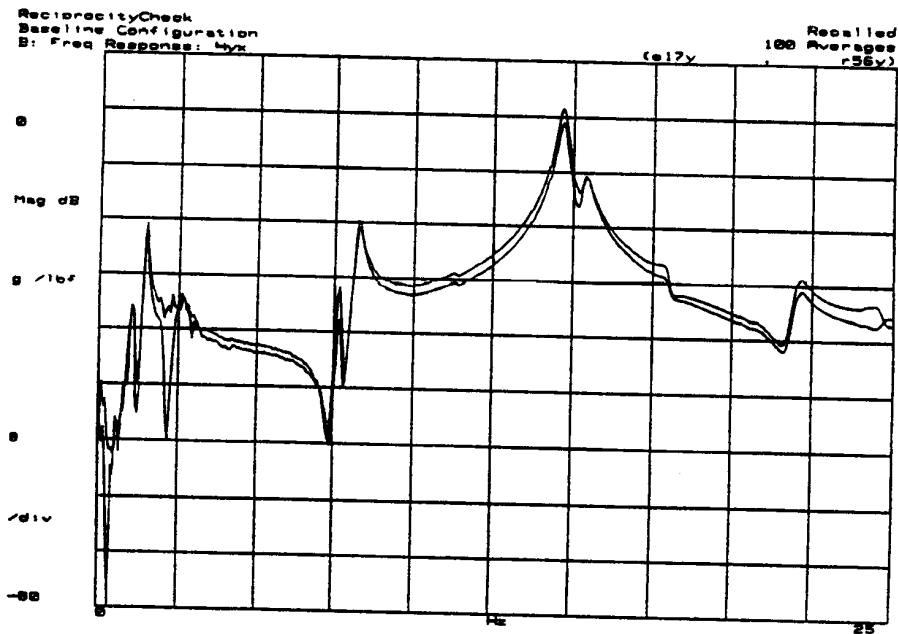


Figure 20. Reciprocity Check for Baseline Configuration (17y - 56y)

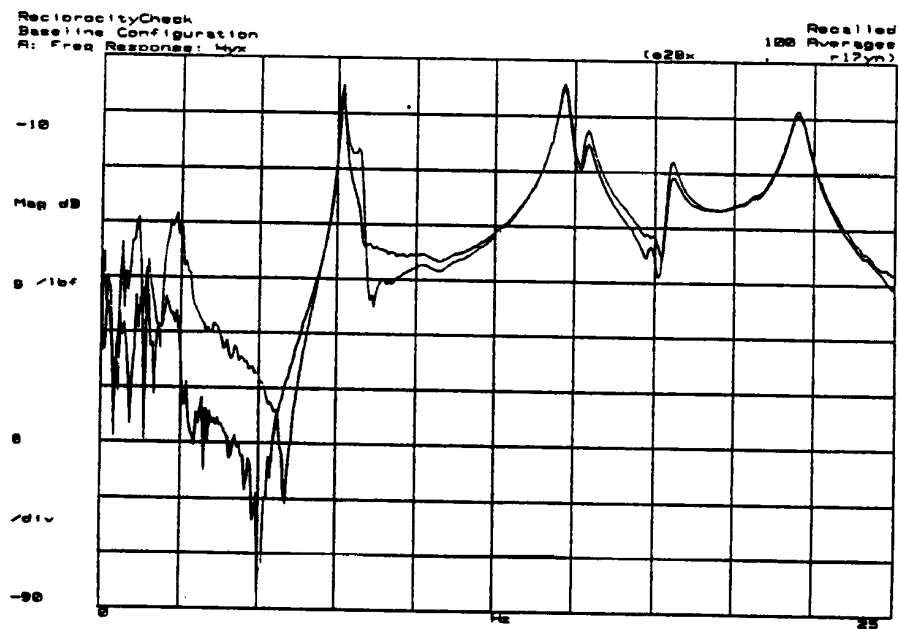


Figure 21. Reciprocity Check for Baseline Configuration (17y - 28x)

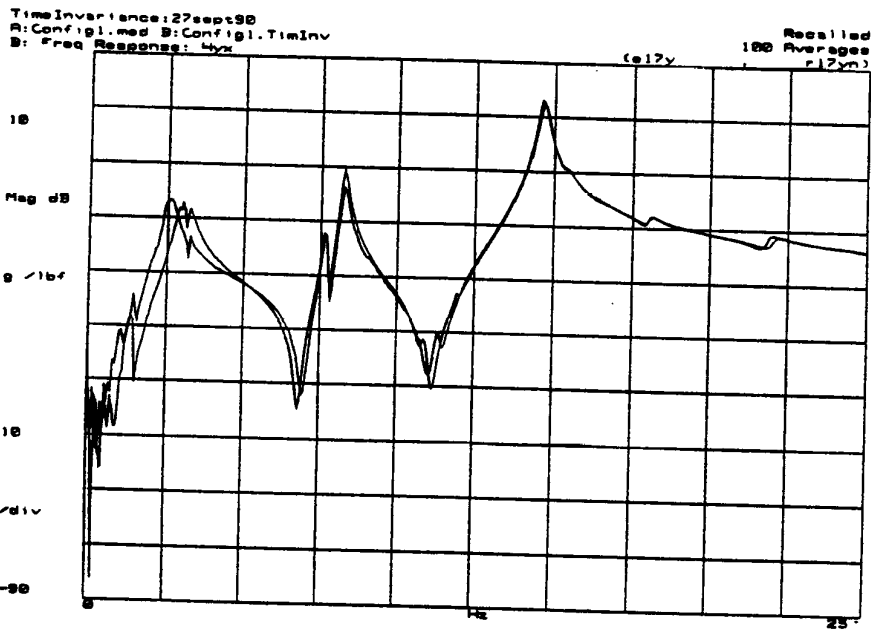


Figure 22. Time Invariance Check: Driving point (17y/17y)

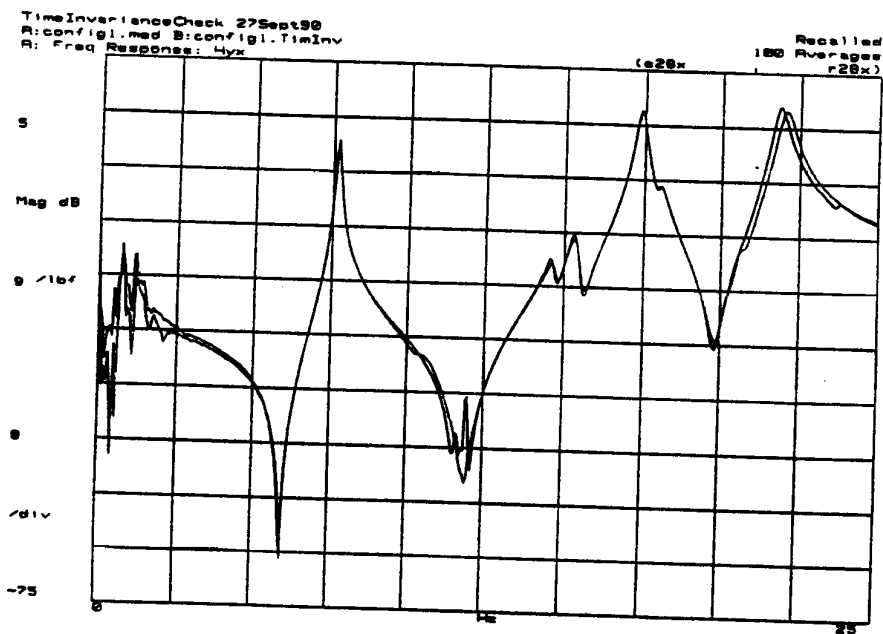


Figure 23. Time Invariance Check: Driving point (28x/28x)

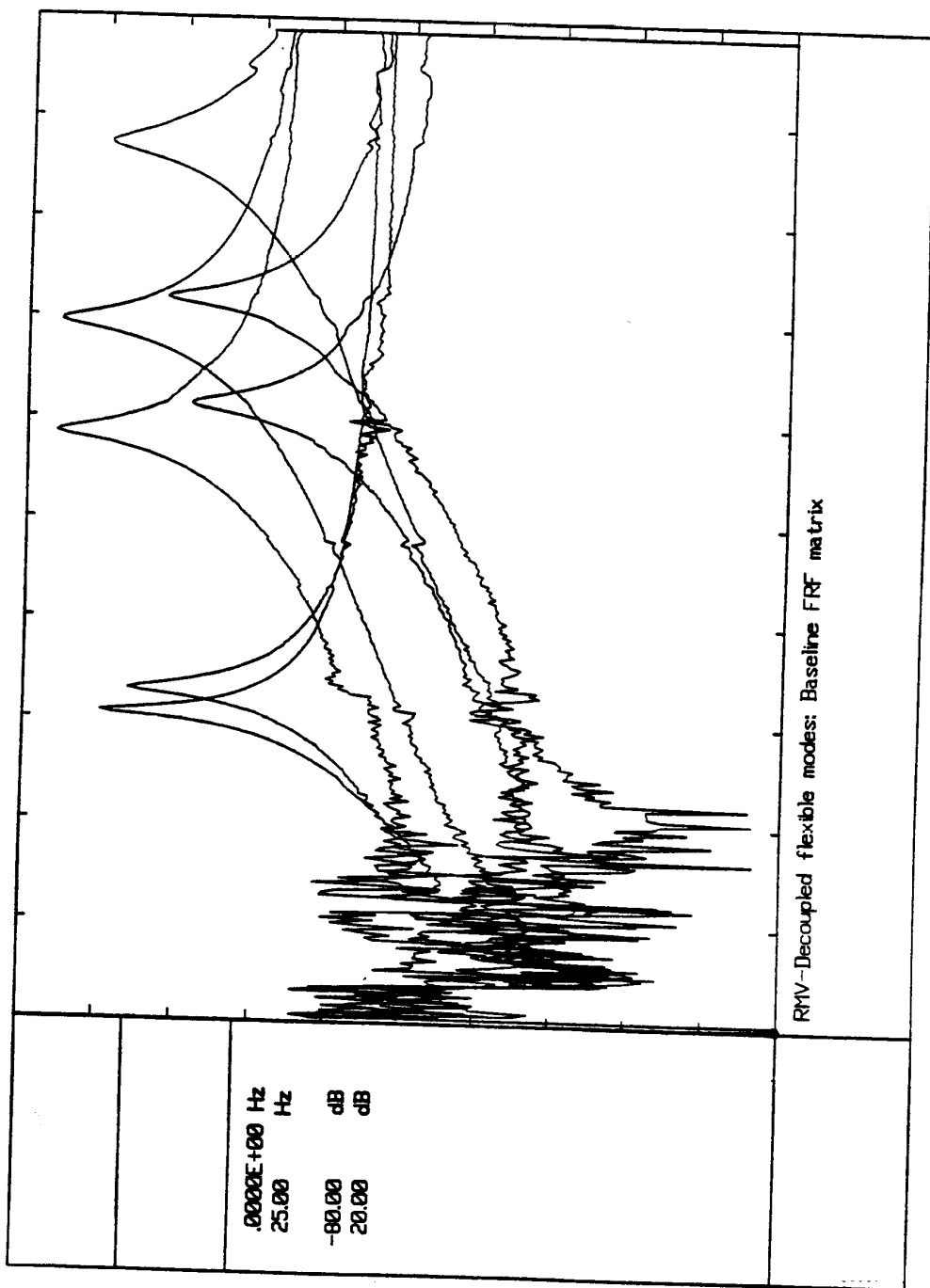


Figure 24. Overview of Decoupled Responses for First Seven Flexible Modes

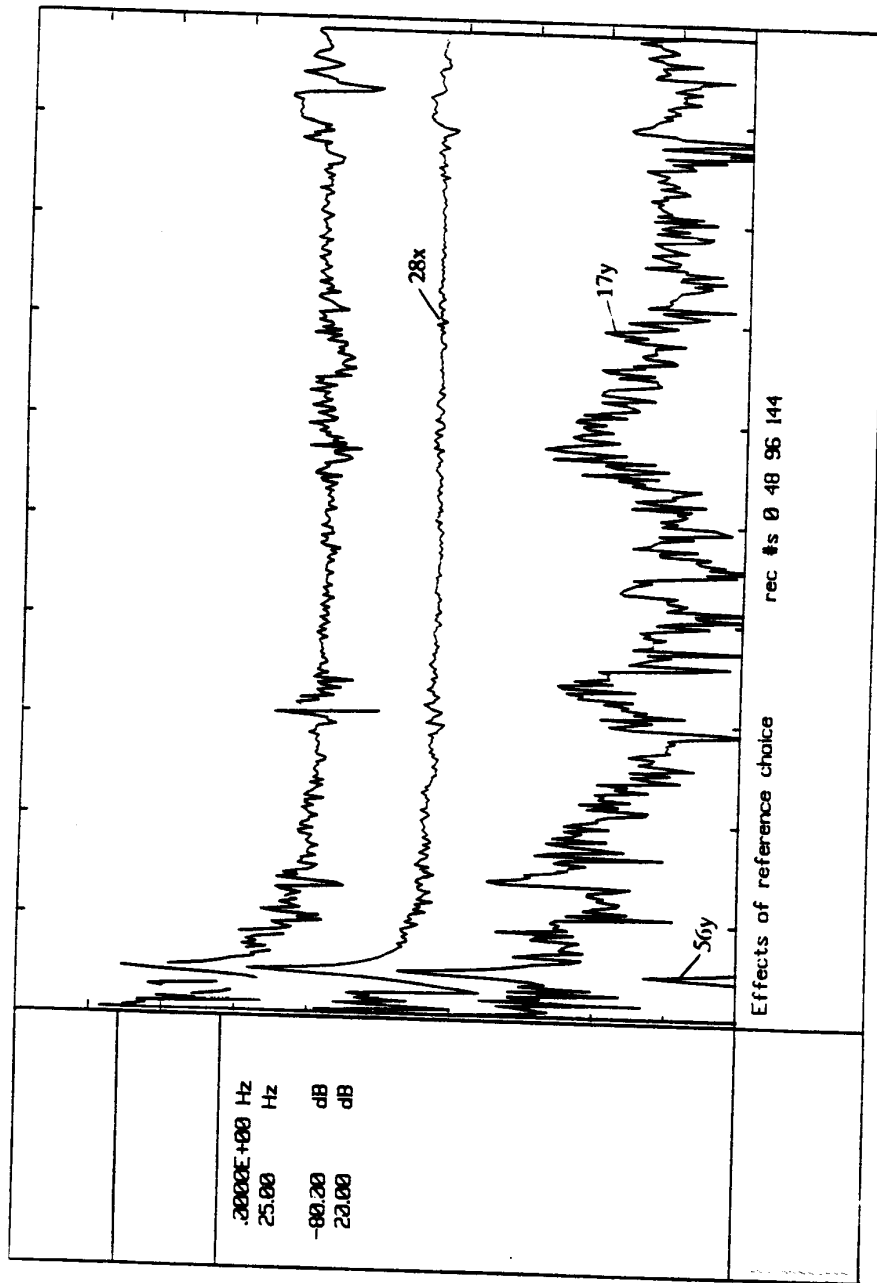


Figure 25. Decoupled FRFs for Different Active References: Mode 1 (Rigid Body Yaw)

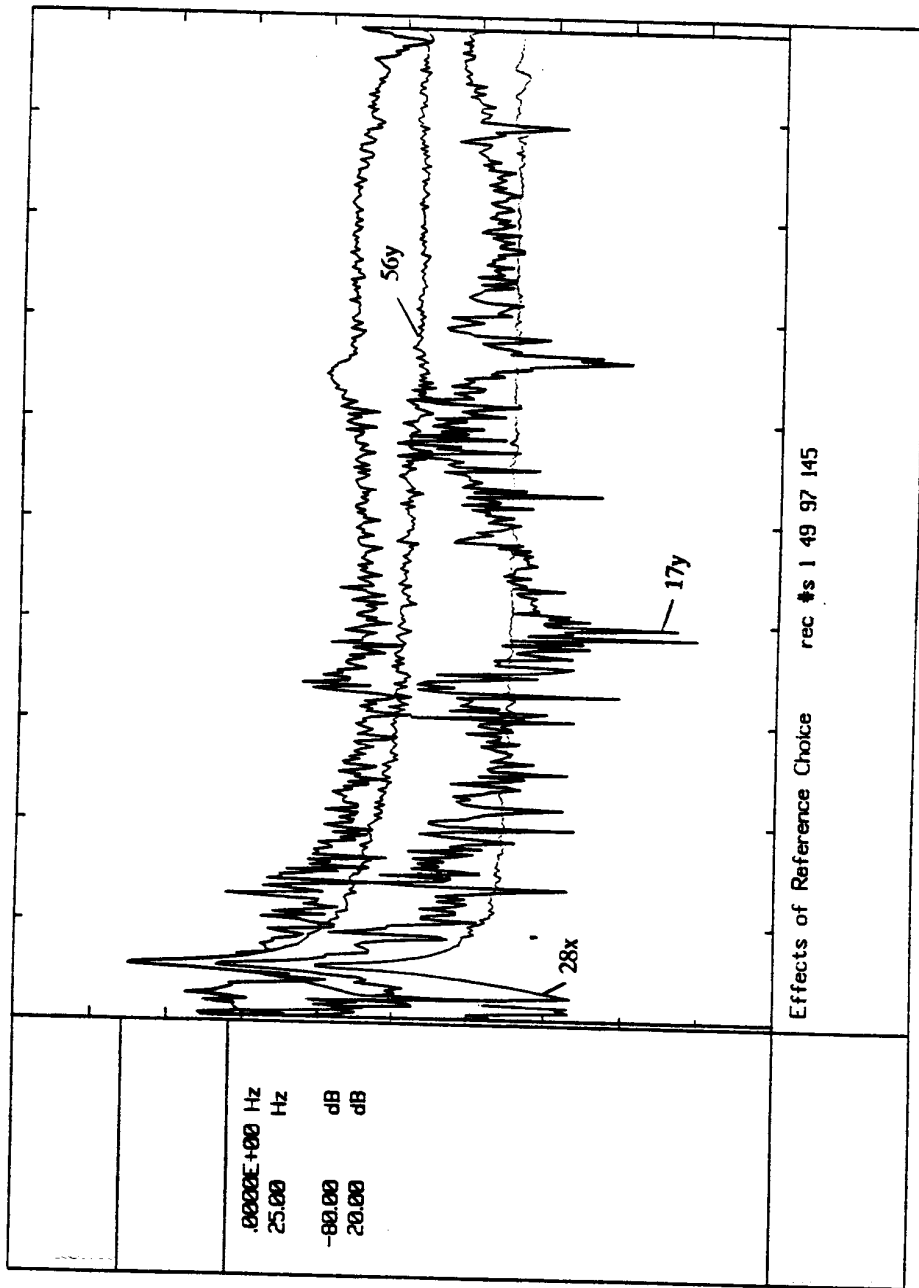


Figure 26. Decoupled FRFs for Different Active References: Mode 2 (Rigid Body Roll)

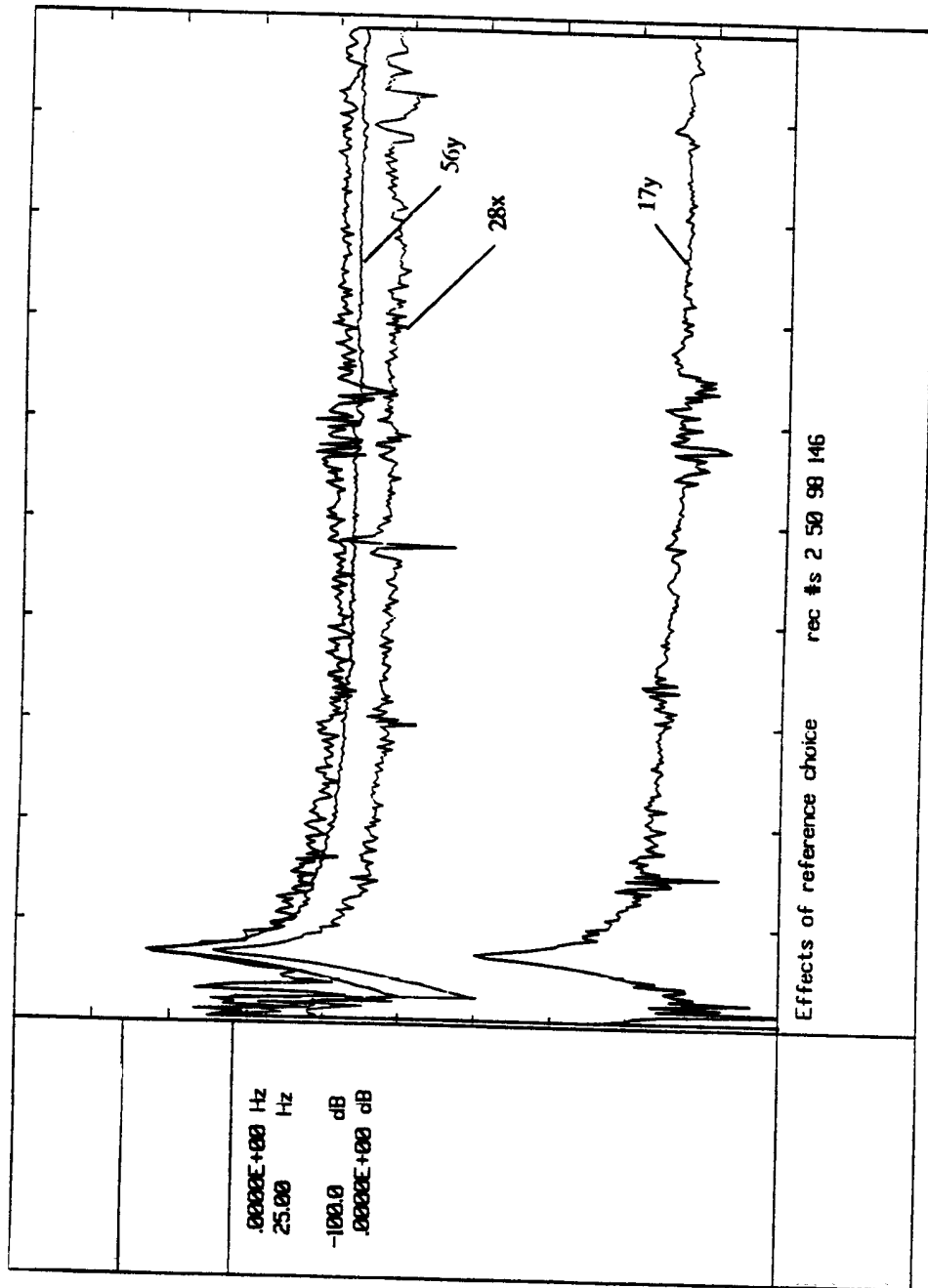


Figure 27. Decoupled FRFs for Different Active References: Mode 3 (Rigid Pitch/Roll)

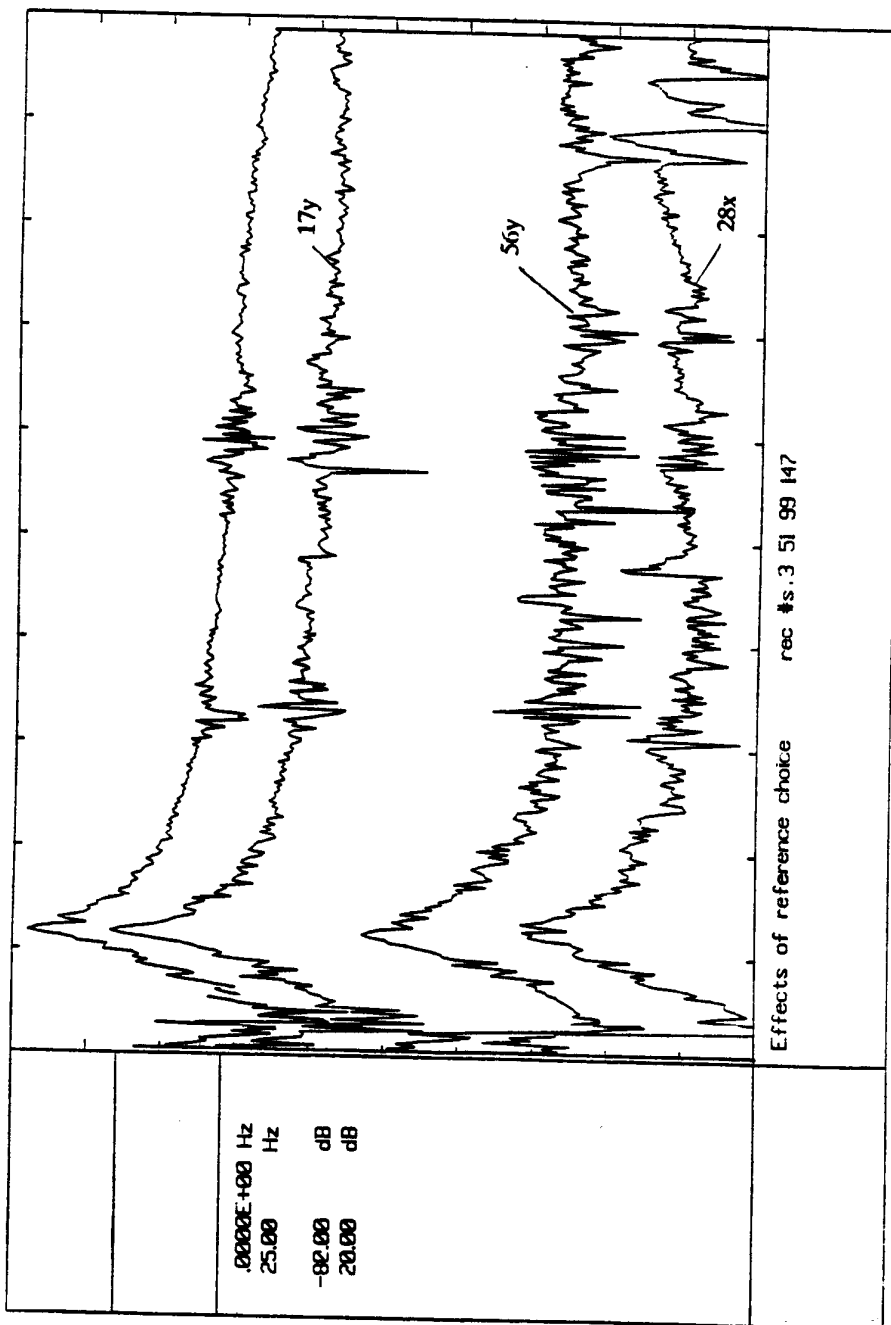


Figure 28. Decoupled FRFs for Different Active References: Mode 4 (Rigid Body Pitch)

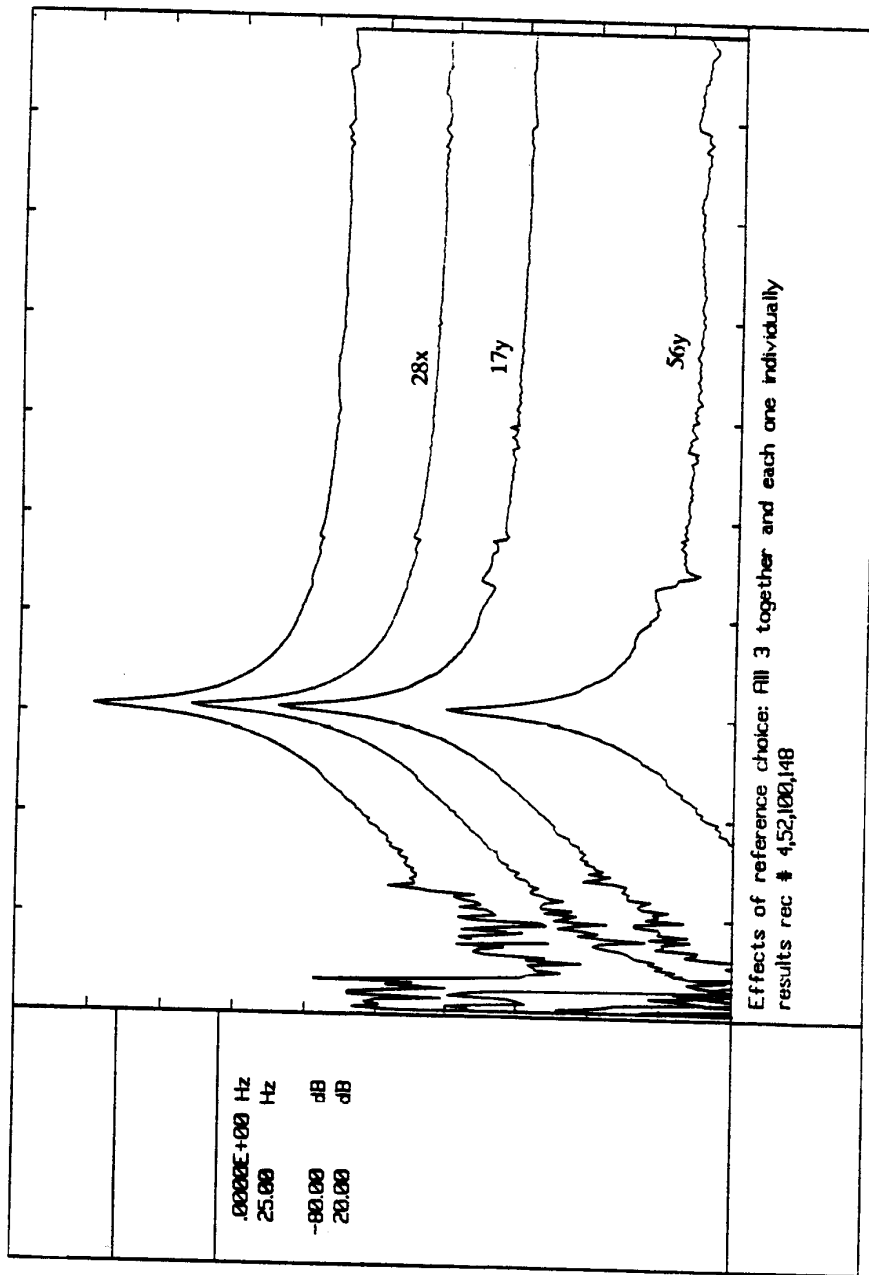


Figure 29. Decoupled FRFs for Different Active References: Mode 5 (Lateral First Bending)

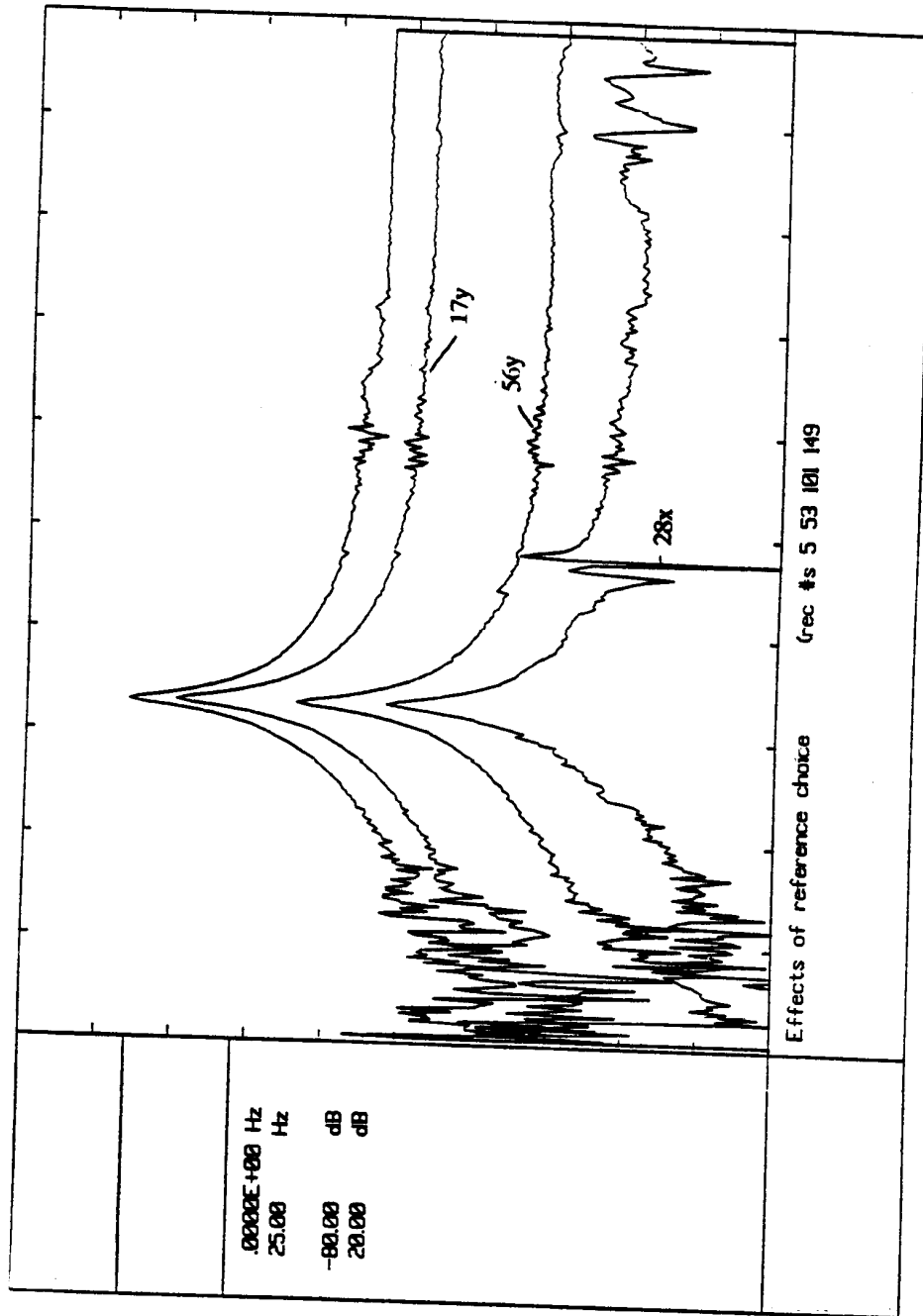


Figure 30. Decoupled FRFs for Different Active References: Mode 6 (Vertical First Bending)

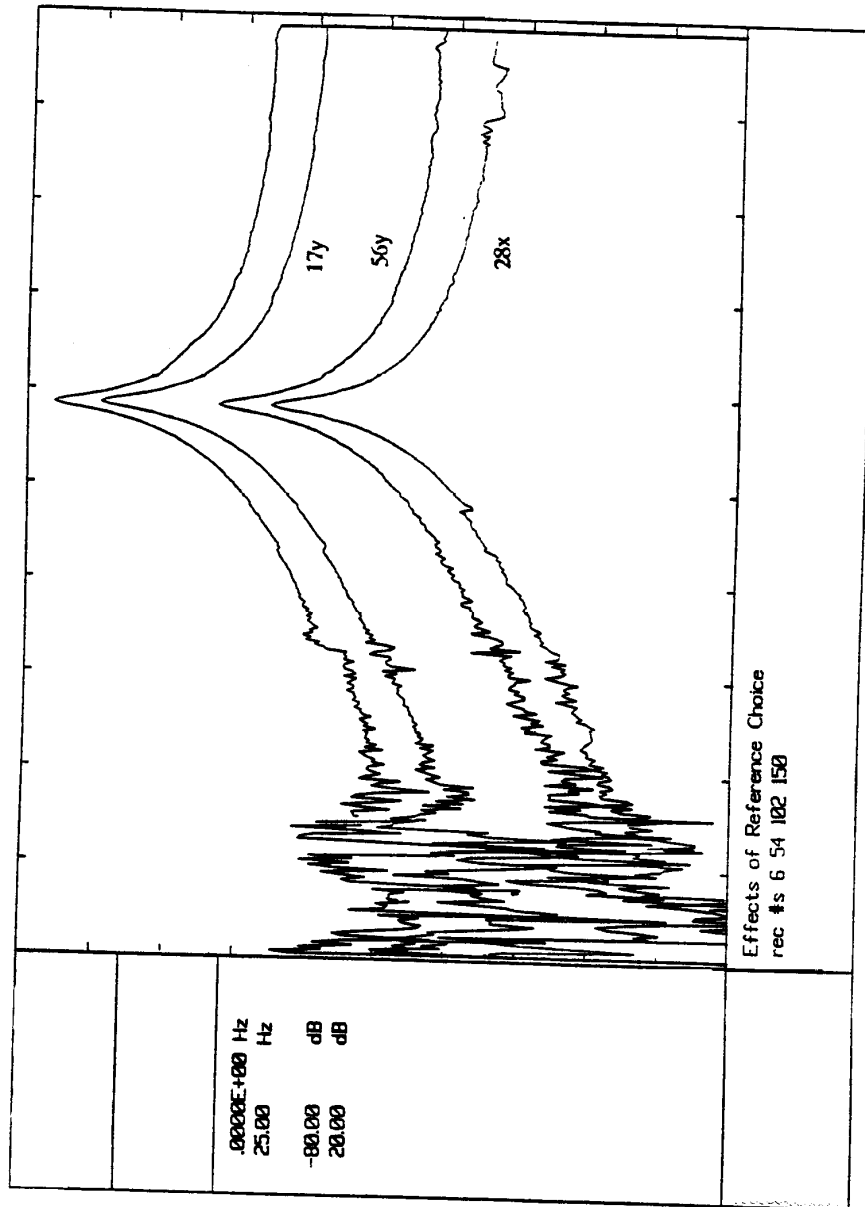


Figure 31. Decoupled FRFs for Different Active References: Mode 7 (Lower Mast Torsion)

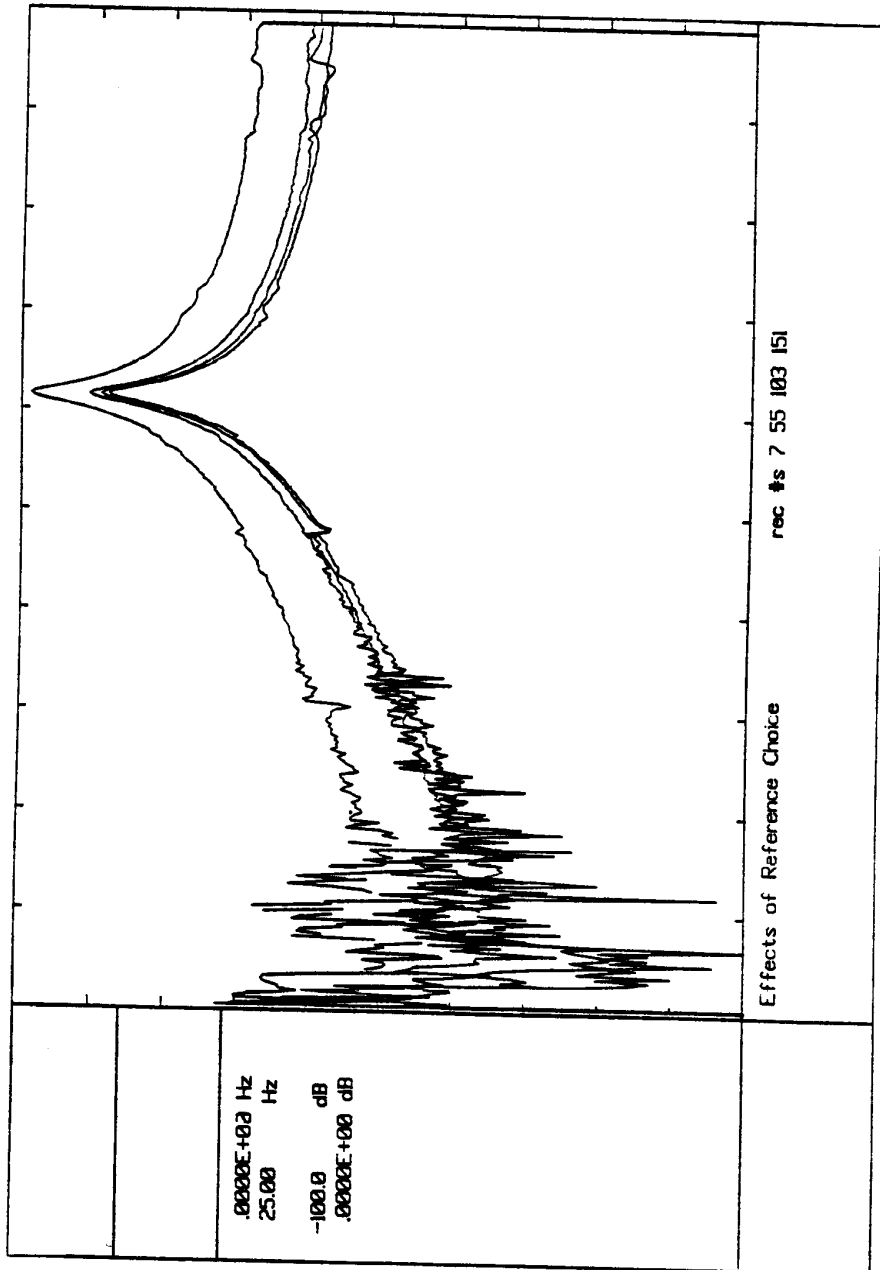


Figure 32. Decoupled FRFs for Different Active References: Mode 8 (Mast Vertical Bending)

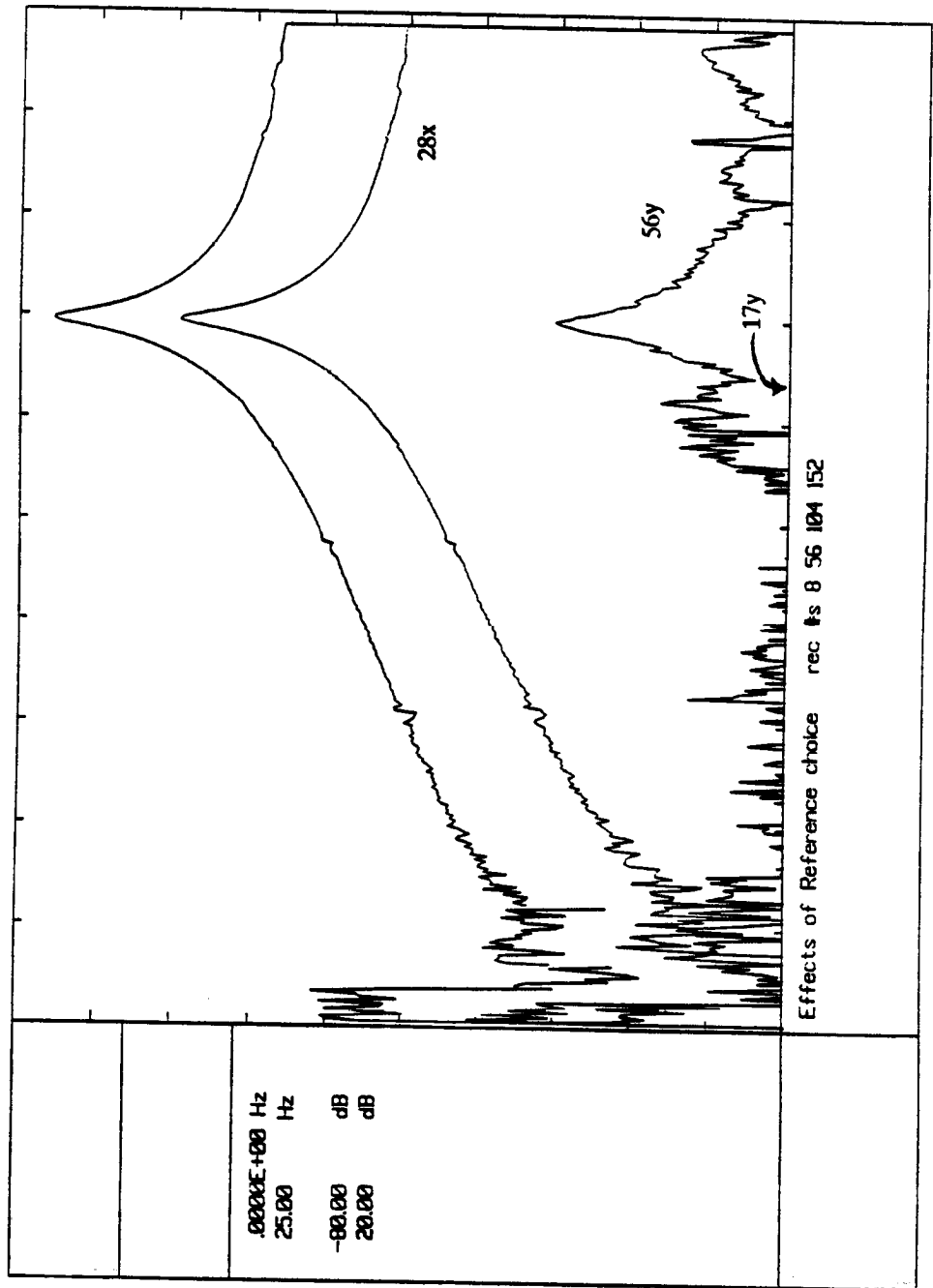


Figure 33. Decoupled FRFs for Different Active References: Mode 9 (Upper Mast/Crossarm Lateral Bending)

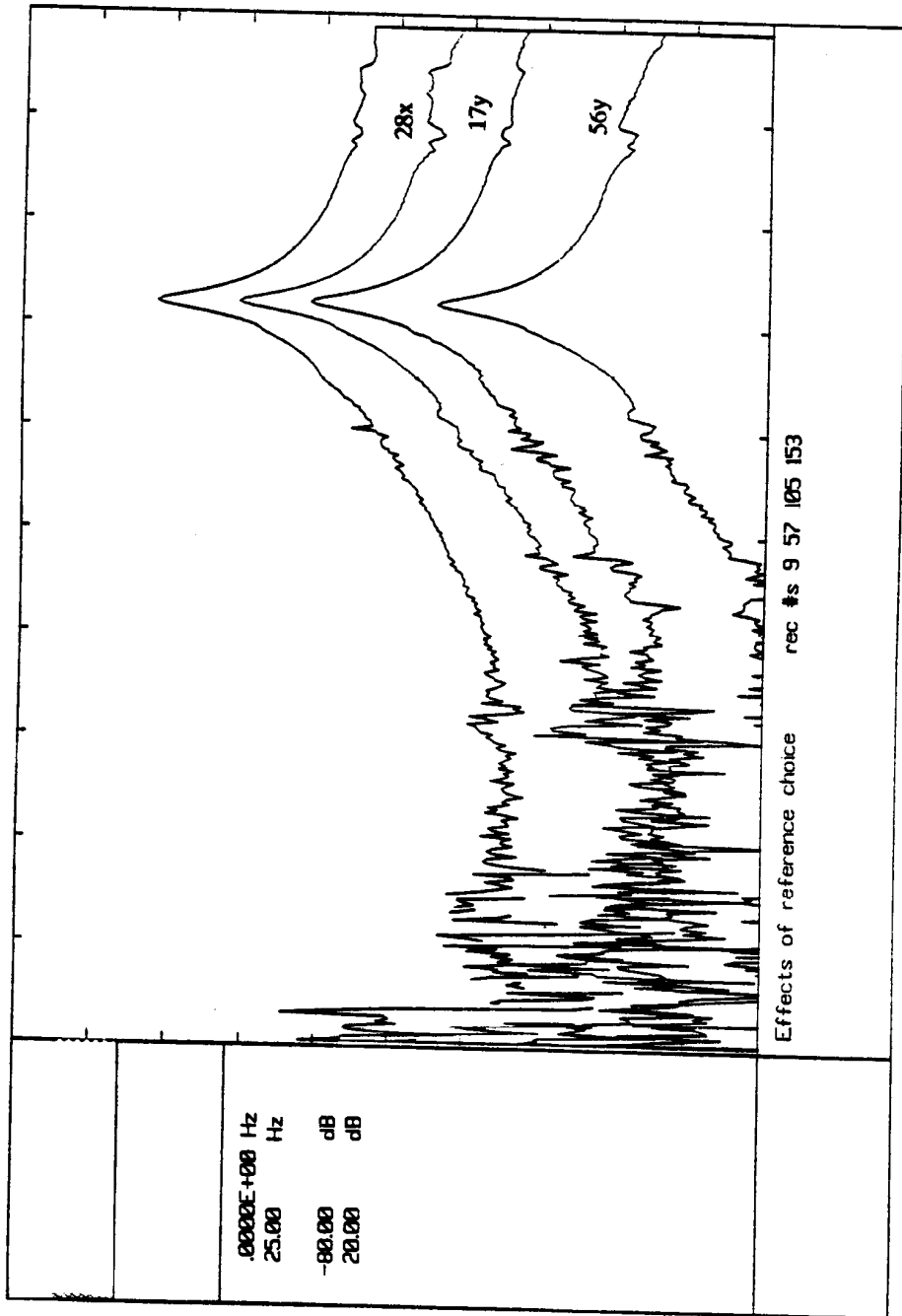


Figure 34. Decoupled FRFs for Different Active References: Mode 10 (Lateral Second Bending)

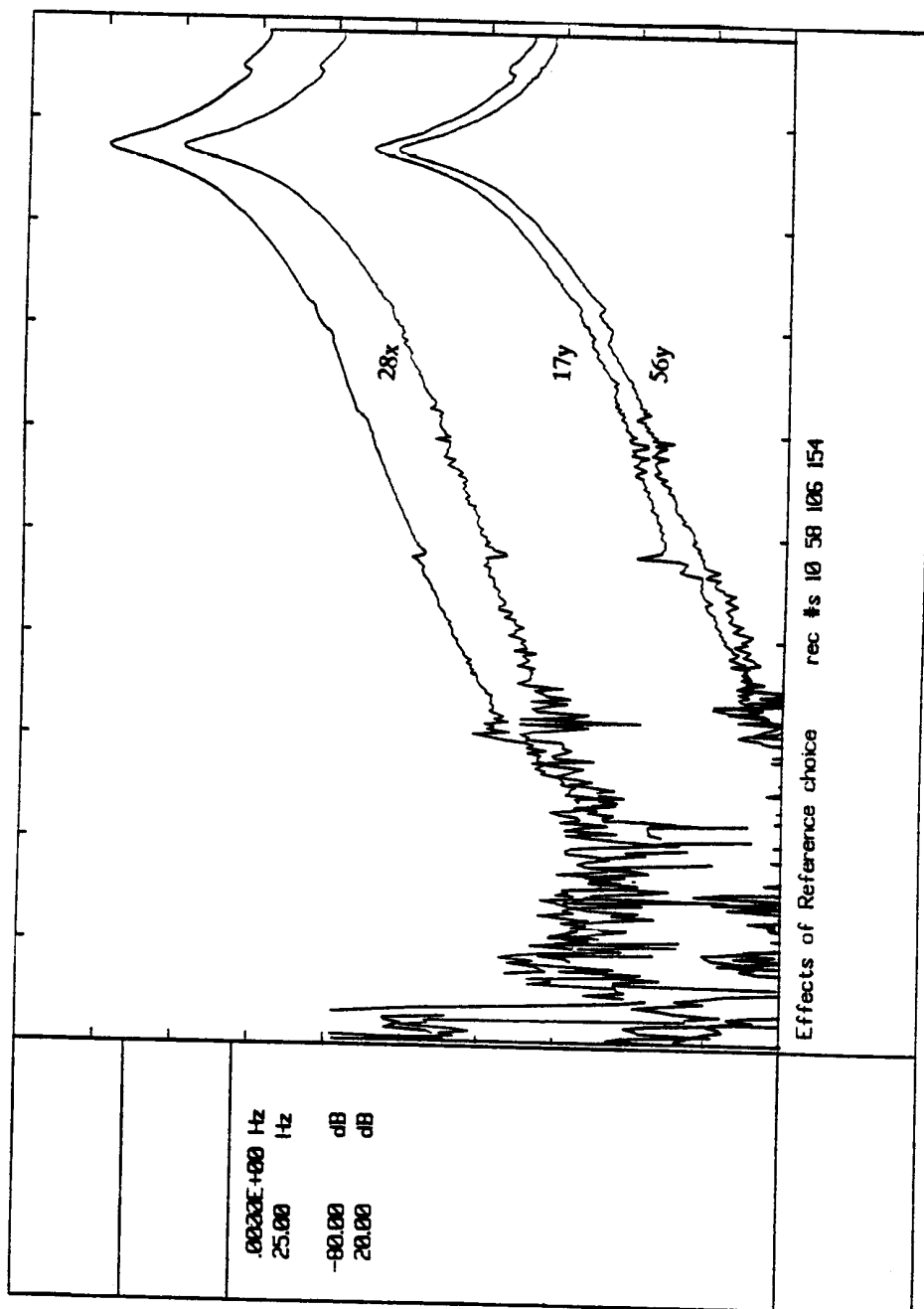


Figure 35. Decoupled FRFs for Different Active References: Mode 11 (Upper Mast Torsion)

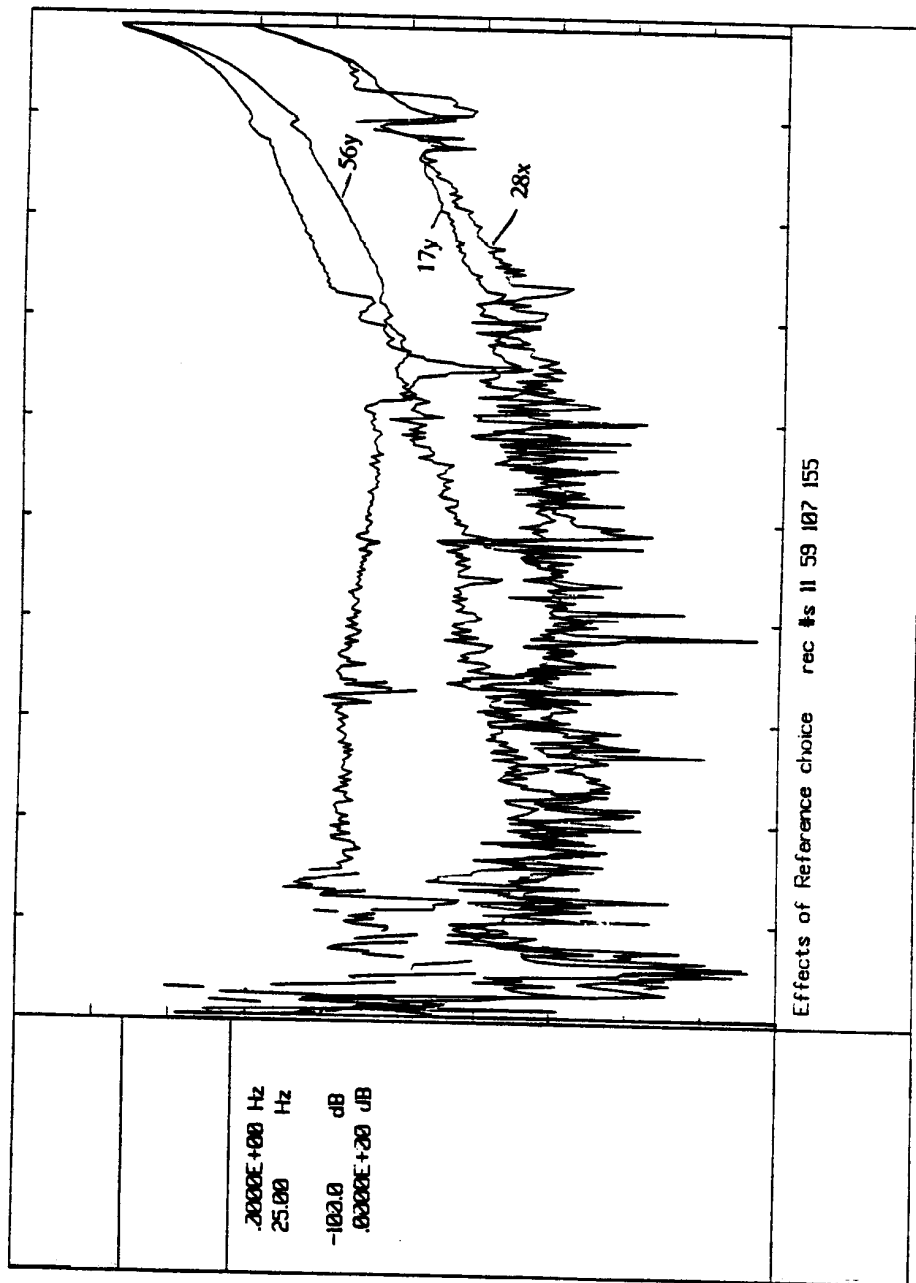


Figure 36. Decoupled FRFs for Different Active References: Mode 12 (Crossarm YZ-plane Bending)

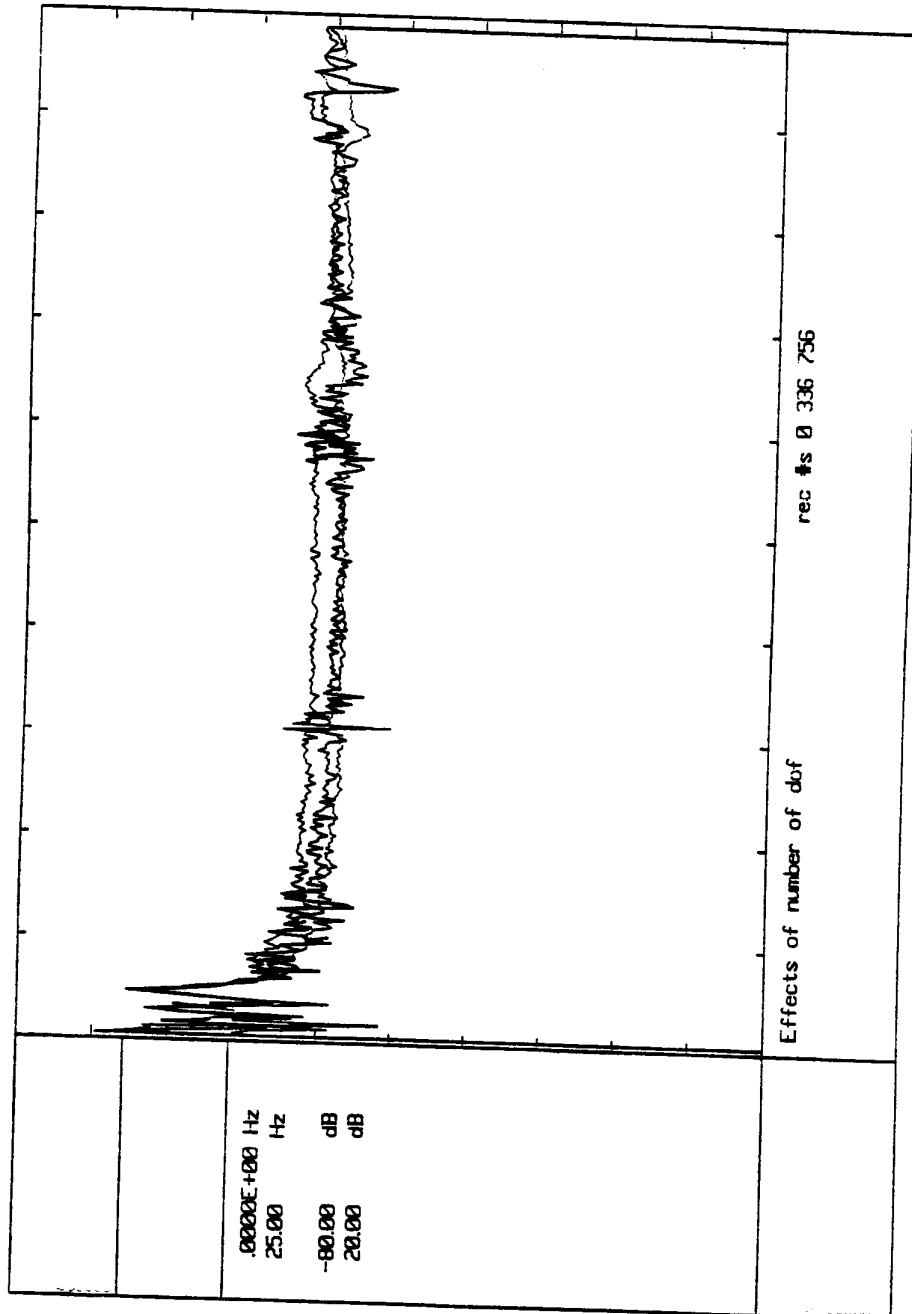


Figure 37. Comparison of Decoupled FRF for 80, 40, and 20 degrees of freedom (Mode #1)

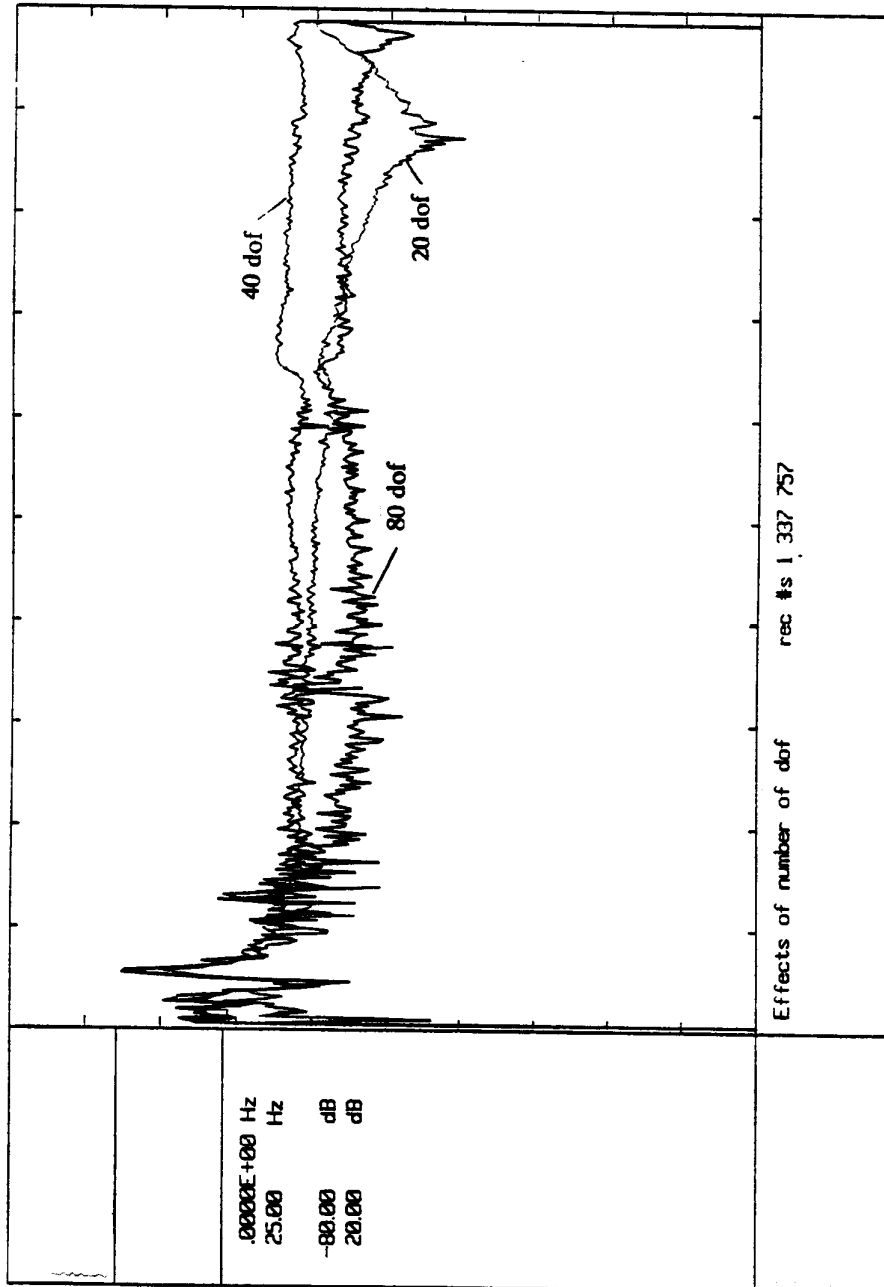


Figure 38. Comparison of Decoupled FRF for 80, 40, and 20 degrees of freedom (Mode #2)

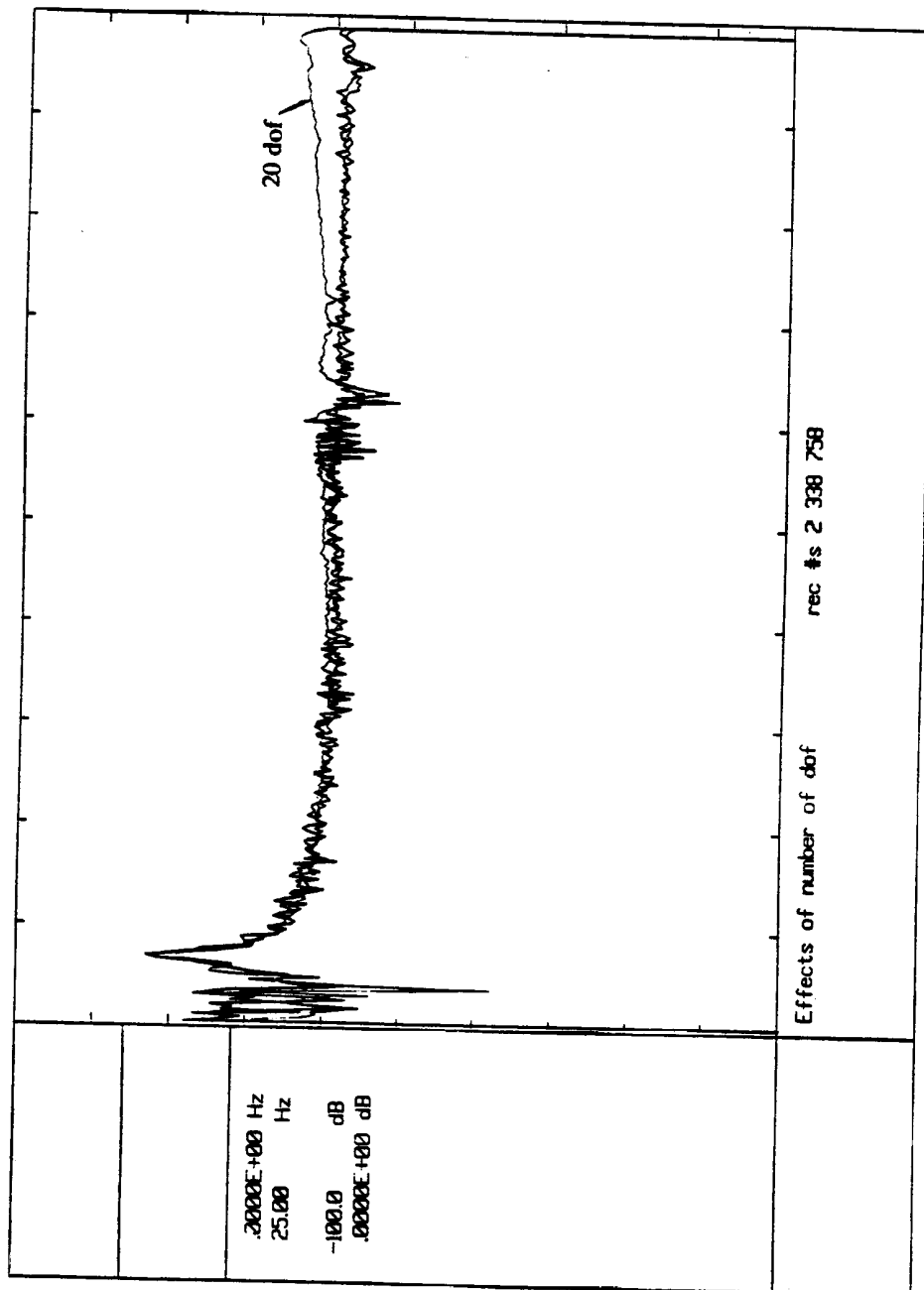


Figure 39. Comparison of Decoupled FRF for 80, 40, and 20 degrees of freedom (Mode #3)

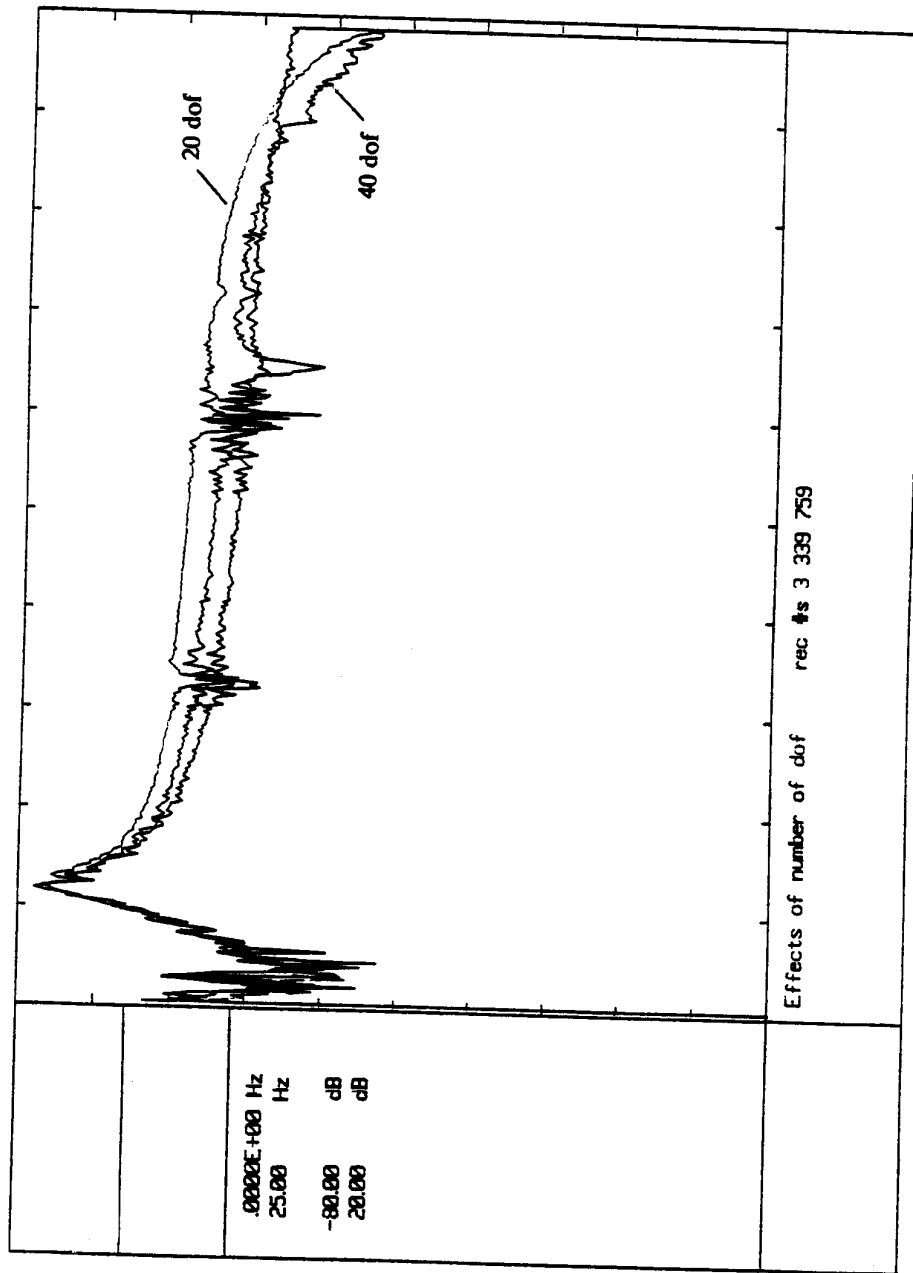


Figure 40. Comparison of Decoupled FRF for 80, 40, and 20 degrees of freedom (Mode #4)

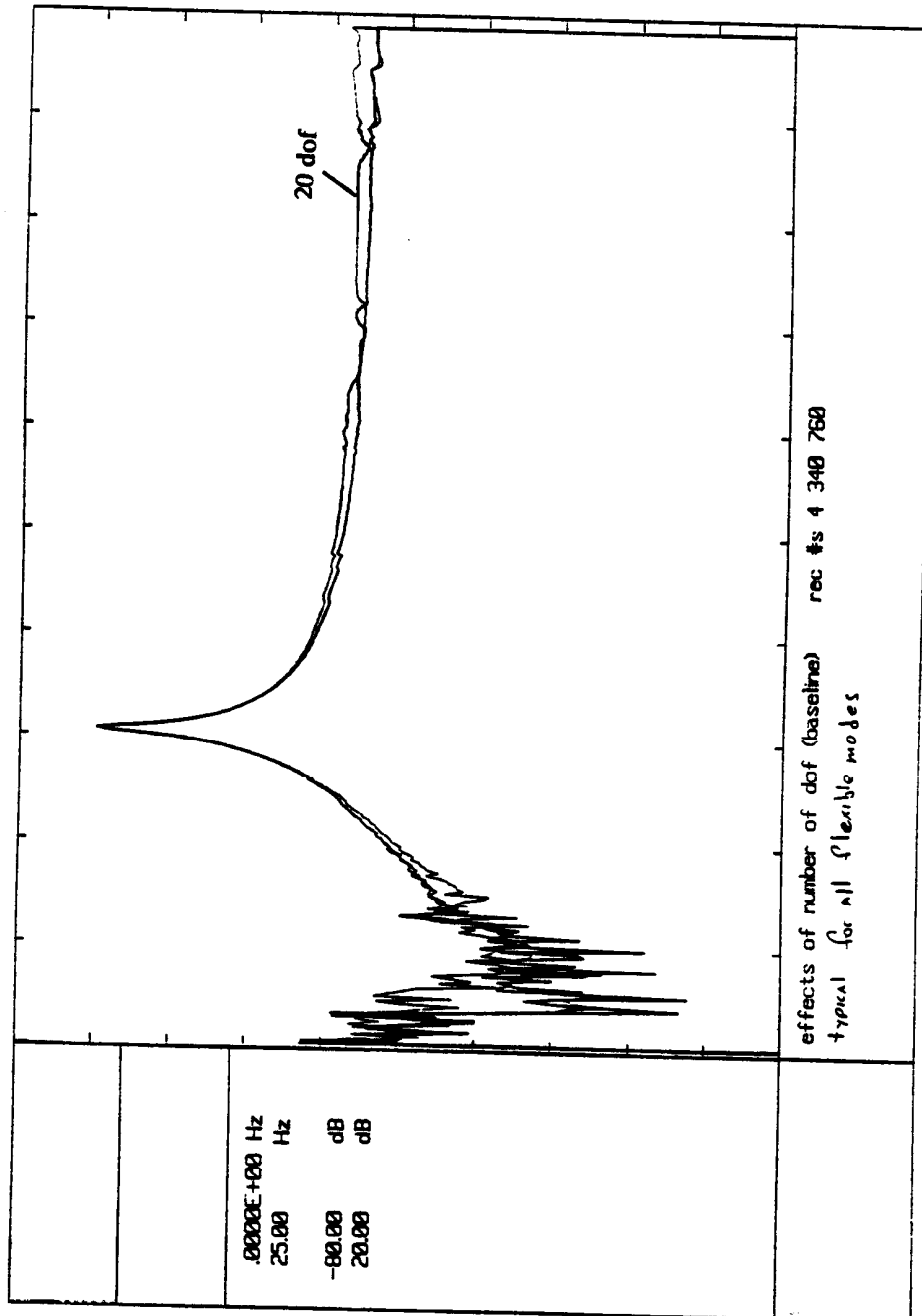


Figure 41. Comparison of Decoupled FRF for 80, 40, and 20 degrees of freedom (Mode #5)

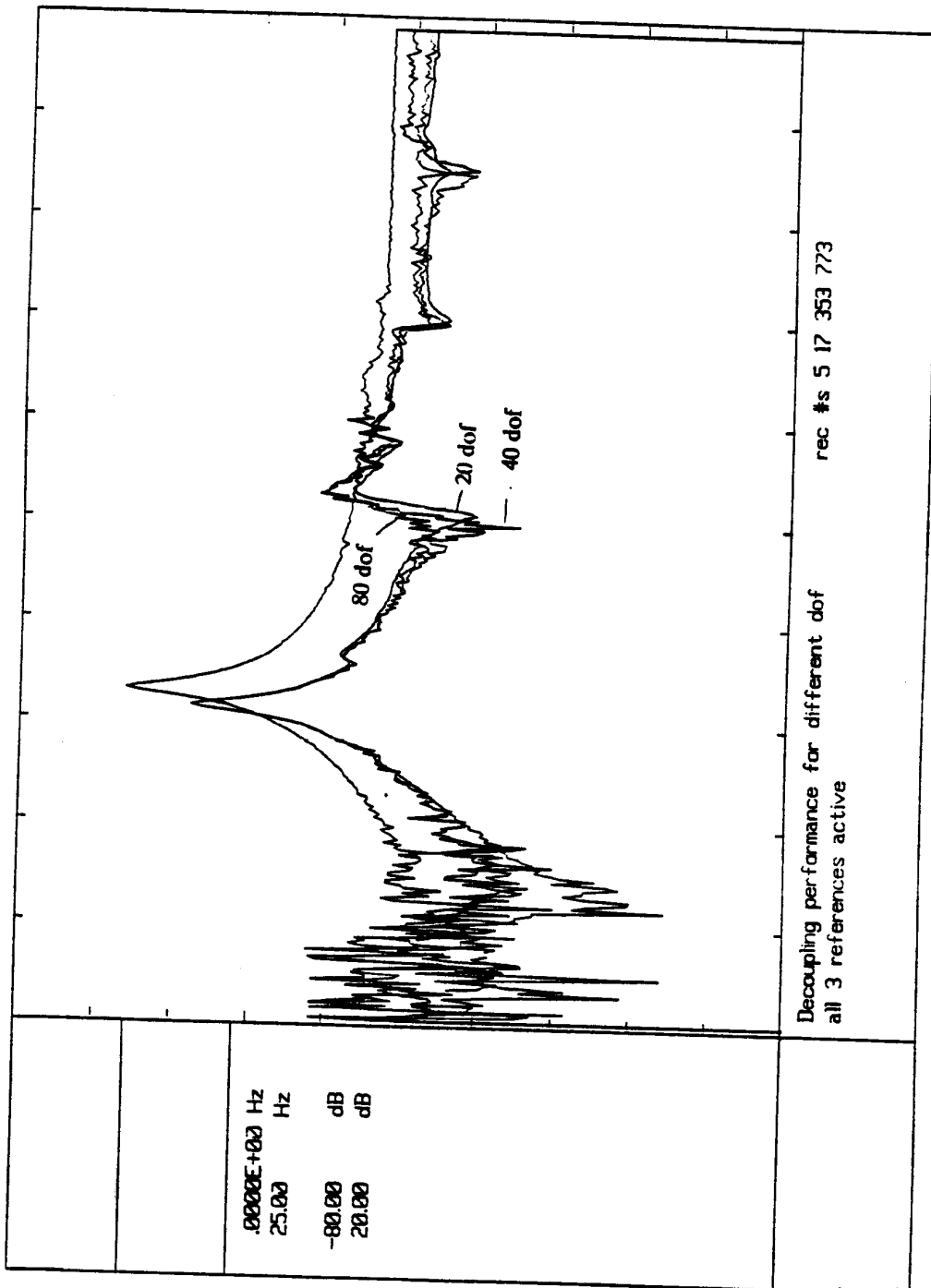


Figure 42. Decoupled FRFs for 80, 40, and 20 degrees of freedom (Mode #6; 1 mass added)

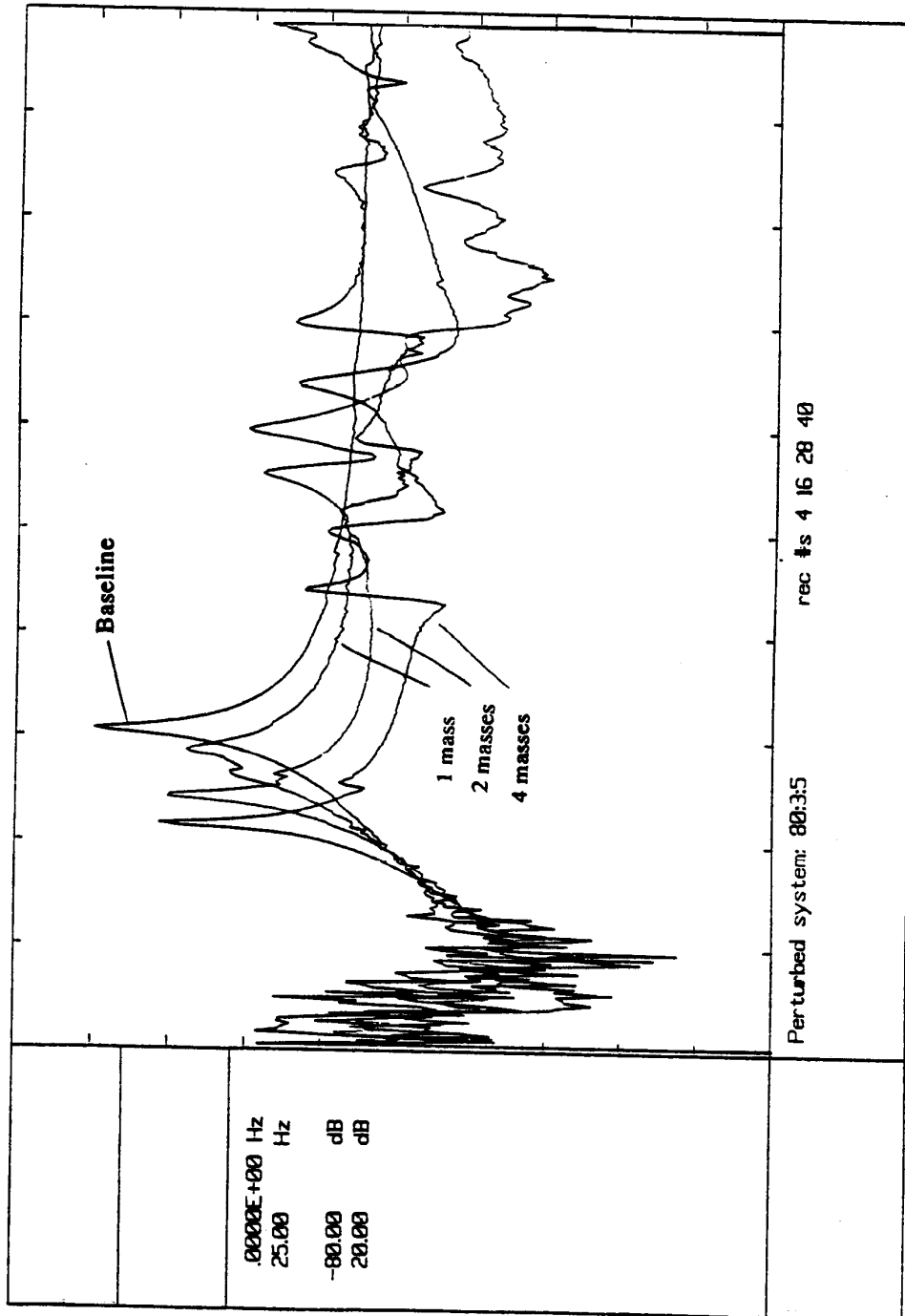


Figure 43. Decoupled FRFs for All Configurations: Mode #5 (Lateral First Bending)

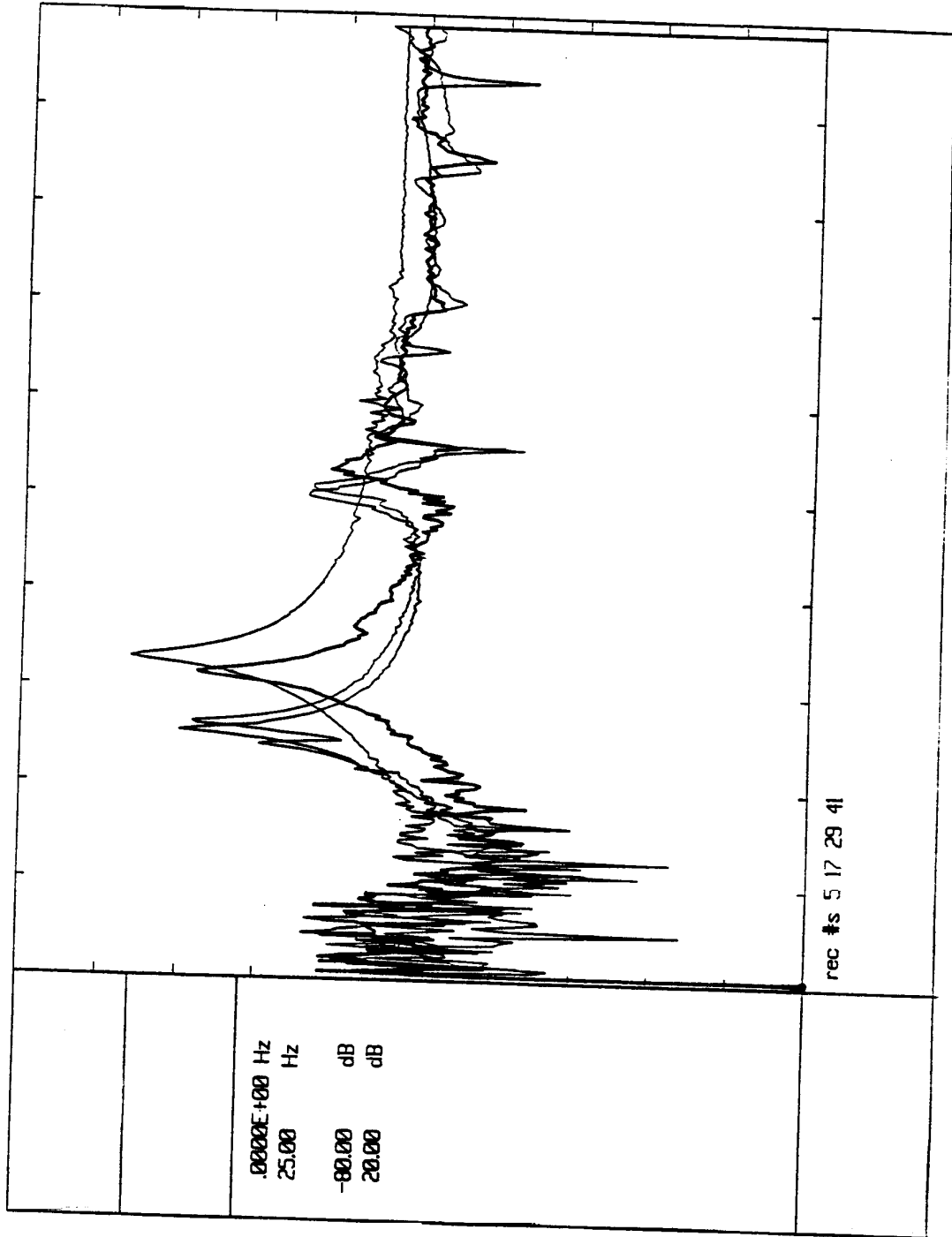


Figure 44. Decoupled FRFs for All Configurations: Mode #6 (Vertical First Bending)

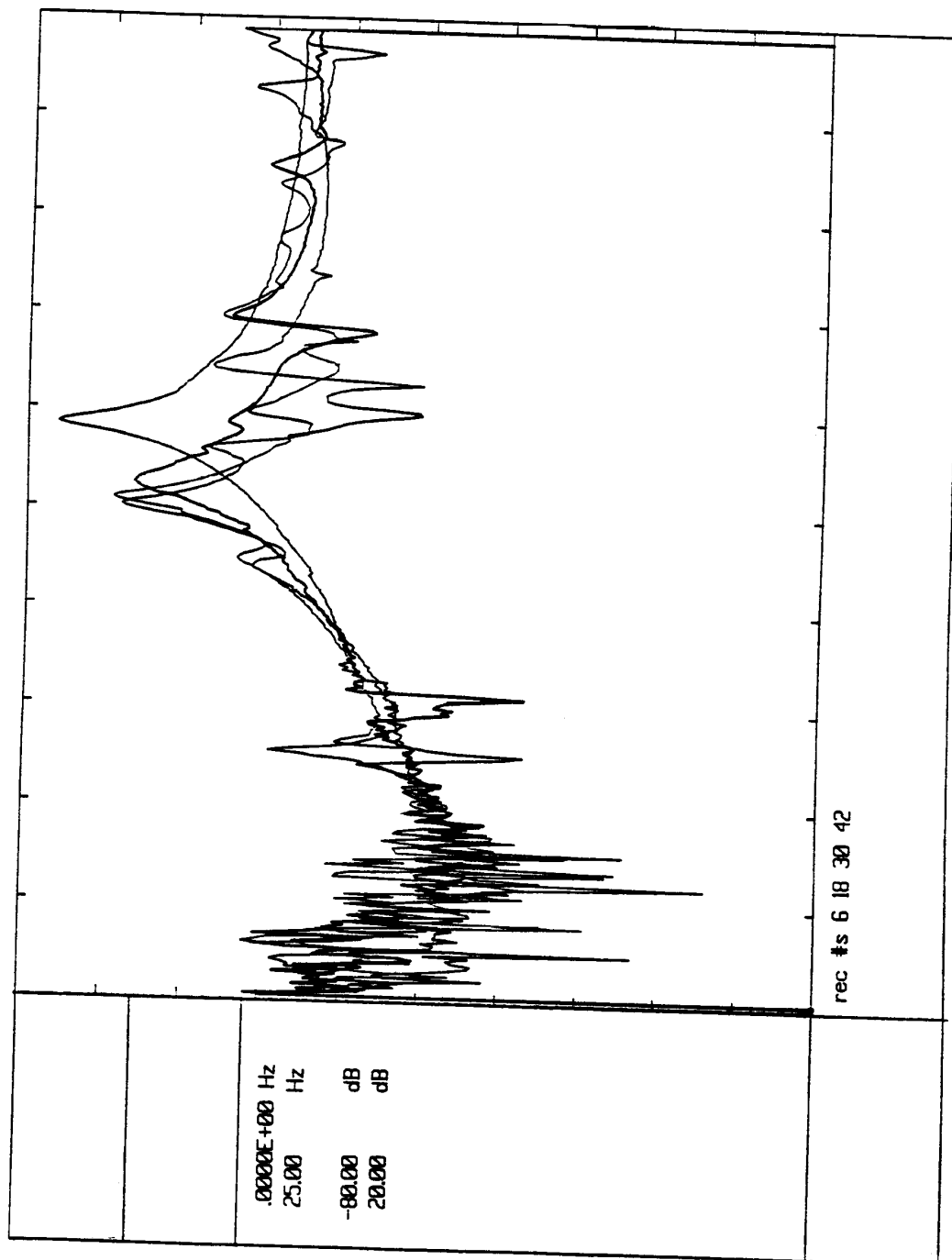


Figure 45. Decoupled FRFs for All Configurations: Mode #7 (Lower Mast Torsion)

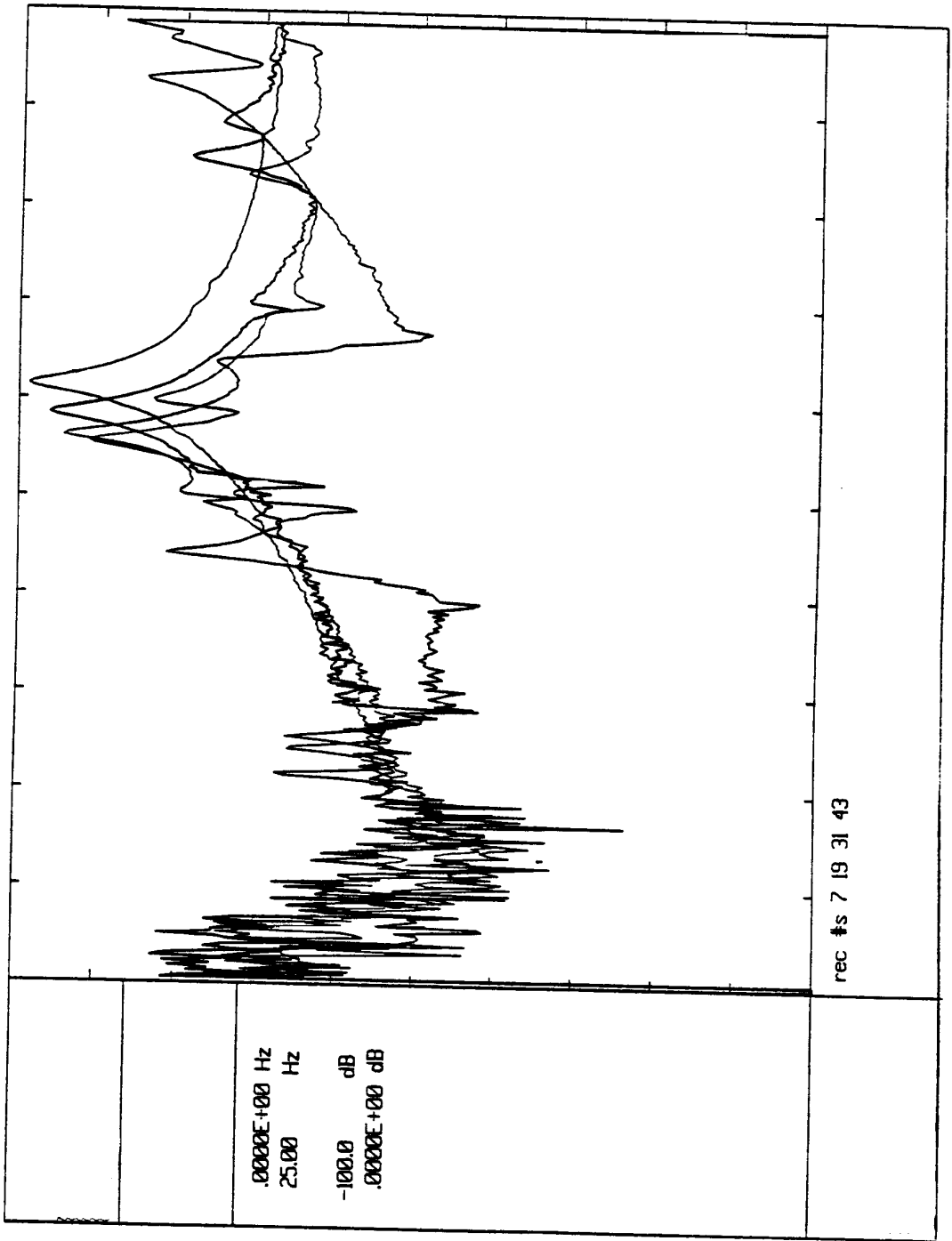


Figure 46. Decoupled FRFs for All Configurations: Mode #8 (Mast Vertical Bending)

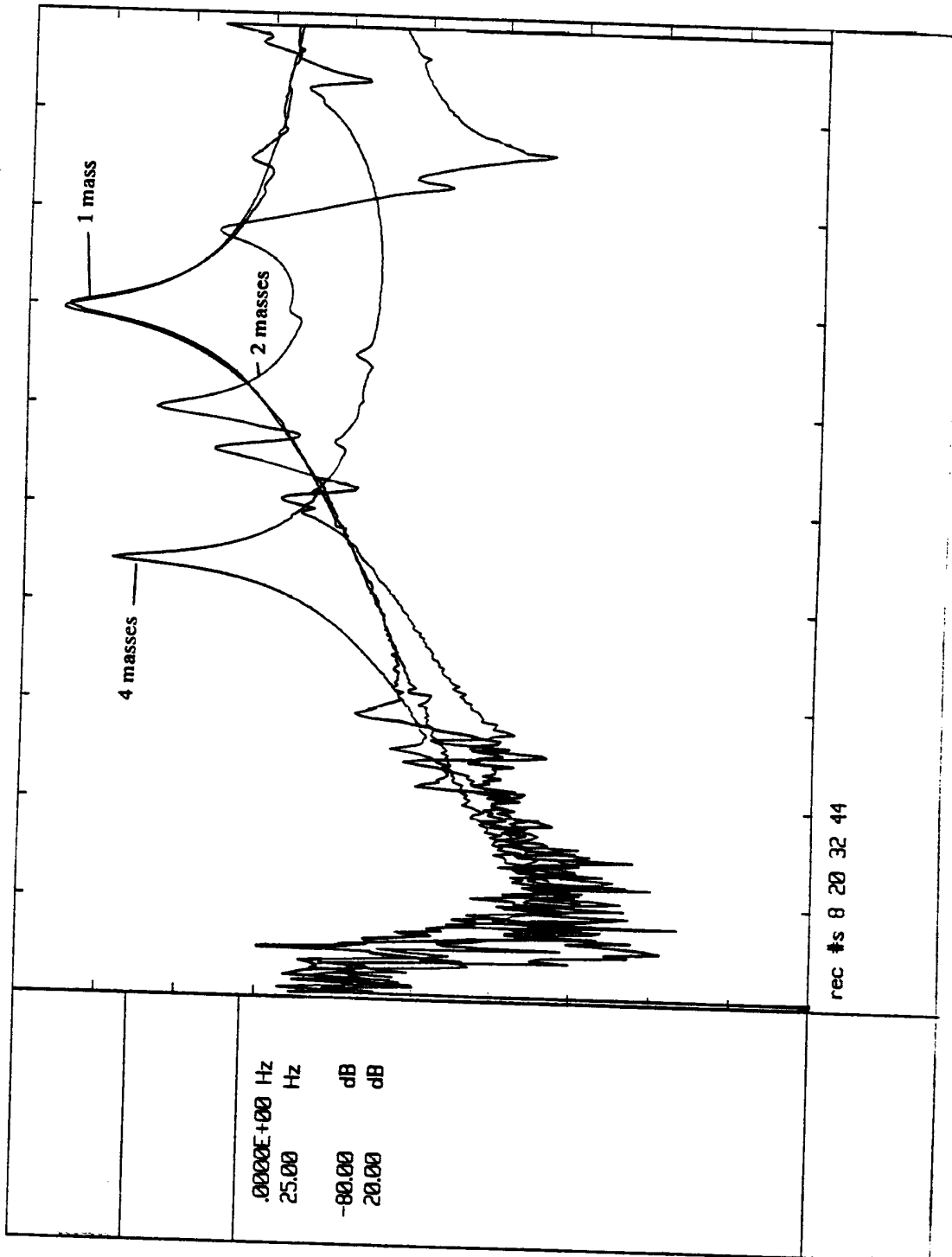


Figure 47. Decoupled FRFs, All Configurations: Mode #9 (Upper Mast/Crossarm Lat Bending)

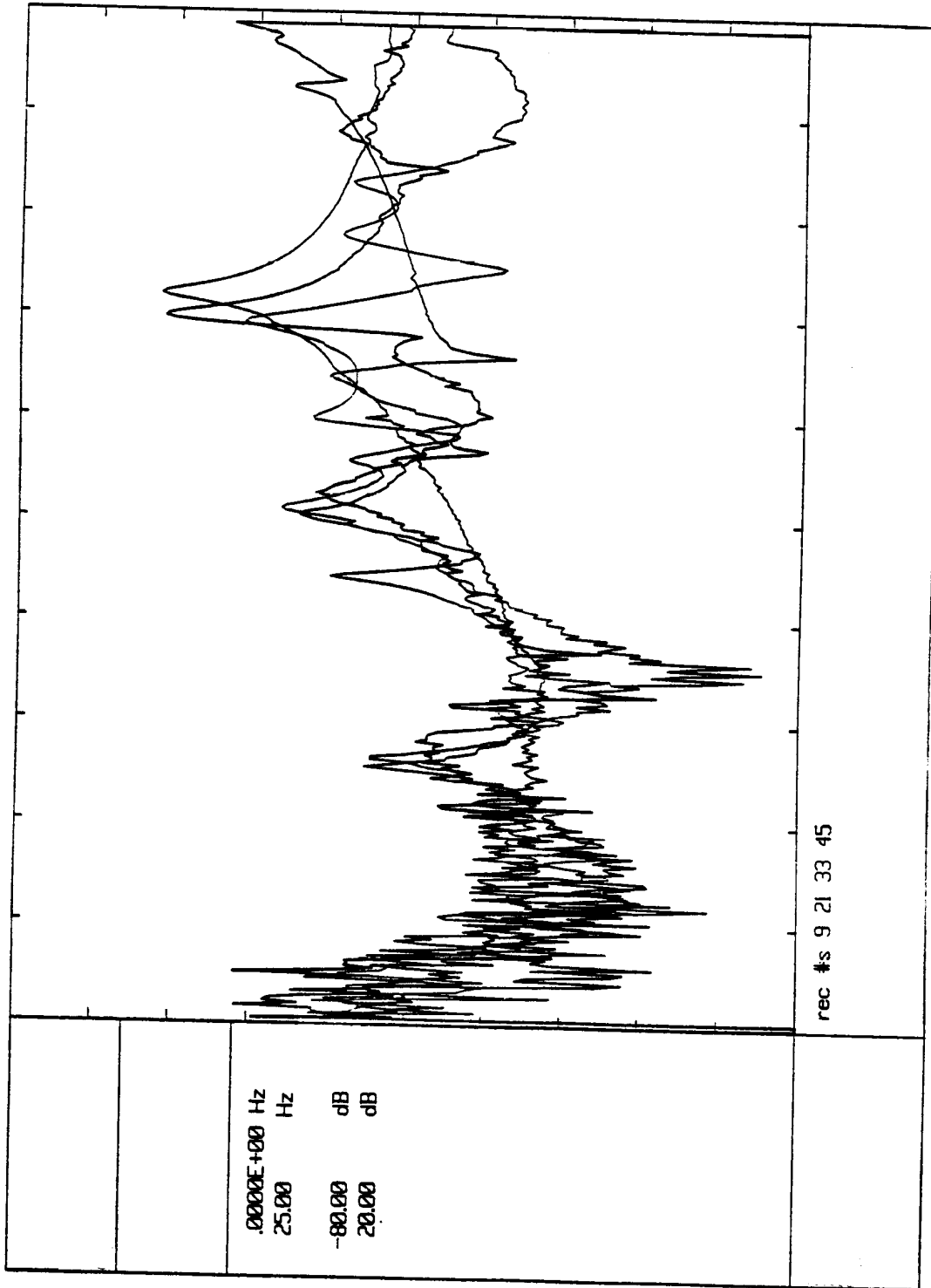


Figure 48. Decoupled FRFs for All Configurations: Mode #10 (Lateral Second Bending)

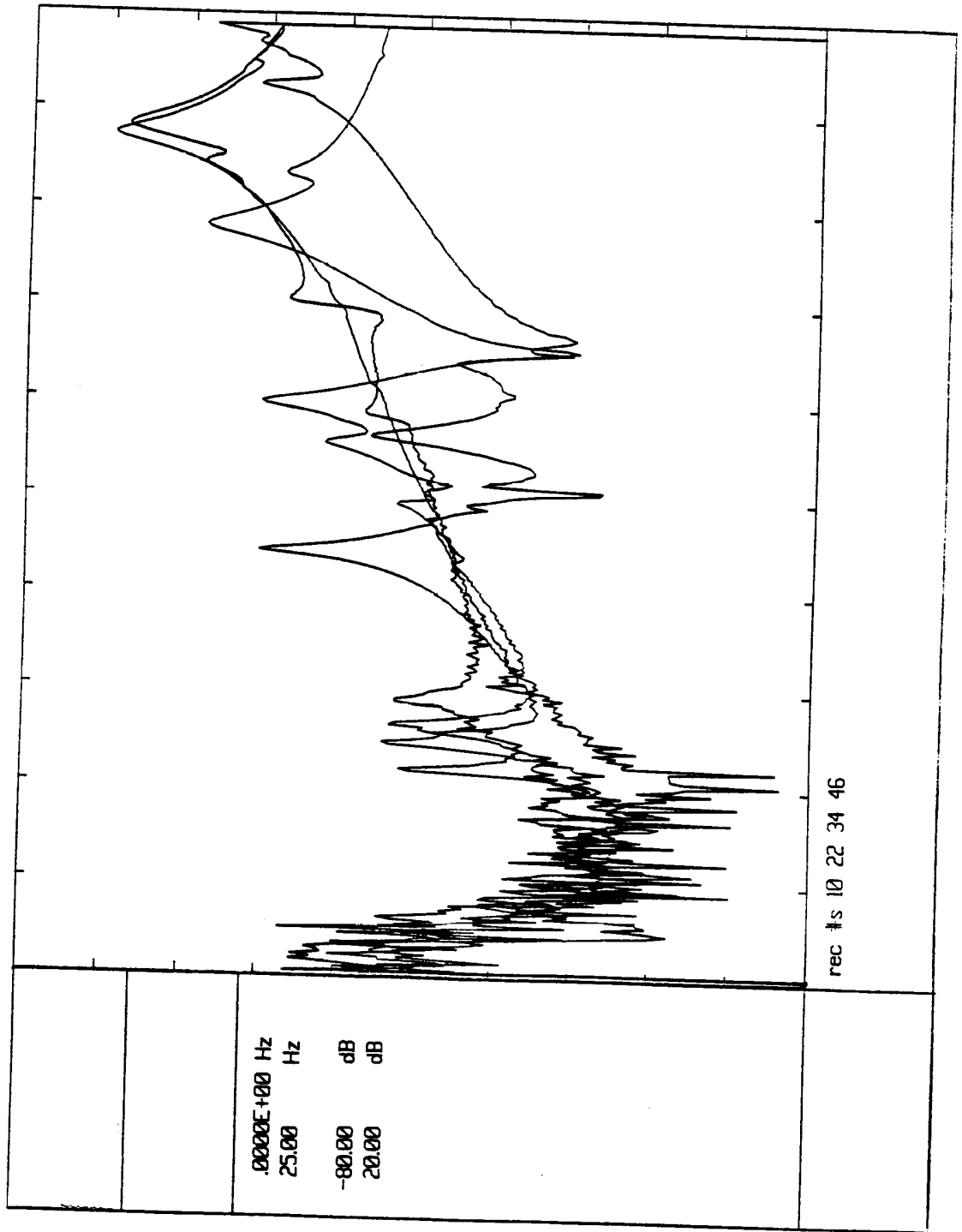


Figure 49. Decoupled FRFs for All Configurations: Mode #11 (Upper Mast Torsion)

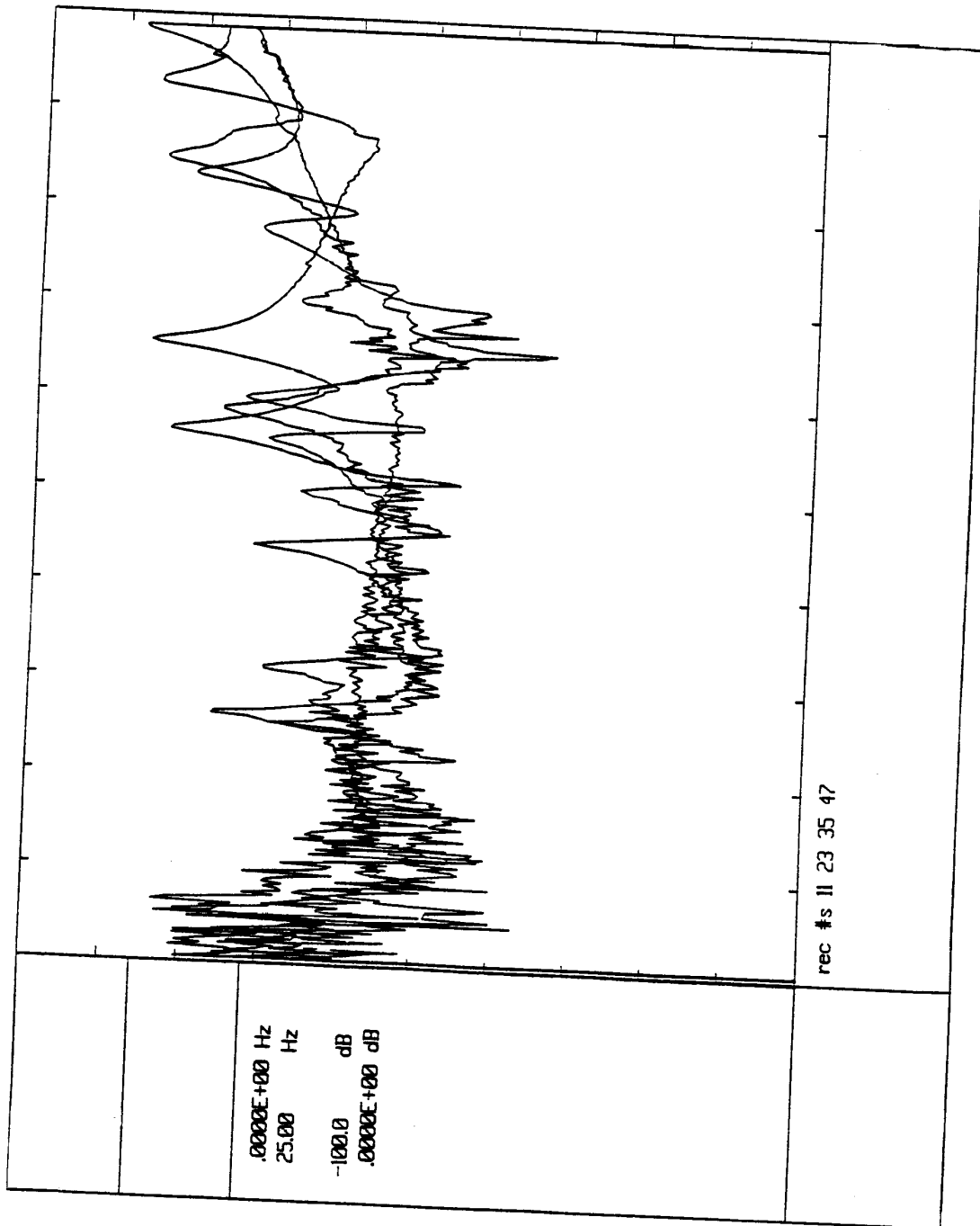


Figure 50. Decoupled FRFs for All Configurations: Mode #12 (Crossarm YZ-plane Bending)

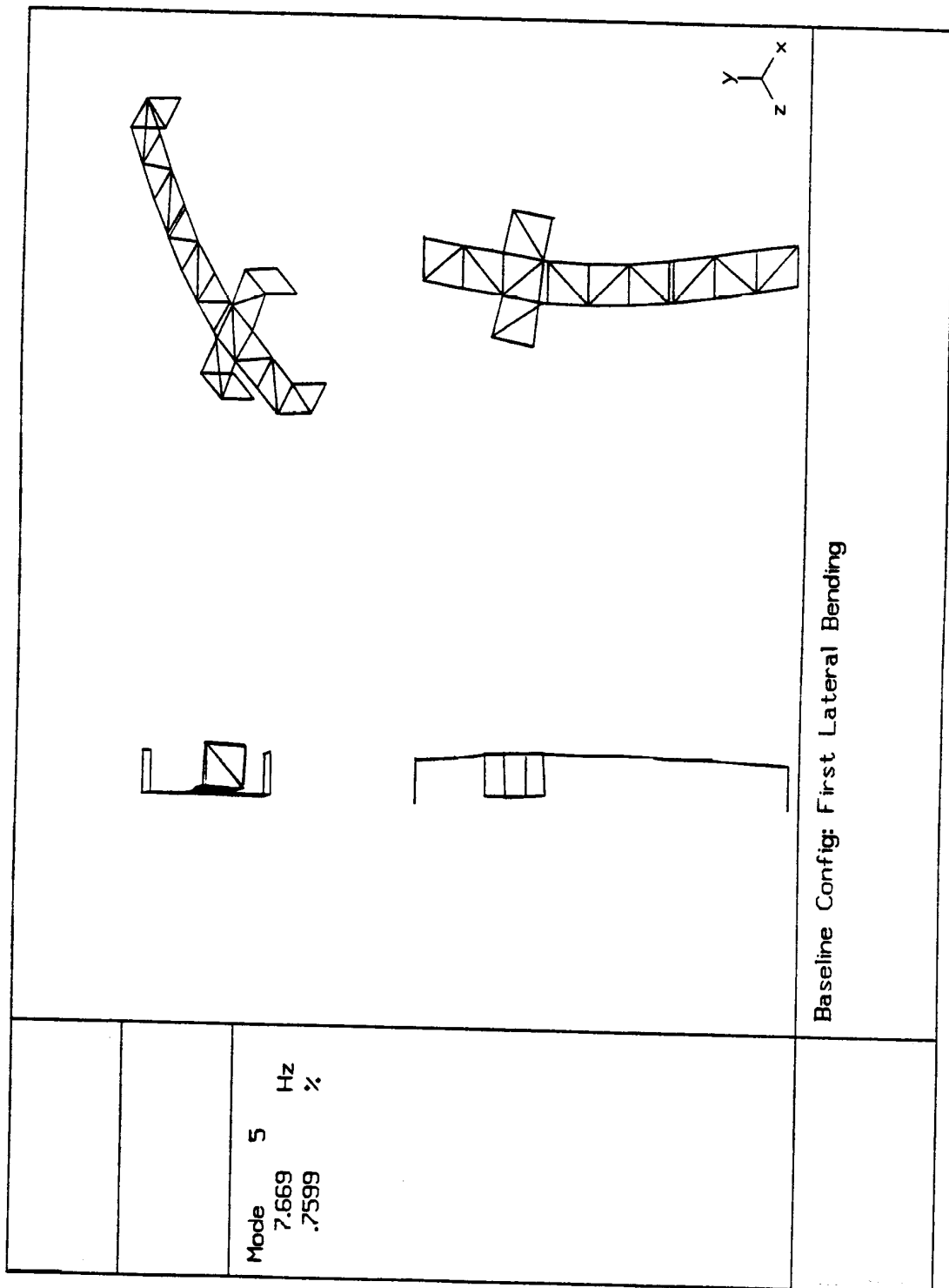


Figure 51. Baseline Mode Shape: First Lateral Bending (mode # 5)

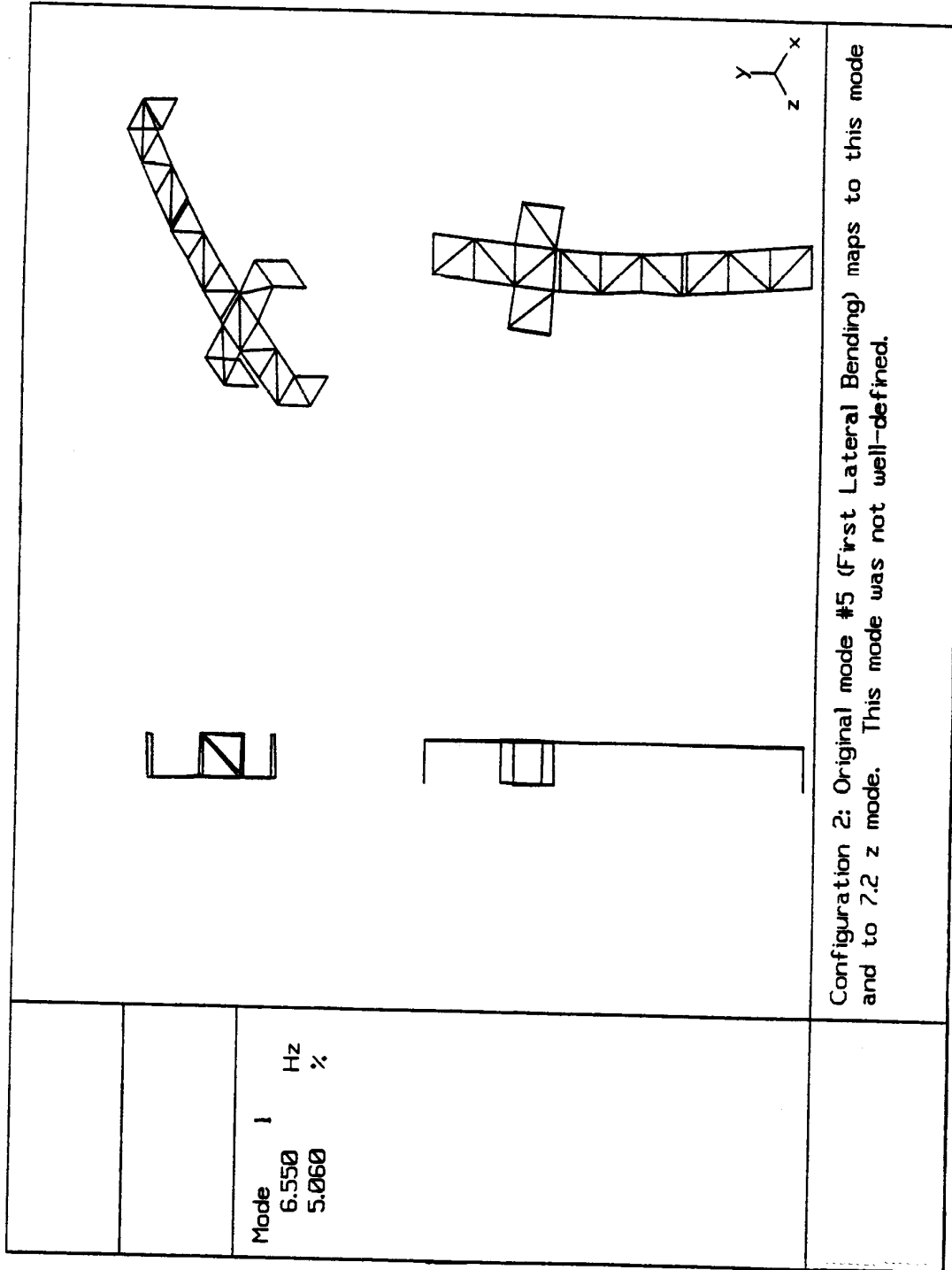


Figure 52. Configuration #2 Mode Shape Containing Baseline First Lateral Bending

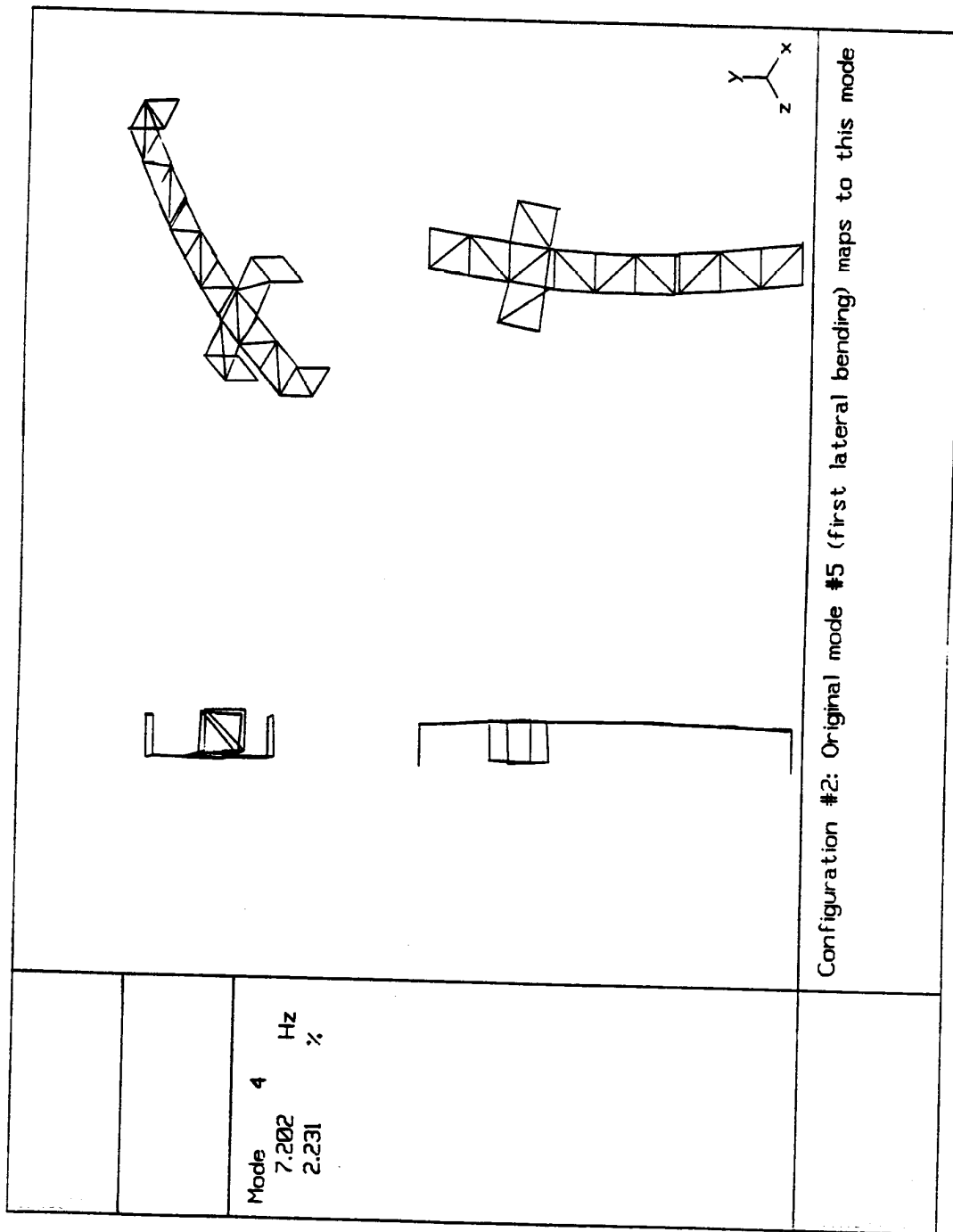


Figure 53. Configuration #2 Mode Shape Containing Baseline First Lateral Bending

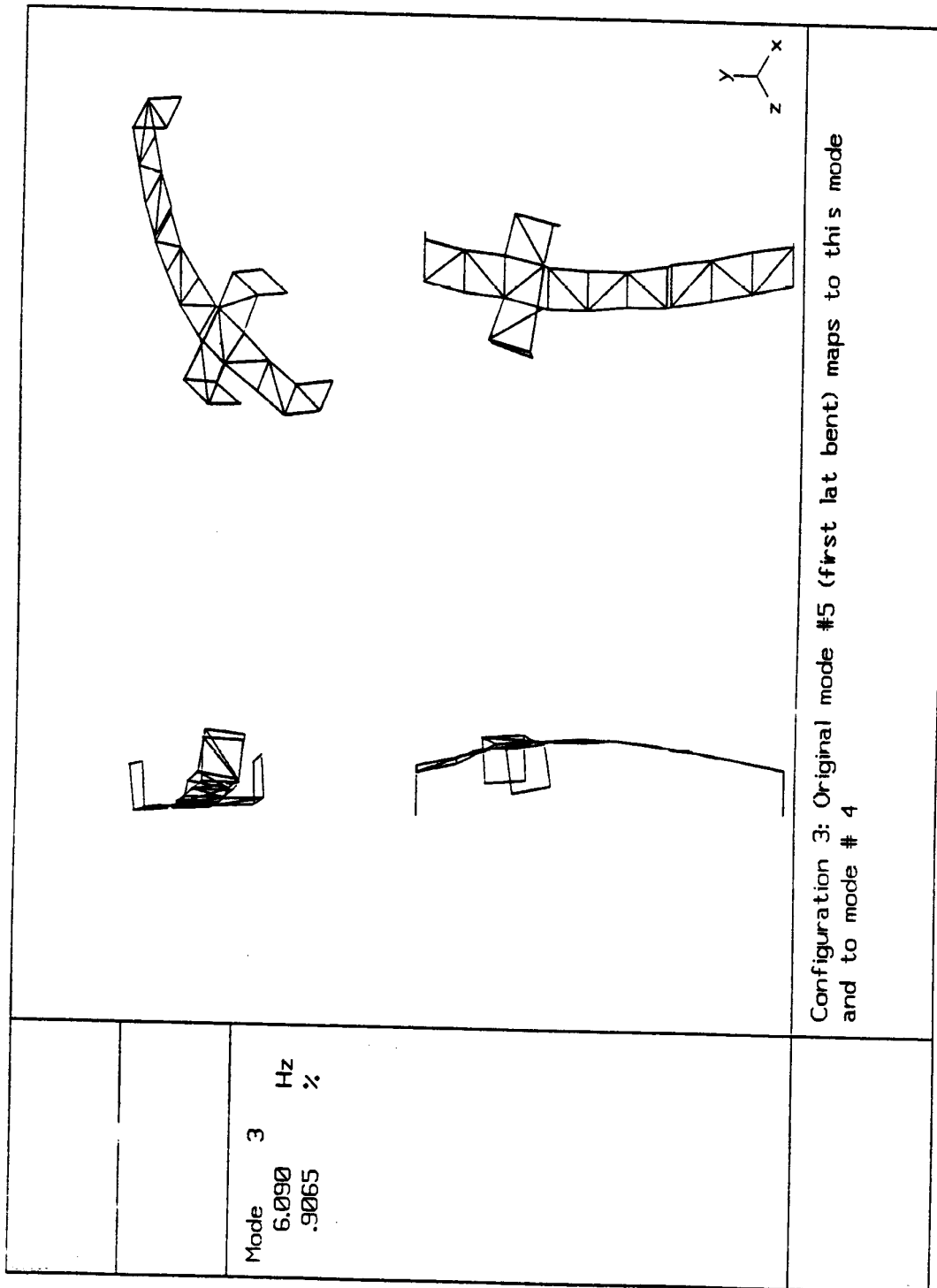


Figure 54. Configuration #3 Mode Shape Containing Baseline First Lateral Bending

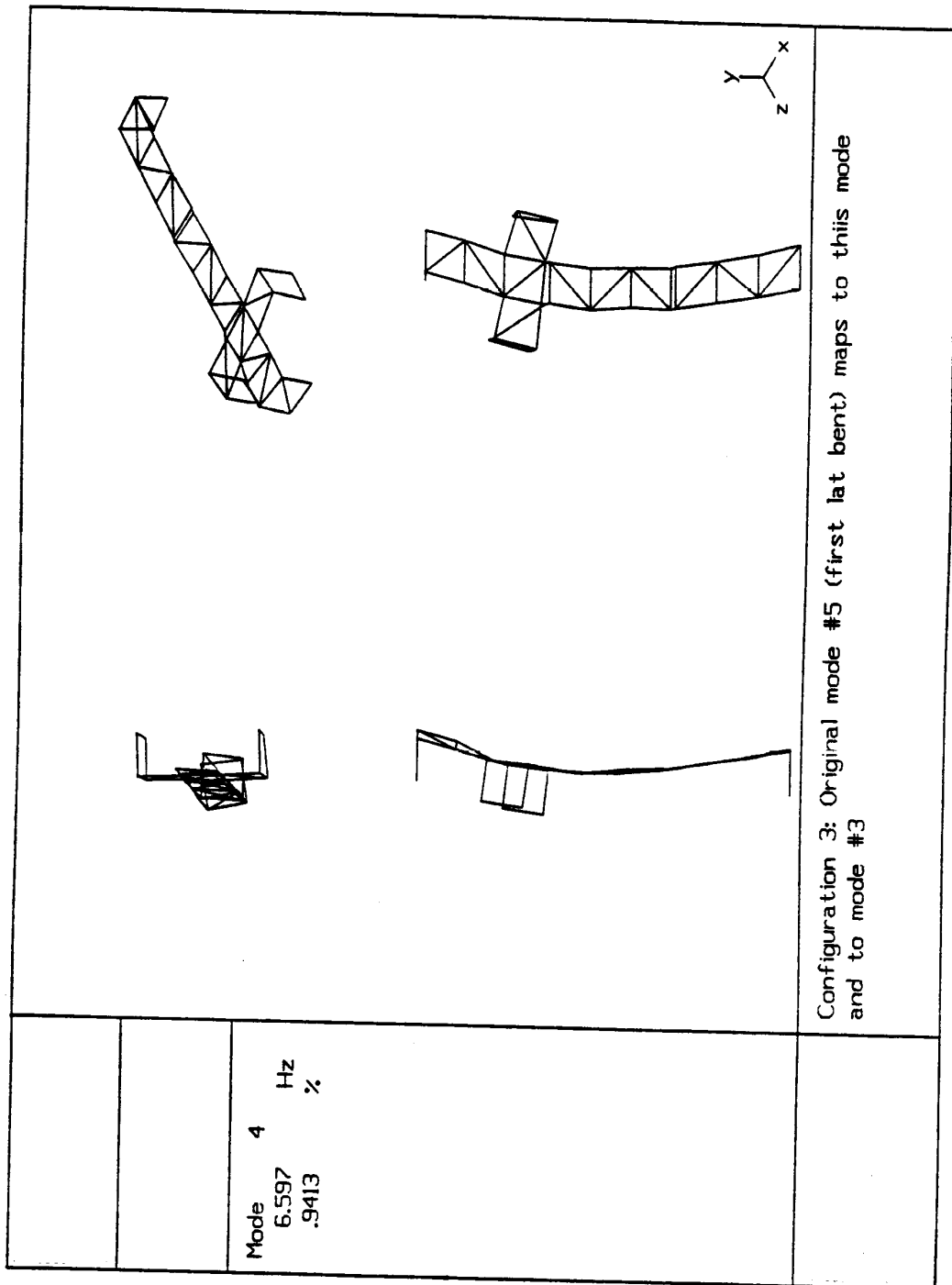


Figure 55. Configuration #3 Mode Shape Containing Baseline First Lateral Bending

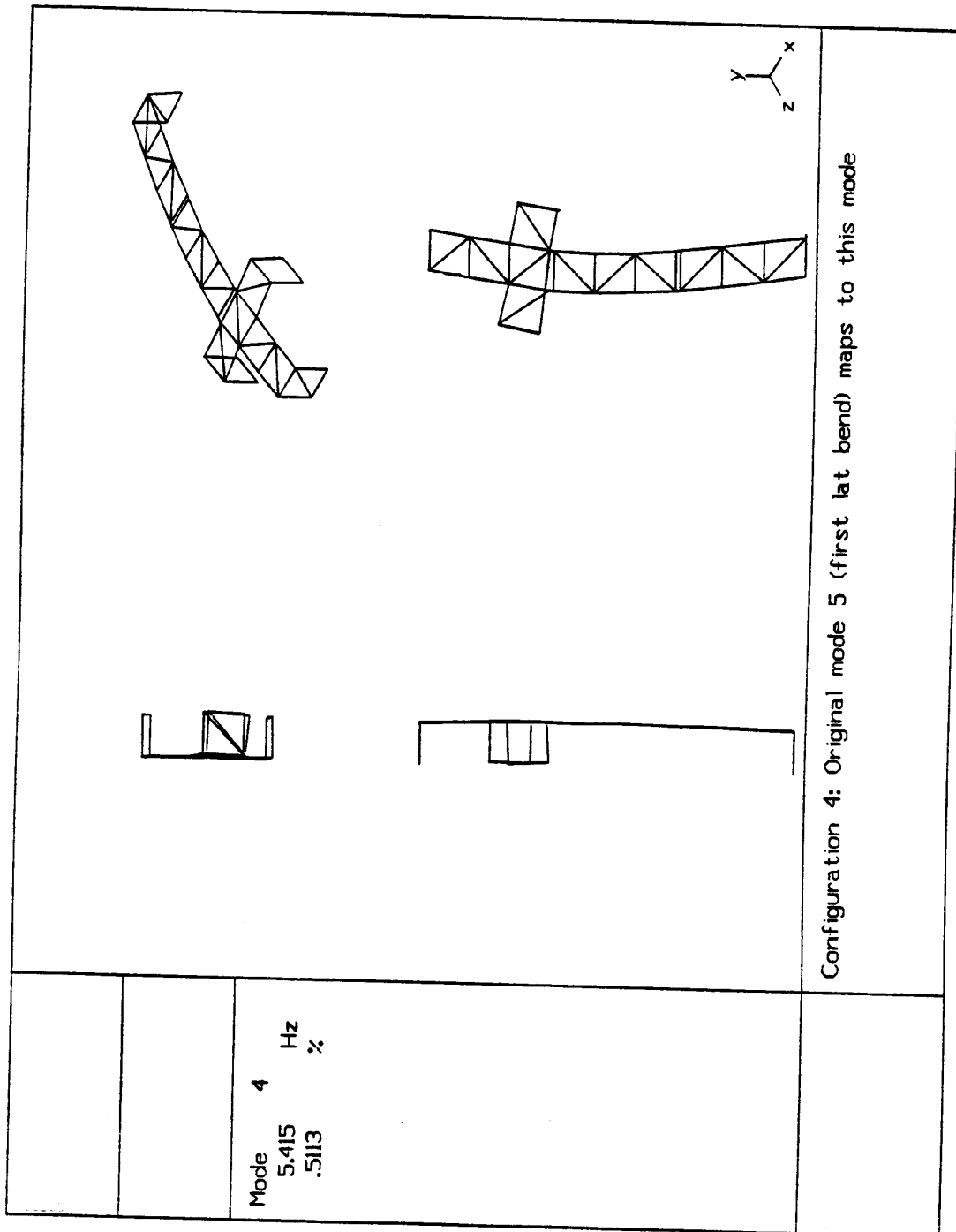


Figure 56. Configuration #4 Mode Shape Containing Baseline First Lateral Bending

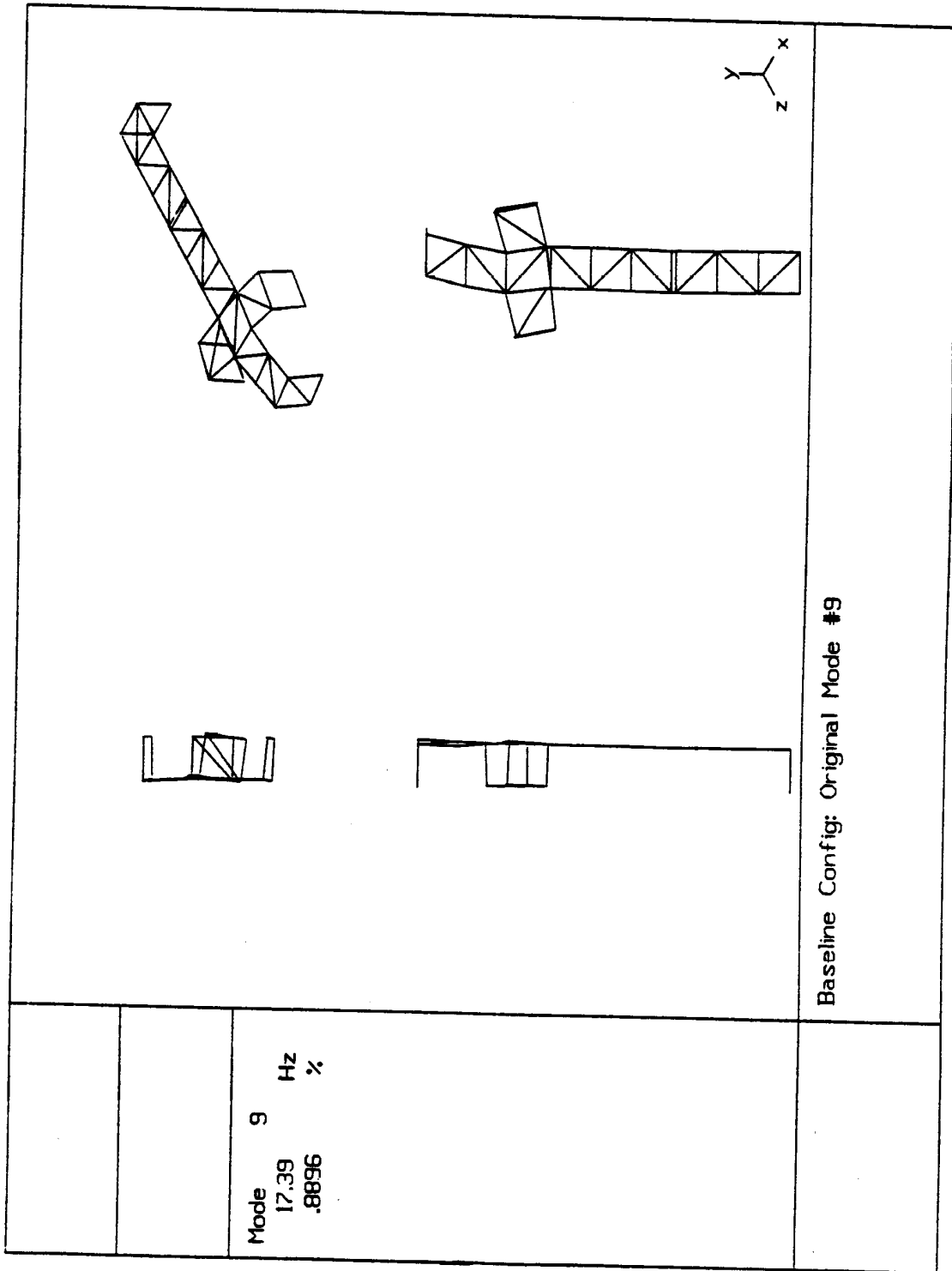


Figure 57. Baseline Mode Shape: Upper Mast/ Crossarm Lateral Bending (mode # 9)

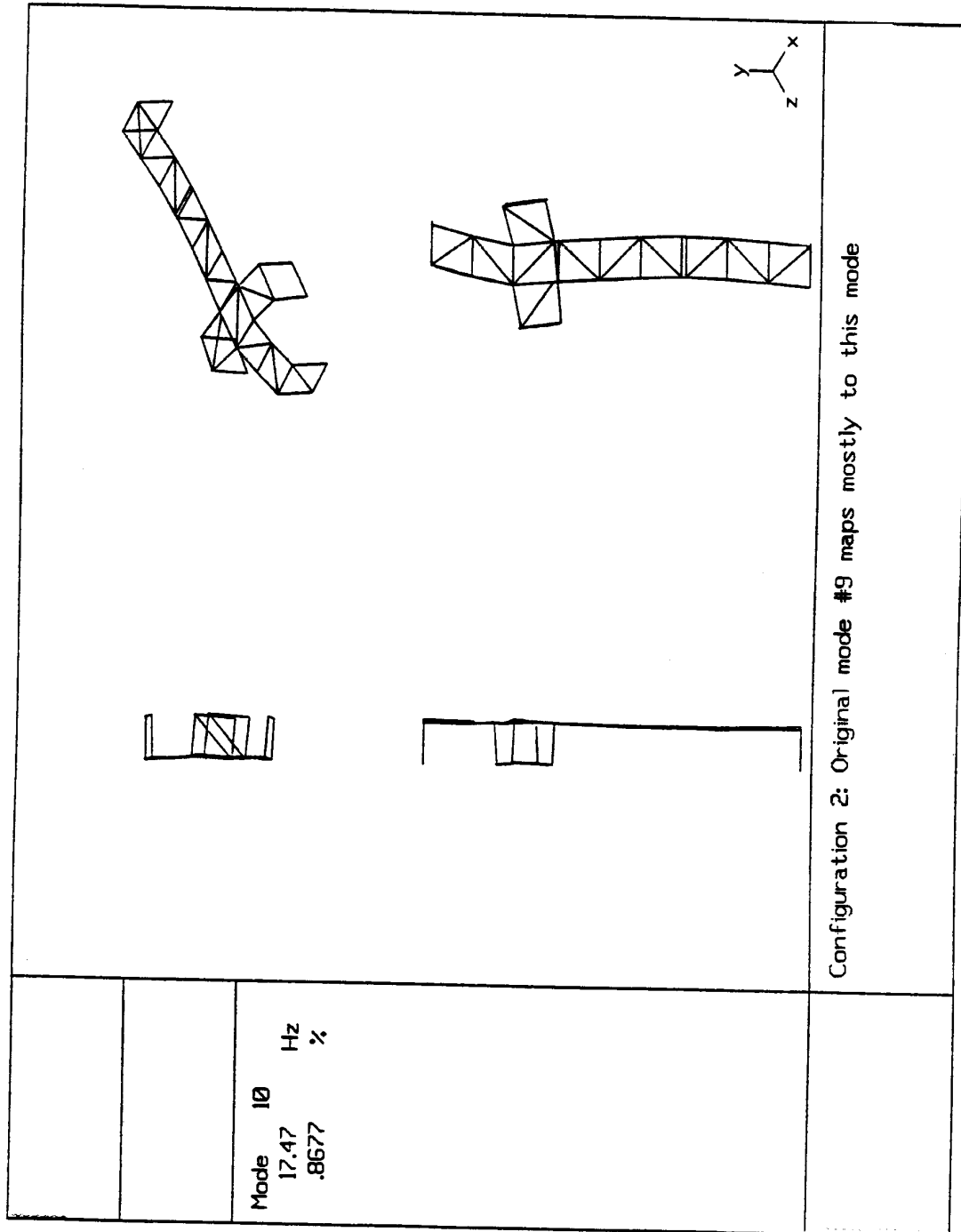


Figure 58. Configuration #2 Mode Shape Containing Baseline Mode #9

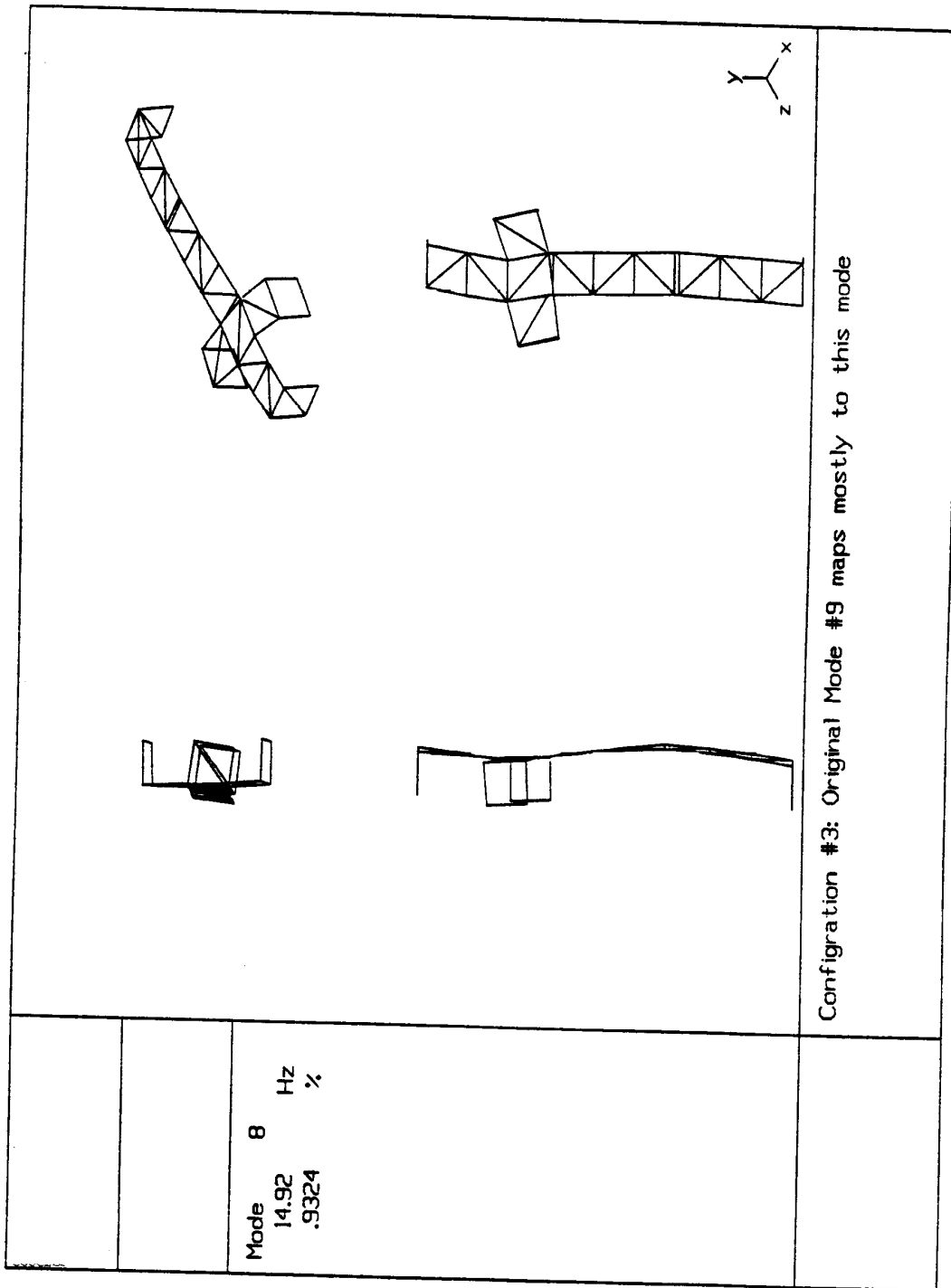


Figure 59. Configuration #3 Mode Shape Containing Baseline Mode #9

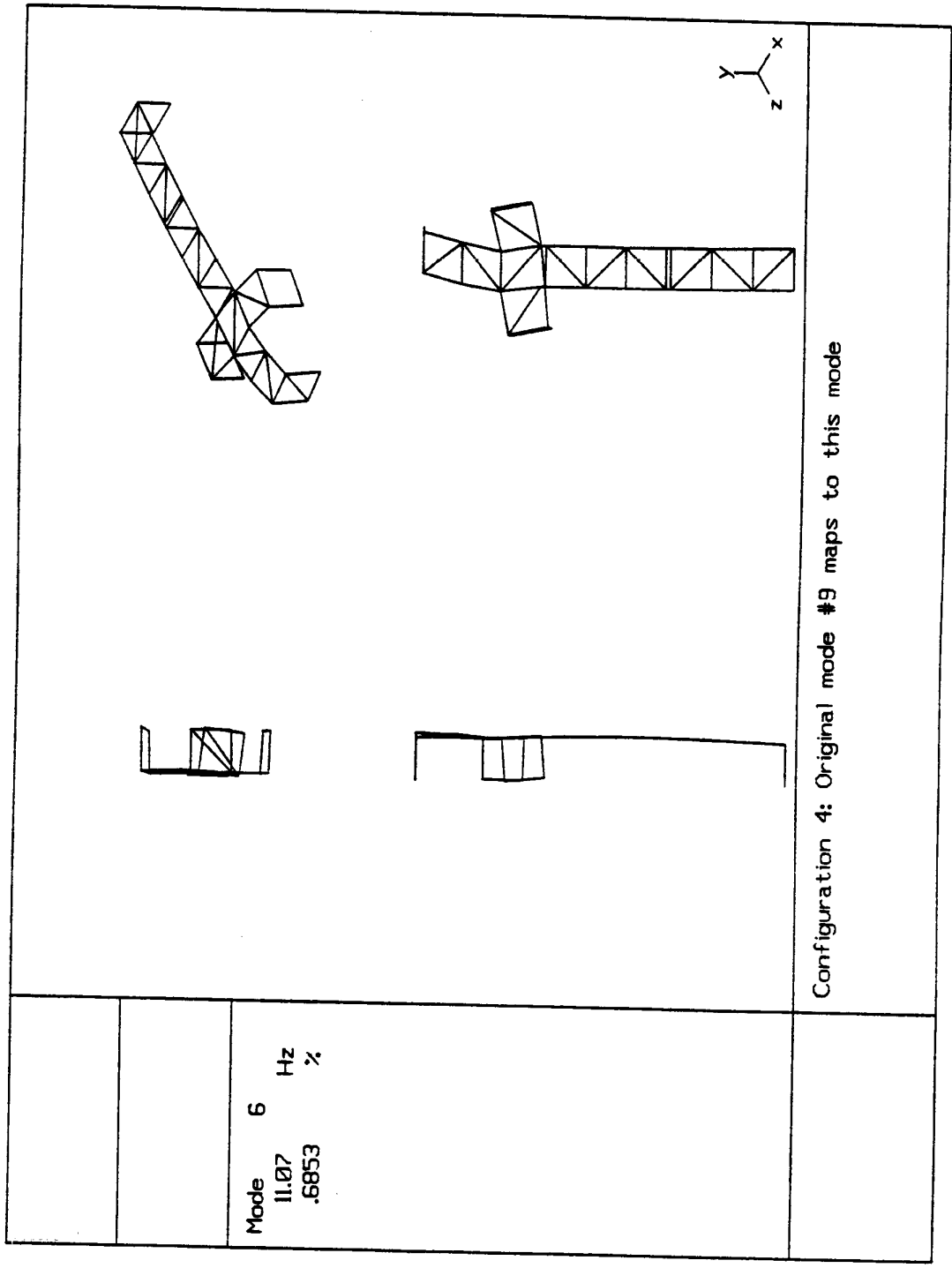


Figure 60. Configuration #4 Mode Shape Containing Baseline Mode #9

## CONCLUDING REMARKS

Several aspects of using this new concept of the reciprocal modal vector, or discrete modal filter, as a modal state observer have been investigated and presented. The modal state observer can be constructed using only experimental data and subsequent data analysis results. The calculation is straightforward and allows the user latitude in choosing calculation parameters. The calculation is also robust provided a reasonable modal model exists and the data is of reasonable quality. The effect of poor data quality was not investigated.

Both the analytical and experimental studies indicated that one can readily extract the response of a particular mode from the measurements. If one then considers a perturbed system, both studies also indicate the reciprocal modal vector is not sensitive to system changes in modal frequency or damping. It is, however, affected by changes in the mode shape or weighting matrix.

The results presented here show that the reciprocal modal vector calculation is straightforward and performs well with frequency response function data, both synthesized and realistic. Additional efforts not reported here indicate that the decoupling appears to also work without the knowledge of any of the inputs, and that similar results can be obtained in the time domain.

The ability to construct a transformation from the physical space to the modal space completely with experimental modal analysis techniques provides the modal analysis community with a powerful tool applicable in a variety of areas that were until now considered beyond the reach of the experimenter. In particular, there appears to be widespread applicability in parameter estimation, analysis, and/or control of structural systems that are nonlinear, time-varying, and/or under the influence of closed loop forces. This includes those applications where the input forces are not known. There may also be some applicability in the area of structural modification prediction techniques as an extension of traditional analytical-experimental correlation applications already mentioned. This is not a complete list.

As stated in the introduction, it is hoped that the concept of modal filtering will eventually lead to the implementation of a practical tool for monitoring the dynamics of structures in the presence of unknown or unmeasurable closed loop forces. For closed loop systems in which the closed loop eigenvectors are constant and identical to the open loop structure, the results presented here clearly indicate that a "modal state monitor" would be straightforward to implement. Unfortunately, most real problems in this area will have changing closed loop mode shapes. Thus, additional efforts must be made to develop a practical tool for modal state monitoring.

## RECOMMENDATIONS

Reciprocal modal vectors and modal filters in general have widespread applicability, yet many aspects of these applications require additional research and development in order to be well-understood. Topics relevant to some of these applications and to this thesis that are recommended for further study are:

1. More detailed investigations of the effect of the number and choice of measurement degrees of freedom on the decoupling performance. In some situations, such as fly-by-wire aircraft, one is often limited in the number of available sensors. Thus, implementation may not be practical in some situations.
2. An investigation into the feasibility of estimating a mass matrix from the reciprocal modal matrix. A logical first step would be to study the observation that was made here concerning the relationship between the reciprocal modal vectors and the modal matrix for the analytical model. Specifically, how is the scaling of the reciprocal modal vector related to mode shape scaling,  $Q_r$ , and actual mass values?

3. Extension of the reciprocal modal vector theory and formulation to include sensors of different types, non-reciprocal systems, and repeated roots. In addition, a study should be performed to investigate the accuracy of scaling factor and complex eigenvalue estimates that can be obtained from the decoupled space.
4. Construction of update schemes to improve both the original estimate and to update the reciprocal vectors in an online sense (for control or observation of time varying systems).
5. Design and analysis of controllers using experimentally determined modal filters as state estimators. This would include studies to identify optimal actuator number and locations to control a given set of modes.
6. Implementation of the reciprocal modal vector calculation in modal parameter estimation algorithms as a standard modal parameter.
7. Implementation of reciprocal modal vectors for online preprocessing of measured data. For applications where the reciprocal modal vector can be considered time-invariant, fast online parameter estimation schemes can be implemented in the modal space. This is because single-degree-of-freedom frequency response functions can be calculated during the data acquisition process merely by first processing the response transducers with the modal filter prior to calculating the frequency response functions. Thus, single-degree-of-freedom pole estimators can provide estimates of pole values with very little computational effort.
8. For the more general case of non-constant closed loop eigenvectors, preprocessing the responses with the modal filter will not result in single-degree-of-freedom frequency response functions. Comparison studies should be made to investigate the performance of multiple-degree-of-freedom pole estimators in the baseline modal space. In addition, if the number of modes in the frequency range considered does not change, then the  $N$ -dimensional modal space can be re-diagonalized via a variety of standard modal parameter estimation techniques. Since  $N$  is known, these techniques might be implemented with a reduced amount of required engineering judgement (possibly in an online sense).
9. For applications involving pole estimates from operating data, a variety of techniques currently exist (e.g. random decrement and any single degree-of-freedom technique) whose performance should be enhanced through the use of modal filters. Implementation of modal filters for these techniques is straightforward and should be pursued. Since the modal filter will change as the mode shapes change, some thought should be given to the construction of weighting functions that might be useful for diagonalizing the operating data. Specifically, what are the best linear combinations of the open loop modal filters that try to decouple the closed loop information (frequency response function or operating data), and how well do they perform? If it is found that linear combinations of the open loop modal filters do not adequately decouple the closed loop systems (or cannot be found in a practical manner), then other approaches should be considered.

## REFERENCES

- <sup>[1]</sup>Zhang, Q., R.J. Allemang, and D.L. Brown, "Modal Filter: Concept and Applications," Proc. of the 8th Int'l Modal Analysis Conference, Orlando, FL, Jan. 1990, pp. 487-496.
- <sup>[2]</sup>Zhang, Q., C.Y. Shih, and R.J. Allemang, "Orthogonality Criterion for Experimental Modal Vectors," Vibration Analysis-Techniques and Applications, ASME publication DE-Vol. 18-4, pp. 251-258.
- <sup>[3]</sup>Meirovitch, L., and H. Baruh, "Control of Self-Adjoint Distributed-Parameter Systems," *J. of Guidance, Control, and Dynamics*, vol. 5 no. 1, Jan.-Feb. 1982, pp. 60-66.
- <sup>[4]</sup>Meirovitch, L., and H. Baruh, "The Implementation of Modal Filters for Control of Structures," *J. of Guidance, Control, and Dynamics*, vol. 8 no. 6, Nov.-Dec. 1985, pp. 707-716.
- <sup>[5]</sup>Allemang, Randall J., Ph.D Dissertation, Department of Mechanical and Industrial Engineering, University of Cincinnati, "Investigation of Some Multiple Input/Output Frequency Response Function Experimental Modal Analysis Techniques," 1980.
- <sup>[6]</sup>Shih, C.Y., Q. Zhang, and R.J. Allemang, "Force Identification by Using Principle and Modal Coordinate Transformation Method," Vibration Analysis-Techniques and Applications, ASME publication DE-Vol. 18-4, pp. 303-309.
- <sup>[7]</sup>Shih, C.Y., Y.G. Tsuei, R.J. Allemang, and D.L. Brown, "Complex Mode Indication Function and its Application to Spatial Domain Parameter Estimation," Proc. 7th Int'l Modal Analysis Conference, Las Vegas, NV, 1989.
- <sup>[8]</sup>Allemang, Randall J., and David L. Brown, "A Correlation Coefficient for Modal Vector Analysis," Proc. 1st Int'l Modal Analysis Conference, Orlando, FL, Nov. 8-10, 1982, pp. 110-116.
- <sup>[9]</sup>Allemang, Randall J., "System Identification for Controls: A Modal Analysis Perspective," Keynote Address, Proc. of the 15th Int'l Seminar on Modal Analysis, Sept. 19-21, 1990.



# Report Documentation Page

1. Report No. NASA CR-179448		2. Government Accession No.		3. Recipient's Catalog No.	
4. Title and Subtitle  Analysis of Structural Response Data Using Discrete Modal Filters				5. Report Date May 1991	
				6. Performing Organization Code	
7. Author(s)  Lawrence C. Freudinger				8. Performing Organization Report No. H-1693	
				10. Work Unit No. RTOP 505-63-40	
9. Performing Organization Name and Address University of Cincinnati, Dept. of MINE Structural Dynamics Research Laboratory Cincinnati, OH 45221-0072				11. Contract or Grant No. G0635, PR A78043C	
				13. Type of Report and Period Covered Contractor Report	
12. Sponsoring Agency Name and Address  National Aeronautics and Space Administration Washington, DC 20546-3191				14. Sponsoring Agency Code	
15. Supplementary Notes  This report was prepared as a theses in partial fulfillment of the requirements of the University of Cincinnati for the degree of Master of Science.					
16. Abstract <p>This thesis describes the application of reciprocal modal vectors to the analysis of structural response data. Reciprocal modal vectors are constructed using an existing experimental modal model and an existing frequency response matrix of a structure and can be assembled into a matrix that effectively transforms the data from the physical space to the modal space within a particular frequency range. In other words, the weighting matrix necessary for modal vector orthogonality (typically the mass matrix) is contained within the reciprocal modal matrix.</p> <p>The ability to extract the response of a particular mode from a system due to whatever forces may be acting on it has broad applicability, from operating data analysis and force identification to vibration control. The underlying goal of this work is mostly directed toward observing the modal state responses in the presence of unknown, possibly closed loop forcing functions, thus having an impact on both operating data analysis techniques and independent modal space control techniques. This study investigates the behavior of reciprocal modal vectors as modal filters with respect to certain calculation parameters and their performance with perturbed system frequency response data.</p>					
17. Key Words (Suggested by Author(s))  Aeroservoelastic; Flight test; Modal filter; Modal test; Reciprocal modal vector; Spatial filter; Vibration control			18. Distribution Statement Unclassified — Unlimited  Subject category 05		
19. Security Classif. (of this report) Unclassified		20. Security Classif. (of this page) Unclassified		21. No. of Pages 78	22. Price A04